The Role of Transient Receptor Potential Melastatin 8 (TRPM8) in the Naked Mole-rat Thermosensation

Dissertation

to obtain the academic degree

Doctor rerum naturalium (Dr. rer. nat.)

submitted to the Department of Biology, Chemistry, Pharmacy

of Freie Universität Berlin

by

Lin Wang

Born in Zhejiang, China

Berlin, Germany, 2024

This work was carried out under the supervision of Prof. Dr Gary Lewin between February 2021 to September 2024 at the Max Delbrück Center for Molecular Medicine in the Helmholtz Association, Berlin, Germany.

1. **Gutachter: Prof. Dr. Gary R. Lewin**
   Max Delbrück Center for Molecular Medicine

2. **Gutachter: Prof. Dr. Ursula Koch**
   Department of Biology, Chemistry, Pharmacy
   Freie Universität Berlin

Disputation am 16.12.2024

DECLARATION OF AUTHORSHIP

I, **Lin Wang**, hereby declare that I alone am responsible for the content of my doctoral dissertation and that I have only used the sources or references cited in the dissertation.

ACKNOWLEDGEMENTS

I extend my deepest gratitude to everyone who assisted, encouraged, supported, and occasionally diverted my attention during my doctoral journey.

My sincere appreciation goes to Prof. Dr. Gary R. Lewin for providing me with the opportunity to study and work within this research group. I am immensely grateful for your magnanimity and for never letting occasional idiosyncrasies affect our interactions. My heartfelt thanks to Dr. Valérie Bégay-Müller. Your rigor and support have granted me profound insights both scientifically and personally.

I am also thankful to our collaborators, Prof. Félix Viana de la Iglesia and Prof. Elvira De la Peña García from the Universidad Miguel Hernández. Though our time together was brief, the experience of working with you was immensely beneficial. The individuals I encountered within the Spanish research group were exceptionally kind and warm-hearted.

I express gratitude to Maria Braunschweig for her unwavering positivity in our conversations and her willingness to understand my perspective while candidly addressing my issues. Big thanks also go to Franziska Bartelt and Kathleen Barda for their support in smoothly conducting experiments within the lab. Thank you to Gabriela Pflanz and Anika Mühlenberg for taking care of the NM-Rs used in my research. Also special thanks to Michael Strehle. Your morning coffees and brief conversations made me feel truly at home within this group, fostering a sense of belonging. I wish to express my gratitude to current and past colleagues who introduced me to the equipment in the laboratory and passed on their valuable technical expertise to me. Special thanks are due to Dr. Shermin Mak and Dr. Wenhan Luo for editing my thesis.

I am fortunate to have received substantial support from my family, ensuring the completion of this work. I am eternally grateful for their understanding and consideration. While I refrain from listing individual family members here, my gratitude knows no bounds. I am deeply appreciative of all the kind-hearted friends who have been by my side not only during cheerful times but also during hard times. Because of all of you, my doctoral life was more joyful than I could have imagined. Lastly, I extend my heartfelt thanks to Kuisong Song, whose love and unwavering support were with me throughout the writing of my thesis.

The acknowledgement may have an end, but gratitude knows no bounds.

The thesis concludes on September 30, 2024, yet the chapters of my life continue.

ABSTRACT

The subterranean naked mole-rat (*Heterocephalus glaber*, NM-R) is a rodent that has attracted growing research interest from a biomedical and zoological perspective. NM-Rs exhibit unique physiological characteristics including eusociality, pain insensitivity, cancer resistance, an unusual immune system, a long lifespan, and the lower basal metabolic rate than expected for its body mass. In addition, NM-Rs are poikilothermic mammals. So far, the precise mechanisms of cold detection processes remain poorly understood. The transient receptor potential melastatin 8 (TRPM8) ion channel is the principal cold receptor in mammals, a better understanding of the role of TRPM8 is needed to improve our current knowledge of the thermosensory system in NM-R.

We used RNAScope and immunofluorescence to better understand the expression and localization of TRPM8 in sensory and non-sensory tissues. TRPM8 is expressed in the NM-R DRGs but more $TRPM8^{+}$ $NF200^{+}$ neurons are found in NM-R compared to mice. Approximately 33.7% of TRPM8-positive neurons also express NF200, indicating a significant presence in myelinated sensory neurons, while 39.33% and 19.14% of these neurons co-express CGRP and TRPV1, respectively. Interestingly, TRPM8 was also observed in large-diameter neurons and was not limited to smaller neurons typically associated with cold sensing in mice. Furthermore, we identified TRPM8 expression in the near lamina I of the dorsal horn of the NM-R spinal cord, which is similar to mice. Notably, we observed abundant and specific *Trpm8* mRNA expression in the neurons of grey matter within the NM-R spinal cord.

A notable discovery was the identification of a unique extended N-terminal sequence in NM-R TRPM8 compared with TRPM8 sequences from more than 30 mammals. We confirmed a unique extended N-terminal variant of the TRPM8 ion channel in NM-Rs using RT-PCR and a custom *Ex-trpm8* probe designed for the 415–854 bp region from the NM-R *Trpm8* mRNA. To explore the functional implications of this extended N-terminal sequence, we performed calcium imaging assays using HEK293T cells expressing NM-R TRPM8. The results demonstrated that the extended sequence significantly diminishes the response of TRPM8 to cold, menthol, and icilin. When this sequence was deleted, TRPM8 function was restored to levels similar to the mouse TRPM8. Additionally, fusing this N-terminal extension to mouse TRPM8 reduced its responsiveness, suggesting that the extended sequence modulates cold sensitivity in NM-Rs.

Further experiments using calcium imaging of cultured NM-R DRG neurons and skin-nerve preparations demonstrated that NM-Rs retain intact cold sensation, which is largely independent of TRPM8. Cold-sensitive neurons were more abundant in NM-Rs than in mice, particularly among larger neurons. Additionally, cold-sensitive fibers in NM-Rs exhibited faster conduction velocities compared to those in mice, suggesting the involvement of alternative pathways for cold detection and potential evolutionary adaptations for rapid cold sensing in subterranean environments.

These findings suggest that NM-Rs may have evolved unique TRPM8 isoforms and alternative mechanisms for cold perception, which may reflect adaptations to their distinct ecological niche. These findings not only advance our understanding of cold detection in NM-Rs but also raise intriguing questions about the evolutionary divergence of TRPM8 function in this species.

ZUSAMMENFASSUNG

Der unterirdisch lebende Nacktmull (*Heterocephalus glaber*, NM-R) ist ein Nagetier, das zunehmendes Interesse aus biomedizinischer und zoologischer Perspektive fährt. Nacktmulle weisen einzigartige physiologische Merkmale auf, darunter Eusozialität, Schmerzunempfindlichkeit, Krebsresistenz, ein ungewöhnliches Immunsystem, eine lange Lebensspanne und eine niedrigere Basalstoffwechselrate als für ihre Körpermasse erwartet. Darüber hinaus sind Nacktmulle poikilotherme Säugetiere. Bislang sind die genauen Mechanismen der Kälteregulation noch unzureichend verstanden. Der Transiente Rezeptorpotential Melastatin 8 (TRPM8) Ionenkanal gilt als der Hauptkälterezeptor bei Säugetieren. Ein besseres Verständnis der Rolle von TRPM8 ist notwendig, um unser derzeitiges Wissen über das thermosensorische System des Nacktmulls zu erweitern.

Wir verwendeten RNAScope Detektion und Fluoreszenzimmunhistochemie, um die Expression und Lokalisierung von TRPM8 in sensorischen und nicht-sensorischen Geweben besser zu verstehen. TRPM8 wird in den Nacktmull-Spinalganglien (DRG) exprimiert, wo mehr $TRPM8^+$ $NF200^+$ Neuronen im Vergleich zu Mäusen zu finden sind. Etwa 33,7 % der TRPM8-positiven Neuronen exprimieren ebenfalls NF200, was auf eine signifikante Präsenz in myelinisierten sensorischen Neuronen hinweist, während 39,33 % und 19,14 % dieser Neuronen CGRP bzw. TRPV1 co-exprimieren. Interessanterweise wurde TRPM8 auch in Neuronen mit großem Durchmesser beobachtet und war nicht auf kleinere Neuronen beschränkt, die typischerweise mit Kälteempfindung bei Mäusen in Verbindung gebracht werden. Des Weiteren identifizierten wir TRPM8-Expression in der Nähe der Lamina I des Rückenmarksdorsalhorns von Nacktmullen, ähnlich wie bei Mäusen. Bemerkenswert war die reichliche und spezifische *Trpm8* mRNA-Expression in den Neuronen der grauen Substanz des Rückenmarks von Nacktmullen.

Eine bemerkenswerte Entdeckung war die Identifizierung einer im Vergleich zu TRPM8-Sequenzen von über 30 anderen Säugetieren einzigartigen verlängerten N-terminalen Sequenz im Genom von Nacktmullen. Wir verifizierten diese verlängerte N-terminale Variante des TRPM8-Ionenkanals mittels RT-PCR und einer speziellen *Ex-trpm8*-Sonde, die für den Bereich 415–854 bp der NM-R *Trpm8* mRNA entworfen wurde. Um die funktionellen Auswirkungen dieser verlängerten N-terminalen Sequenz zu untersuchen, führten wir Kalzium-Imaging-Experimente mit HEK293T-Zellen durch, die NM-R TRPM8 exprimierten. Die Ergebnisse

zeigten, dass die verlängerte Sequenz die Reaktion von TRPM8 auf Kälte, Menthol und Icilin signifikant vermindert. Als diese Sequenz aus dem NM-R *Trpm8* Gen entfernt wurde, wurde die Sensitivität auf ein Niveau ähnlich dem von Maus-TRPM8 wiederhergestellt. Umgekehrt verringerte eine Fusion der NM-R N-terminalen Erweiterung an Maus-TRPM8 dessen Empfindlichkeit, was darauf hindeutet, dass die verlängerte Sequenz die Kälteempfindlichkeit bei Nacktmullen moduliert.

Weitere Experimente mit Kalzium-Imaging an kultivierten NM-R-DRG-Neuronen und Haut-Nerven-Präparaten zeigten, dass Nacktmulle ihre intakte Kälteempfindung beibehalten, die weitgehend unabhängig von TRPM8 ist. Kälteempfindliche Neuronen waren bei Nacktmullen häufiger als bei Mäusen, insbesondere größere Neurone. Darüber hinaus zeigten kälteempfindliche Fasern bei Nacktmullen höhere Leitungsgeschwindigkeiten im Vergleich zu Mäusen, was auf die Beteiligung alternativer Wege der Kältewahrnehmung und mögliche evolutionäre Anpassungen für schnelles Kälteempfinden in unterirdischen Lebensräumen hinweist.

Die aufgeführten Ergebnisse legen nahe, dass Nacktmulle einzigartige TRPM8-Isoformen und alternative Mechanismen für die Kältewahrnehmung entwickelt haben, was möglicherweise Anpassungen an ihre spezifische ökologische Nische widerspiegelt. Diese Erkenntnisse erweitern nicht nur unser Verständnis der Kältewahrnehmung bei Nacktmullen, sondern werfen auch interessante Fragen zur evolutionären Divergenz der TRPM8-Funktion in dieser Spezies auf.

TABLE OF CONTENTS

List of tables

List of figures

List of abbreviations

AFM	Atomic Force Microscopy
AM	acetoxymethyl
AMC	Aδ-mechano-cold
AMH	Aδ-mechano-heat
AMTB	*N-(3-aminopropyl)-2-[(3-methylphenyl)methoxy]-N-(2-thienylmethyl)benzamide*
ANKTM1	Ankyrin-like with transmembrane domains protein 1
ANOVA	Analysis of variance
ARD	Ankyrin repeat domain
BAT	Brown adipose tissue
BLAST	Basic Local Alignment Search Tool
BSA	Bovine serum albumin
$CaCl_2$	Calcium chloride
CC	C-cold
CGRP	Calcitonin gene-related peptide
CMC	C-mechano-cold
CMCH	C-mechano-cold-heat
CMH	C-polymodal
CMR1	cold- and menthol-sensitive receptor 1
CNS	Central Nervous System
CO_2	Carbon dioxide
CTD	Carboxyl-terminal domain
CV	conduction velocity
DAPI	4',6-diamidino-2-phenylindole
DH	Dorsal horn
DMEM	Dulbecco's modified eagle medium
DMSO	Dimethyl sulfoxide
DNA	Deoxyribonucleic acid
DRG	Dorsal root ganglia
E	Embryonic
e.g.	Exempli gratia(lt.) - for example
EDTA	Ethylenediamine tetraacetic acid
EGFP	Enhanced Green Fluorescent Protein
FBS	Fetal bovine serum
FCS	Fetal calf serum
GFP	Green fluorescent protein
GLR	Glutamate receptor
HBSS	Hank's buffered salt solution
HEK293	Human embryonic kidney cells 293
HMMs	Hidden Markov Models
HRP	Horseradish peroxidase
HSPCs	Hematopoietic stem/progenitor cells
Hz	Hertz
IB4	Isolectin B4

iBAT	interscapular brown adipose tissue
IFR	Instantaneous firing rate
IRES	Internal ribosomal entry site
KCl	Potassium chloride
KO	Knockout
Kv	Voltage-gated potassium
LB	Lysogeny broth
$MgCl_2$	Magnesium chloride
MHR	Melastatin homology regions
Min	Minutes
mRNA	Messenger RNA
ms	Millisecond
n	Sample size
NaCl	Sodium chloride
NaOH	Sodium hydroxide
NBAT	Neck brown adipose tissue
NCBI	National Center for Biotechnology Information
NK	Natural killer
NM-R	Naked mole-rat (*Heterocephalus glaber*)
NO	Nitric oxide
NS	Non-significant
P	Postnatal
PBS	Phosphate-buffered saline
PBST	Triton X-100 in PBS
PCR	Polymerase chain reaction
PFA	Paraformaldehyde
PLL	Poly-L-lysine
POA	Preoptic area
RAMs	Rapid adapting mechanoreceptors
RFP	Red fluorescent protein
RT	Room temperature
RT-PCR	Reverse transcription polymerase chain reaction
SAMs	Slow adapting mechanoreceptors
SEM	Standard error of the mean
SIF	Synthetic interstitial fluid
Sk.mu	Skeletal muscle
Ta	Ambient temperature
Tb	Body temperature
TDE	2’2-thiodiethanol
TRP	Transient Receptor Potential
TRPA	Transient Receptor Potential Ankyrin
TRPA1	Transient receptor potential ankyrin 1
TRPC	Transient receptor Potential Canonical
TRPM	Transient Receptor Potential Melastatin
TRPM	Transient Receptor Potential Mucolipin
TRPM3	Transient receptor potential cation channel subfamily M member 3

TRPM8	Transient receptor potential cation channel subfamily M member 8
TRPN	Transient receptor Potential NOMPC
TRPP	Transient Receptor Potential Polycystin
TRPV	Transient Receptor Potential Vanilloid
TRPV1	Transient receptor potential cation channel subfamily V member 1
TRPV2	Transient receptor potential cation channel subfamily V member 2
TRPV3	Transient receptor potential cation channel subfamily V member 3
UCP1	Uncoupling protein 1
UV	ultraviolet
VSL	Voltage sensor-like
w/v	weight per volume
WAT	White adipose tissue
WT	Wild-type

1 Introduction

1.1 African mole-rat family

The African mole-rat family, *Bathyergidae*, encompasses a diverse group of subterranean rodents found primarily in sub-Saharan Africa (Buffenstein, Park, et al., 2021; Cox et al., 2020) (Figure 1).

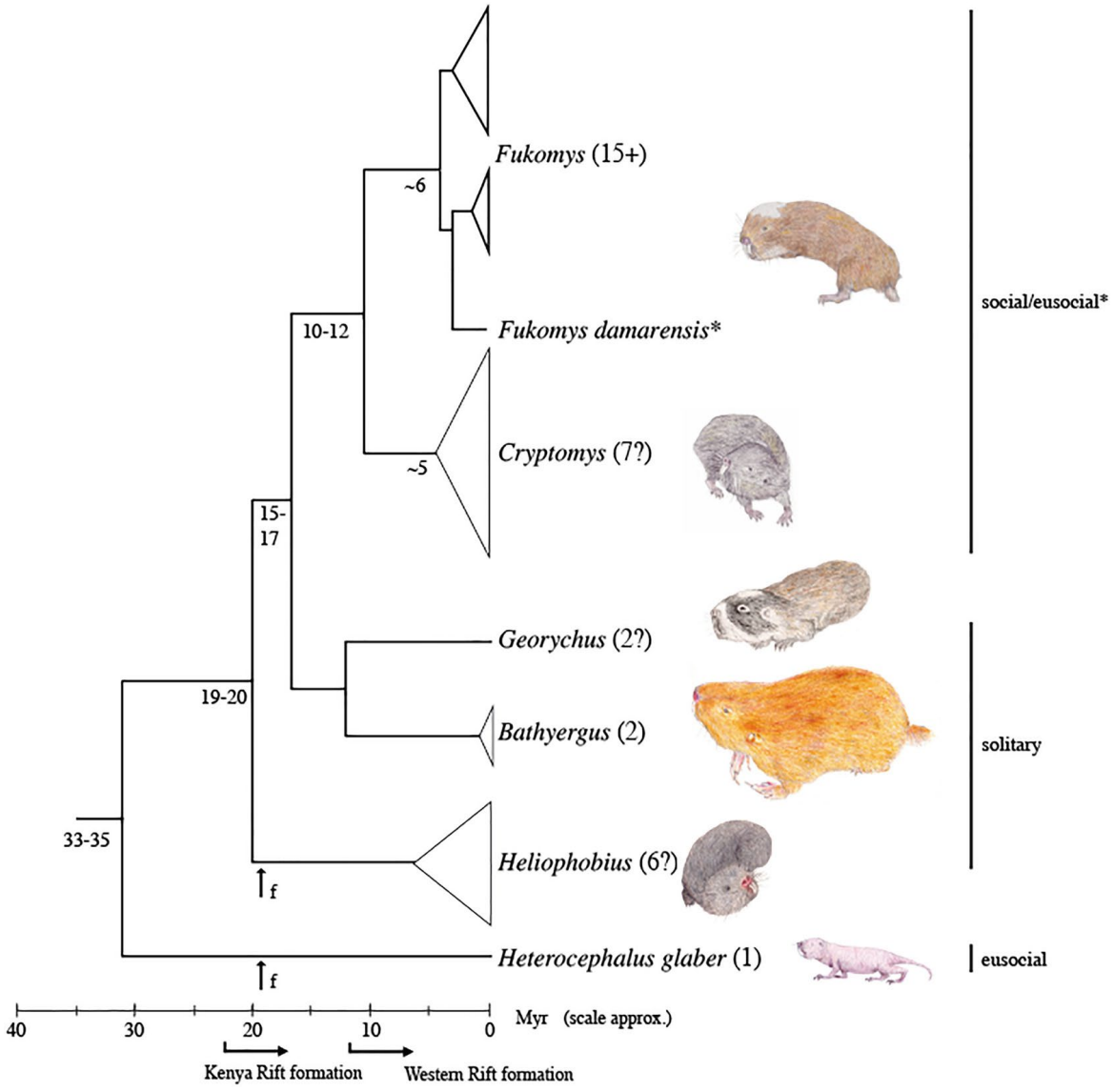

Figure 1. Genus-level phylogeny of the African mole-rats.
The divergence times in millions of years (myr) based on mitochondrial and nuclear gene analyses. Fossil calibration points are marked by "f." Numbers in parentheses indicate current species estimates per genus. Image adapted fromImage was adapted from Buffenstein et al., 2021; Cox et al., 2020.

This family consists of several genera, including the well-known Naked mole-rat (*Heterocephalus glaber,* NM-R), the Giant mole-rats (*Bathyergus*), the Damaraland mole-rat (*Fukomys damarensis*), the Common mole-rat (*Cryptomys hottentotus hottentotus*), the Emin's mole-rat (*Heliophobius emini*), and the Cape mole-rat (*Georychus capensis*) (Buffenstein, Park, et al., 2021; Morhart, 2015). A recent comparative study of all African mole-rat genera highlighted unique adaptations in their limb morphology, particularly the humeral and tibio-fibular morphologies, which are the key to their fossorial lifestyle (Montoya-Sanhueza, Šaffa, et al., 2022). NM-R is unique in its eusocial structure and exceptional physiological adaptations to an underground lifestyle, including reduced metabolic rates that allow them to thrive in hypoxic environments (Šumbera, 2019).

African mole-rats are well-adapted to life beneath the surface. Their strong, clawed front feet enable efficient digging, while the dense fur provides insulation against the cold and damp soil of their burrows. Their relatively small, underdeveloped eyes and the absence of external ears reflect physiological adaptations to the living environment where sight and sound are not absolutely necessary. Instead, these rodents heavily rely on a heightened sense of touch and vibrations to communicate and navigate their extensive burrow systems (Begall et al., 2015). These burrows are not mere shelters but complex structures that offer protection from predators, enable access to food sources, and serve as communal living spaces that facilitate mole-rats' social organization and breeding strategies (Begall et al., 2015).

Thermal biology plays a critical role in the survival of African mole-rats, with various adaptations that help them to manage thermal stress in the strictly subterranean habitat. Hairless NM-Rs, in particular, exhibits thermoregulatory behaviors such as huddling to conserve or share heat. In fact, their unique physiological traits enable them to tolerate a wide range of temperatures (Sahd, 2021). Temperature preferences, however, vary across species within the family. This reflects their ecological adaptations and habitat preferences that can range from the cold, moist soils to warm arid conditions (Oosthuizen & Bennett, 2022).

In the last decade, studies have successfully identified the functional anatomy of African mole-rats, revealing significant disparities in the postcranial skeleton among species (Gomes Rodrigues et al., 2016). These differences are thought to reflect adaptations to their specific digging styles and the soil types encountered in their natural habitats. Morphological evolution of the skull and the postcranial skeleton in these rodents reflects their life in burrows,

highlighting the profound influence of subterranean living on their physical appearance (Gomes Rodrigues et al., 2016; Montoya-Sanhueza, Bennett, et al., 2022).

The specific features of African mole-rats including their physical features, behavioral traits, and ecological roles, are summarized in the table below (Montoya-Sanhueza, et al., 2022; Šumbera, 2019) (Table 1). Data is collected from recent studies on *Bathyergidae* family members, emphasizing the diversity and evolutionary strategies of these remarkable animals in facing subterranean challenges.

Table 1. Summary of African Mole-Rats (*Bathyergidae* Family) characteristics and adaptations.
Source: Compiled from Montoya-Sanhueza et al. 2022, Šumbera 2019, and additional literature on *Bathyergidae* family adaptations from peer-reviewed journals accessible via PubMed and similar databases.

Feature	Description
Size	Small, ranging from 4 to 15 cm in length (without tail), indicating significant size variation within the family.
Body shape	Robust with strong, clawed front feet for efficient burrowing.
Fur	Dense fur provides insulation and protection from the subterranean environment, expect for NM-R.
Eyes	Small and underdeveloped, reflecting adaptation to a lightless habitat.
Ears	Absent external ears, adapted to minimize dirt ingress during digging.
Senses	Highly developed senses of touch and smell are crucial for navigation and communication.
Social behavior	Some species exhibit complex social structures, including eusocial colonies of up to 300 members, while others are solitary.
Breeding	In eusocial species, cooperative breeding occurs, where all colony members contribute to raising the offspring, whereas solitary species do not exhibit cooperative breeding.
Diet	Primarily herbivorous, feeding on roots, tubers, and other underground plant materials.
Adaptations	Specially adapted to a subterranean lifestyle, including physiological and morphological traits.
Burrow systems	Extensive networks provide protection from predators, food and water sources, and nesting areas.
Ecosystem	Contribute to soil aeration, improve drainage, and help control pest populations and diseases.
Lifespan	Typically live 5 to 20 years, with some species, like the NM-R, reaching up to 30 years in captivity.

1.2 *Heterocephalus glaber* (Naked mole-rat)

Among the African mole-rat family, NM-R, being a small, hairless rodent with powdery gray skin, is of particular interest, not only owing to its eusocial structure but also its remarkable physiological traits, which are part of a broader evolutionary context shared with its relatives (Browe et al., 2020). Their lifespan is exceptionally long compared to other rodents, with some individuals living for more than 30 years, and 37 years being the maximum recorded in our lab so far. They also display higher resistance to cancer and do not experience menopause (Wong et al., 2022). In comparison, while the Damaraland mole-rat also exhibits eusociality, its average lifespan is shorter, ranging between 10-15 years, though some individuals have reached at least 15 years (Jacobs & Oosthuizen, 2023).

1.2.1 Habitat and ecological niche of the Naked mole-rat

NM-R is a subterranean rodent that inhabit complex, underground burrow systems and live among highly socialized, eusocial colonies which can accommodate up to 300 individuals. The colonies are clustered into a strict hierarchical structure which consists of a single breeding female, the queen, and other members that serve as workers, soldiers, and occasional breeders under specific conditions. Such system of social complexity provides an unparalleled model for studying social behaviors among social vertebrates (Krebs & Clutton-Brock, 1991; Pamenter, 2022).

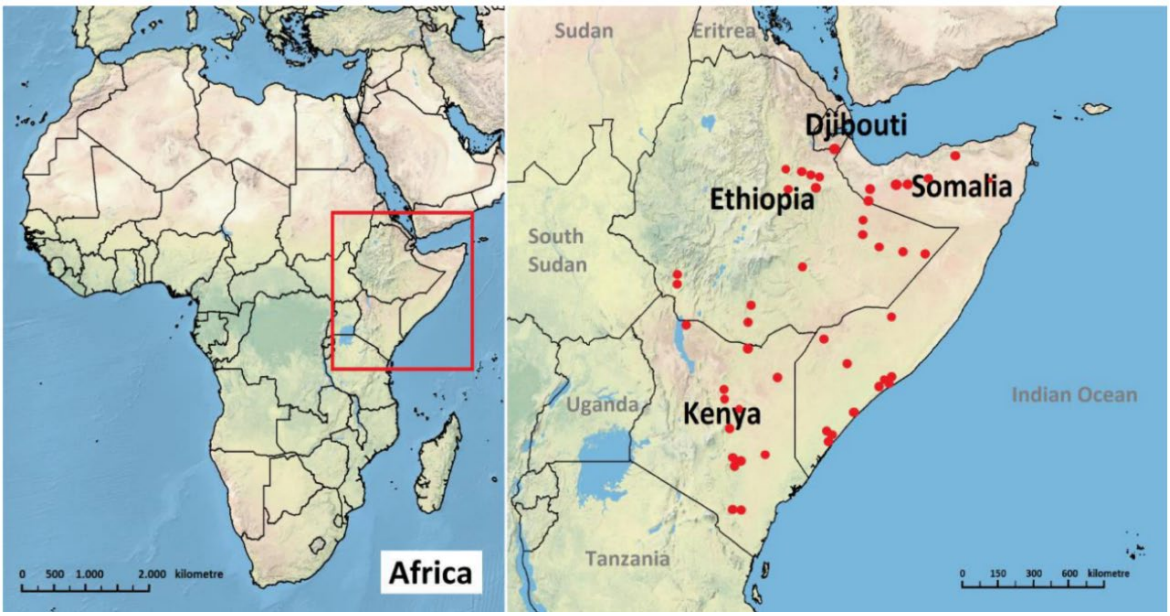

Figure 2. Distribution of *Heterocephalus glaber* in the horn of Africa, the presence of NM-R is represented by red dots.
Image was adapted from Morhart, 2015.

Being native to the arid regions of East Africa (Figure 2), including parts of Ethiopia, Kenya, and Somalia, NM-Rs construct elaborate underground burrows that allow extension of their habitat for several miles beneath the surface (Morhart, 2015). These tunnels, which are about 183-244 cm in depth, provide a sanctuary from predators and extreme environmental conditions. NM-Rs are primarily herbivores. Their diet consists of mainly roots and tubers, and is occasionally supplemented by insects and fungi. They get water from the food. Specific features that enable their adaptations to the subterranean lifestyle include powerful jaws and sharp incisors which can be used for gnawing through roots and excavating tunnels, providing them specific digging abilities required for survival underground. Moreover, sensitive vibrissae aid their navigation through dark environments (Buffenstein, Park, et al., 2021).

1.2.2 Unique physiological and behavioral traits

Remarkably, NM-Rs have evolved to thrive in hypoxic conditions, owing to their altered lung structure, special hemoglobin properties, and a highly efficient metabolic strategy that minimizes energy expenditure while maximizing oxygen utilization during respiration (Browe et al., 2020; Pamenter, 2022). Furthermore, NM-Rs are intriguing subjects for biomedical research due to their resistance to cancer and their unique pain insensitivity. Studies on their sensory system, specifically their olfactory and pain receptors, have provided insights into potential mechanisms behind these phenomena (Beery et al., 2016). The NM-R serves as an exceptional model for studying aging, social behavior, and disease resistance, due to its unique immunological and hematopoietic characteristics. Among them, NM-Rs harbor macrophages with a typical M1 pro-inflammatory gene signature (Bégay et al., 2022; Gorshkova et al., 2023), a higher myeloid-to-lymphoid cell ratio, with lack of natural killer cells (Bégay et al., 2022; Hilton et al., 2019) and a unique CD8 αβT cell population (Lin et al., 2024). In addition, their hematopoietic stem/progenitor cells retain neotenic traits (Emmrich et al., 2022). Interestingly, the size of the spleen in NM-Rs correlates with social status, with higher-ranking individuals having larger spleens and greater antimicrobial defenses, suggesting that social interactions may influence immune function and longevity (Bégay et al., 2022).

In addition to their immune system adaptations, NM-Rs exhibit evolutionary changes in their pain perception mechanisms. Research by Eigenbrod et al., 2019 analyzed RNA transcripts across several subterranean rodent species, including NM-Rs, and discovered multiple alterations in ion channels associated with pain. These evolutionary modifications suggest that

natural selection has driven the suppression of pain responses in some of species, likely as an adaptation to their harsh subterranean environments.

Thermoregulation is a vital physiological process that allows organisms to maintain their core body temperature (Tb) within a narrow optimal range, despite varying environmental conditions. This is crucial for sustaining metabolic functions and overall homeostasis. Unlike most mammals, NM-Rs exhibit a unique form of thermoregulatory ability, called poikilothermic endothermy, which reflects that their Tb can vary with ambient temperature (Ta), resembling reptiles, in addition to internal metabolic heat generation like other mammals (Buffenstein, Amoroso, et al., 2021) (Figure 3). To better understand how NM-Rs manage their thermal environment, a closer look at their current thermoregulatory strategies will be discussed in Section 1.5.

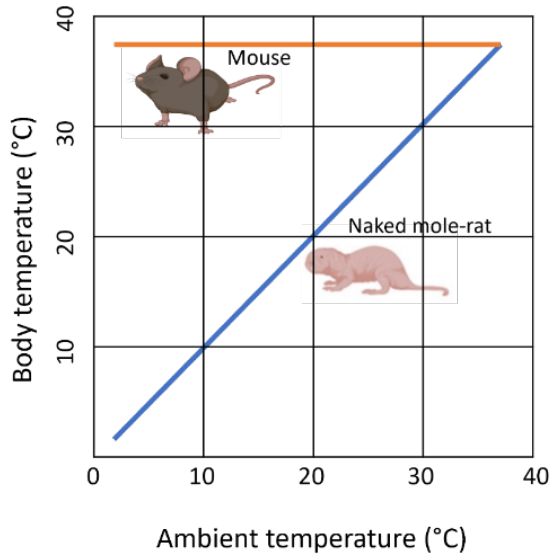

Figure 3. Body surface temperatures of NM-R were dependent on the ambient temperature. This figure illustrates the contrasting thermoregulation strategies between the naked mole-rat (blue line) and the mouse (orange line). While the mouse is able to maintain a stable body temperature across a broad range of ambient temperatures, NM-R exhibits a more variable thermoregulatory response. Image modified from Buffenstein, Amoroso, et al., 2021.

NM-Rs reside in large, complex burrow systems that buffer against the extreme surface temperatures of their native habitats in East Africa. These burrows provide a relatively stable microclimate, protecting them from extreme heat and cold. NM-Rs have a lower basal metabolic rate compared to other rodents, which reduces their overall heat production and energy requirements. This is advantageous in their hypoxic and hypercapnic underground environment. However, little is known about the molecular mechanisms of thermosensation and thermoregulation in NM-Rs.

1.3 Thermosensation and thermoregulation in mammals

Thermosensation is the process by which organisms detect and respond to changes in temperature. In mammals, this sensory capability is crucial for maintaining homeostasis and triggering appropriate behavioral and physiological responses to thermal stimuli (Tan & Knight,

2018). The brain integrates such multimodal sensory information, culminating in a cohesive understanding of the environment, which is vital for survival (Follmann et al., 2018).This process relies on a diverse range of thermal molecular receptors within sensory cells, which detect temperature changes and initiate signaling pathways that transduce these stimuli into neural signals (Figure 4).

Thermosensation is closely linked to thermoregulation, a vital physiological mechanism that allows mammals to maintain their core Tb within a sustainable range despite environmental fluctuations (Figure 4). Together, thermosensation and thermoregulation allow organisms to adapt to and manage changes in external temperatures.

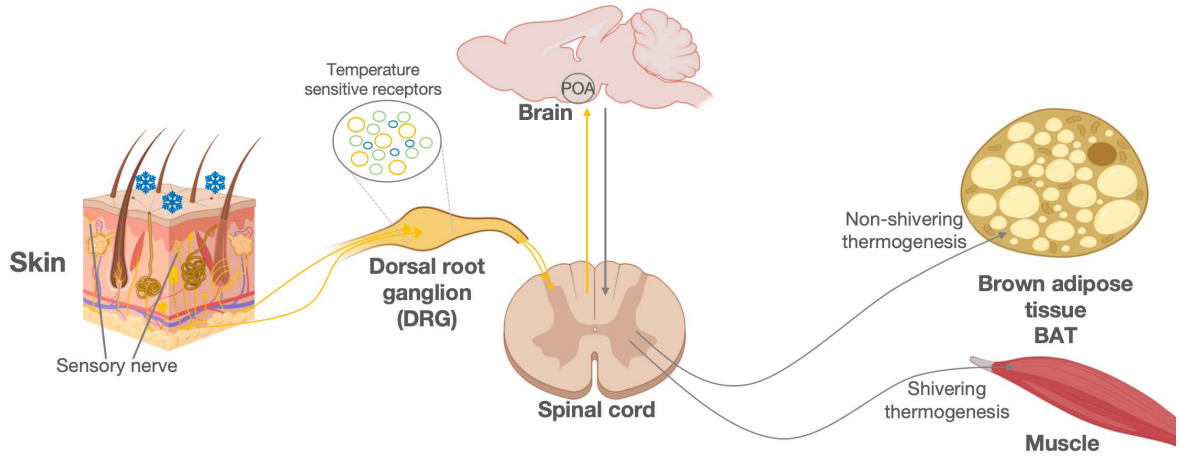

Figure 4. Cold thermoregulation pathways in mouse.
Temperature-sensitive receptors in the skin detect environmental temperature changes and send signals via sensory nerves to the dorsal root ganglion (DRG). These signals are then transmitted to the spinal cord and the preoptic area (POA) in the brain for processing. The brain coordinates the thermogenic responses of the body, including shivering thermogenesis in muscles and non-shivering thermogenesis in brown adipose tissue (BAT), to regulate Tb. The figure illustrates the thermoregulatory process in mammals, highlighting the role of the skin, sensory nerves, DRG, spinal cord, and brain. Drawn with biorender.

In the initial phase of thermoregulation, thermoreceptors (temperature sensitive receptors) in the skin detect changes in environmental temperature and transmit this information via sensory nerves to the dorsal root ganglion (DRG). From the DRG, signals travel to the spinal cord and are relayed to the preoptic area (POA) of the brain for processing.

Specialized thermosensitve ion channels, such as ThermoTRP channels, can sense a variety of temperatures by converting thermal energy into electrical impulses (Patapoutian et al., 2003). Mammals employ diverse strategies for thermoregulation to either produce or dissipate heat

(Figure 4). The first is metabolic heat production i) shivering thermogenesis which involves rapid muscle contractions to generate heat, and ii) non-shivering thermogenesis which primarily occurs in brown adipose tissue (BAT), where heat is produced through metabolic processes (Figure 4) (Betz & Enerbäck, 2018; Oelkrug et al., 2015). The second is evaporative cooling through mechanisms such as panting to help in heat dissipation by promoting the evaporation of water from the skin and respiratory surfaces (Betz & Enerbäck, 2018; Romanovsky, 2014). The third is insulative adaptations and behavioral strategies in which features like fur provide insulation, while behaviors such as burrowing or seeking shade help to maintain an optimal Tb (Romanovsky, 2014).

1.3.1 Roles of thermosensation in mammals

Temperature is a significant factor affecting physiological functions, behaviors, and seasonal activities in animals (Geiser, 2004; Hoffstaetter et al., 2018). It also influences metabolic reaction rates, protein folding speeds, enzyme activity, and the stability of cellular membranes. Animals use temperature cues to prey, synchronize mating activities, and respond to environmental changes. Thus, thermosensation is one of the fundamental sensory functions essential for animal survival.

Animals perceive temperature in two main ways: environmental temperature perception and Tb perception. Environmental temperature perception helps animals in distinguishing between harmless and harmful temperatures in their surroundings, guiding them to environments that are suitable for their survival and reproduction while avoiding potentially harmful temperatures (Colditz & Hine, 2016; Laursen et al., 2016; Wetsel, 2011). Perception of their own Tb helps in maintaining temperature stability, a critical aspect of all living organisms. Endothermic animals employ various physiological and behavioral responses to protect their Tb and ensure relative constancy, whereas ectothermic animals seek for environments that enable them to attain an appropriate Tb.

Regardless of whether being endothermic or ectothermic, animals have the ability to sense changes in the external environment (Laursen et al., 2016; Myers et al., 2009) to drive numerous biological processes within organisms that are highly sensitive to temperature. High temperatures potentially possess greater risks to organisms than low temperatures, as high temperatures may lead to irreversible damage to cellular membranes and proteins. Among vertebrates, somatosensory neurons are responsible to detect environmental temperatures by

sensing the changes in skin temperature and then depolarize neurons through temperature sensitive ion channels, thus generating action potentials (Bagriantsev & Gracheva, 2015).

In addition to the perception of environmental temperatures, animals also need to constantly monitor their own Tb. Homeostasis/maintenance of Tb is a fundamental physiological process, that all organisms must comply. Temperature homeostasis is a neural regulatory process that integrates external environmental information with animal responses to maintain internal stability. This process involves the sensing of environmental and internal temperature states, followed by the transmission of information to the brain, and eventually the initiation of appropriate responses through outgoing signals from the brain (Seebacher, 2009). The temperature regulation system includes both core Tb, which refers to the stable temperature of vital organs such as the heart and brain, and peripheral temperatures, which pertain to the temperature of the skin and extremities. These components are crucial for driving temperature regulation behaviors, such as shivering, and triggering autonomous responses, like vasodilation or vasoconstriction, to maintain overall thermal balance (Jessen, 1981; Roberts, 1988).

1.3.2 Skin nerve fibers and their role in thermosensation

Thermosensation relies on specialized nerve fibers located in the skin, which respond to various temperature stimuli (Zimmermann et al., 2009). These nerve fibers can be broadly categorized based on their conduction velocities and the types of stimuli they respond to. The primary types involved in thermosensation are C-fibers (< 1.5 m/s), Aδ fibers (~1.5 to 10 m/s), and Aβ fibers (> 10 m/s) (Koltzenburg et al., 1997), each playing distinct roles in temperature detection (Figure 5).

C-fibers are unmyelinated and respond to a variety of sensory modalities. Among these, C-polymodal (CMH) fibers are capable of detecting noxious heat (~40°C), cold, and mechanical stimuli, playing a critical role in the perception of pain (Julius & Basbaum, 2001). C-mechano-cold (CMC) fibers are specifically tuned to sense cold temperatures, with low peak firing frequencies and a bimodal distribution of temperature thresholds, typically around 27–29°C and 17–22°C, as well as mechanical forces, and are essential for the sensation of cold (Zimmermann et al., 2009). Additionally, C-mechano-cold-heat (CMCH) fibers can detect both cold and high heat (>45°C), alongside mechanical stimuli, highlighting their versatility in environmental responsiveness (Julius & Basbaum, 2001). The C-cold (CC) fibers are particularly sensitive to

cooling, with peak activity observed around 28°C, making them crucial for fine-tuned cold detection.

Aδ fibers are thinly myelinated and conduct signals more rapidly than C-fibers. The Aδ-mechano-heat (AMH) fibers primarily respond to mechanical and thermal stimuli around 40°C, enabling the rapid perception of sharp, localized heat pain (Julius & Basbaum, 2001). Aδ-mechano-cold (AMC) fibers are crucial for detecting mechanical and cold stimuli, particularly at temperatures below 28°C, and play a key role in eliciting fast reflexive responses to cold (Simone & Kajander, 1997). However, most of Aδ fibers are not thermosensitive, and C-fibers are predominantly responsible for the prolonged sensation of warmth and burning pain.

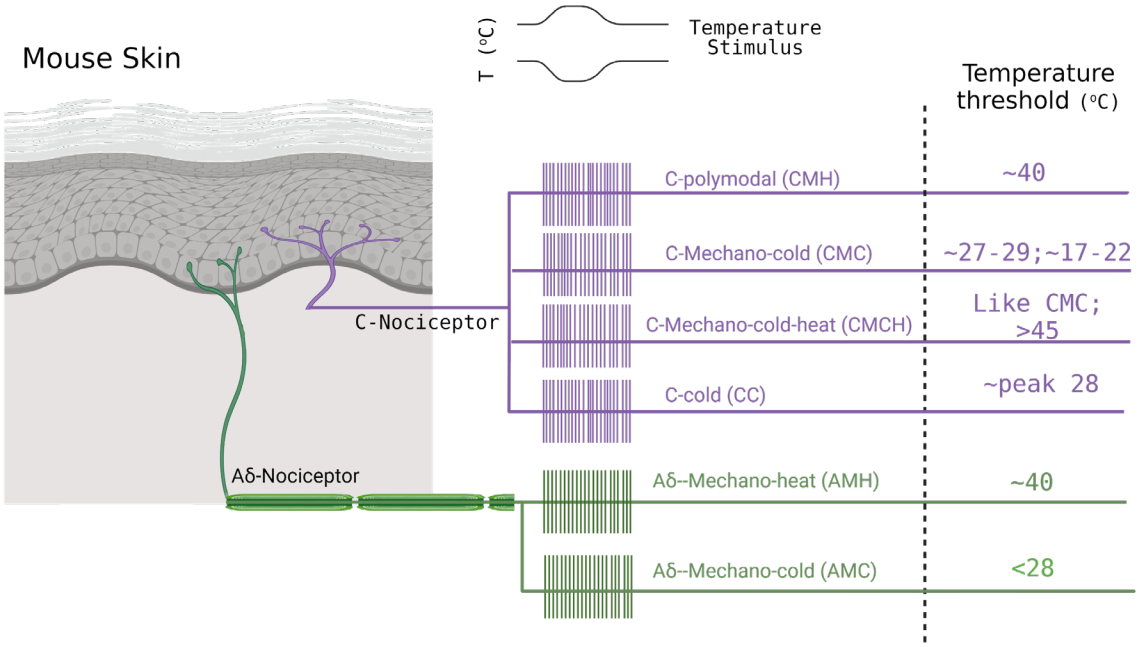

Figure 5. Types of skin nerve fibers involved in thermosensation in mouse.
The different types of skin nerve fibers involved in thermosensation, including their anatomical distribution and the specific temperature stimuli they detect. The fibers are categorized into three main groups: C-fibers (unmyelinated, shown in purple), Aδ fibers (thinly myelinated, shown in green). Each fiber type is associated with specific thermosensory functions. Image was generated from Zimmermann et al., 2009. Drawn with biorender.

Aβ fibers are heavily myelinated and primarily associated with mechanoreception, including sensations of touch and pressure (Lewin & Moshourab, 2004). They do not play a direct role in cold detection but are essential for the rapid transmission of touch-related stimuli (Milenkovic et al., 2008).

1.3.3 The mechanisms of thermosensory perception

The process of temperature perception is believed to begin with sensation by specific receptor proteins which are localised within the free nerve endings in the skin, tongue, and gut (Nilius & Owsianik, 2011). In most cases, this process seems to occur through direct activation of the temperature-gated ion channels on the surface membrane of sensory neurons, rather than through any indirect means. A key aspect involves the conversion of temperature information into electrical signals, a process mediated by the temperature-sensitive receptors specific to certain temperature ranges. Several researches have identified receptors within the skin that respond to environmental temperature changes (Hoffstaetter et al., 2018; Kashio & Tominaga, 2022; Lumpkin & Caterina, 2007; Wetsel, 2011). All temperature-sensitive channels discovered so far are part of the extensive TRP (transient receptor potential) family.

TRP channels are non-selective cation channel proteins localised on cellular or intracellular organelle membranes which are crucial for sensing various physiological stimuli such as temperature, light, mechanical forces, etc… As such, they are vital for the survival and behavioral responses of organisms (Nilius & Voets, 2008). The discovery of the first TRP channel coding gene in *Drosophila melanogaster* paved the way for identification of similar genes across a broad spectrum of organisms, from vertebrates to invertebrates (Montell & Rubin, 1989). All TRP channels share highly conserved sequence features and functional domains in their protein structures. Based on the amino acid sequence homology and structural domain characteristics, TRP channels can be categorized into seven subfamilies: TRPC (Canonical), TRPV (Vanilloid), TRPA (Ankyrin), TRPN (NOMPC), TRPM (Melastatin), TRPML (Mucolipin), and TRPP (Polycystin) (Wang, 2017). Among these, a set of TRP channels, collectively termed as ‘Thermo TRP’, is involved in temperature sensing within organisms. These channels are expressed in the sensory nerve endings located in the skin and other peripheral tissues, as well as in neurons of the DRG. Each Thermo TRP channel is directly activated by a specific temperature range, allowing for precise temperature detection (Patapoutian et al., 2003). Thermo TRP channels contain specific residues, domains, or domain interactions that enable them to be activated by particular temperature ranges.

Research on temperature-sensitive channels mainly focuses on rodents. The types and functions of temperature-sensitive channels in mammals are briefly outlined in the Figure 6. Mammals have evolved ion channels which are capable of sensing a wide temperature range from 0-60°C. These temperature-sensitive channels are part of the TRP family, which is divided into multiple

subtypes. Each subtype of TRP channel is tuned to a specific temperature range, allowing mammals to detect and respond to both cold and hot stimuli (Kashio & Tominaga, 2022).

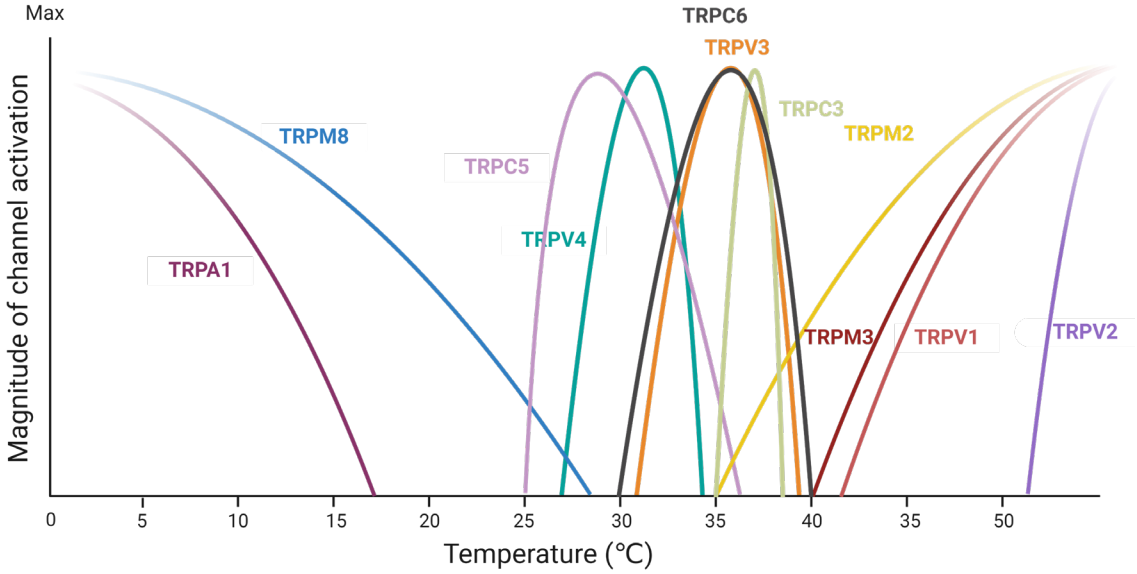

Figure 6: Temperature activation ranges of temperature-sensitive TRP channels.
Each curve represents the magnitude of channel activation in response to temperature changes. The Y-axis in this figure represents the relative magnitude of channel activation, indicating how strongly each temperature-sensitive TRP channel is activated across different temperature ranges. TRPA1: activated by temperatures below 17°C. TRPM8: activated by temperatures between 8°C and 28°C. TRPC5: activated by temperatures between 25°C and 37°C. TRPV4: activated by temperatures between 27°C and 34°C. TRPM3: activated by temperatures above 40°C. TRPV3: activated by temperatures between 31°C and 39°C. TRPC3: activated by temperatures around 35°C to 39°C. TRPM2: activated by temperatures above 35°C. TRPV1: activated by temperatures above 42°C. TRPV2: activated by temperatures above 52°C. TRPC6: activated by temperatures around 30°C to 40°C. Each TRP channel is color-coded for clarity. Inspired from Patapoutian et al., 2003, drawn with biorender.

1.3.4 Cold-activated temperature-sensitive channel

The short transient receptor potential channel 5 (TRPC5) is identified as the cold receptor that functions within the temperature range of 25-37°C. It is expressed in various organs and tissues, including the brain, vascular smooth muscle, adrenal medulla, and in certain cell types such as activated T cells and monocytes (Bernal et al., 2021; Chen et al., 2020). Activation of TRPC5 in response to innocuous low temperatures plays important roles in various regulatory or adaptive processes, including modulation of nerve activity, local metabolism, vascular changes, and transcriptional activation (Chen et al., 2020; Zimmermann et al., 2011). Cold-induced activation of TRPC5 is augmented by Gq-linked receptor activation, indicating a complex

interaction between cold sensing and other cellular signaling pathways (Zimmermann et al., 2011).

The transient receptor potential melastatin 8 (TRPM8), cloned by McKemy et al. in 2002, is expressed in the DRG and trigeminal ganglia neurons. It is responsible for temperature sensations, serving as the primary molecular entity for transducing innocuous low temperatures (Bautista et al., 2007, 2007; McKemy et al., 2002; Paricio-Montesinos et al., 2020; Reimúndez et al., 2023). Apart from being cold-activated, the TRPM8 channel is also responsive to chemical cooling compounds such as menthol, hence it is commonly termed as cold- and menthol-sensitive receptor 1 (CMR1). In mammals, TRPM8 serves as a crucial receptor for sensing innocuous low temperatures, with an activation threshold below 26°C (McKemy, 2018). However, TRPM8 functions beyond mere temperature sensation. Knockout studies on mice lacking the *Trpm8* gene have shown an impaired ability to discern between temperatures of 30°C and significantly lower temperatures, such as 15°C, underscoring the integral role of TRPM8 in temperature discrimination (Dhaka et al., 2007; Milenkovic et al., 2014). Moreover, the application of TRPM8 channel antagonists in mice and rats led to a notable decrease in core Tb, suggesting a broader physiological role of TRPM8 channels in thermoregulation that is not limited to the mere perception of environmental temperatures. This finding has been reinforced by additional studies which indicates the involvement of TRPM8 in heat loss and food intake, ultimately affecting Tb and energy balance (Iftinca & Altier, 2020; Reimúndez et al., 2018). Recent research has also highlighted the role of TRPM8 in oral thermosensation through its participation in the oral cooling sensation, suggesting that it is critical for the thermoregulatory responses to cold (Li et al., 2024). Furthermore, regulation of central and peripheral circadian rhythms by TRPM8, along with their involvement in the oscillations of Tb, highlight its significant influence on the thermal homeostasis of body (Reimúndez et al., 2023).

In 2003, Story et al. discovered a multimodal ion channel coded by the temperature-sensitive channel the transient receptor potential ankyrin 1 (TRPA1) which is sensitive to both temperature and chemical stimuli (Story et al., 2003). Initially known as ANKTM1 (ankyrin-like with transmembrane domains protein 1), TRPA1 is expressed in nociceptive sensory neurons. It is activated by cold stimuli at temperatures lower than those activating TRPM8 channels, typically below 17°C. As 17°C is close to the threshold for human nociceptive low temperatures, some consider mammalian TRPA1 channels to be the detectors of nociceptive cold, and hence a harmful cold receptor (Story et al., 2003). Studies on TRPA1 knockout mice

have suggested its minor role in peripheral cold sensation but a primary role in visceral nerve cold sensation (Fajardo et al., 2008). Further investigation on the involvement of TRPA1 in cold sensation and its response to an array of chemical irritants such as allicin, cinnamaldehyde, and allyl isothiocyanates, confirmed its significant role in the somatosensory system as a primary sensor for noxious chemical stimuli (Bautista et al., 2006). Moreover, research has also demonstrated that TRPA1 is involved in acute heat sensation, indicating that this channel contributes not only to cold detection but also plays a role in nociceptive responses to noxious heat stimuli (Vandewauw et al., 2018).

In addition to TRP channels, recent studies have identified the role of glutamate receptors in cold-sensing mechanisms. The cold-sensing receptor encoded by the glutamate receptor gene, particularly the GLR-3 receptor in *C. elegans*, and its mammalian homolog, the kainate receptor GluK2, which represent a novel class of cold sensors have been recently discovered. These channels, traditionally known for their roles in neurotransmission, have been shown to also mediate cold sensation through mechanisms distinct from their conventional synaptic signaling roles. Characterization of mice lacking the GluK2 receptor and the identification of GLR-3-mediated cold-avoidance behavior in *C. elegans* have significantly expanded our understanding on the molecular basis of cold sensation beyond the previously identified TRP channels (Cai et al., 2024; Gong et al., 2019). However, TRPM8 remains the primary receptor for cold sensing.

The interactions between cold and warm-activated receptors contribute to the overall thermosensory system (Vriens et al., 2014). While warm-activated receptors such as TRPV1, TRPV2, TRPV3, and TRPV4, also play critical roles in thermosensation by detecting a range of warm to hot temperatures (Hellenthal et al., 2021; Hinman et al., 2006; Paulsen et al., 2015; Pertusa et al., 2014), the detailed mechanisms and functions of warm-activated receptors are beyond the scope of this study which will focus specifically on only the cold-activated TRPM8 receptor.

1.3.5 Diversity of thermoreceptors in vertebrates

Studies have found variation in the Thermo TRP homologs during vertebrate evolution. While most ThermoTRP members found in mammals can be traced back to a common ancestor of fish and tetrapods (Baldwin & Ko, 2020), significant differences among the Thermo TRP of extant vertebrates exist. For instance, genome sequencing has revealed a trend of gene loss for certain Thermo TRP homologs in fish species. This loss is likely an adaptation to their wide-ranging and often extreme ecological niches, such as the Antarctic and Arctic (York, 2023;

York & Zakon, 2022). Remarkably, while fish like the zebrafish (*Danio rerio*) can tolerate temperatures from 14–35°C, and carp (*Cyprinus carpio*) can survive between 3–35°C, genome sequencing of 12 fish species did not reveal the presence of TRPM8, suggesting that this cold-sensing channel may have been lost in certain fish lineages (York & Zakon, 2022). The loss of TRPM8 could be a key factor that enables fish to thrive across such a wide range of temperatures. In contrast, amphibians such as the African clawed frogs (*Xenopus laevis*) and western clawed frogs (*Xenopus tropicalis*) retain TRPM8 channels with higher activation thresholds (Myers et al., 2009). Furthermore, TRPM8 channels in amphibians are activated at significantly lower temperatures, reflecting their lower basal Tb compared to endothermic animals (Lu et al., 2022). The activation threshold of TRPM8 also correlates with habitat temperature. In a study of eight vertebrate species, Yang et al., 2020 found a positive correlation between TRPM8 cold activation thresholds and species' environmental temperatures, with emperor penguins having the lowest and African elephants the highest cold activation currents. In birds, chickens have a TRPM8 half-maximal activation temperature 5°C higher than in mammals, further indicating adaptations to higher core Tb (Hoffstaetter et al., 2018). This demonstrates how TRPM8 channels have evolved differently across vertebrate species, reflecting their environmental adaptations.

In addition to TRPM8, other Thermo TRP channels show striking diversity across vertebrate species, further contributing to their ability to detect and respond to different thermal environments. The TRPV1 channel, primarily associated with heat sensation, demonstrates significant species-specific variability in its activation temperature. In zebrafish, TRPV1 is activated at temperatures exceeding 32°C, whereas in African clawed frogs, the threshold is 40°C, in mice, it is 42°C, and in chickens, it reaches 46° (Gau et al., 2013; Gracheva et al., 2011). This pattern reflects an increase in the activation temperature of TRPV1 as the core Tb of the organism rises. For fish, the relatively low activation threshold of TRPV1 (32°C) correlates with their limited tolerance to warm temperatures, where temperatures above this threshold are often unsuitable for their survival (York, 2023).

Birds and mammals, both endothermic animals, maintain relatively constant core Tb. Interestingly, birds have higher core Tb (40–44°C) and basal metabolic rates than mammals (36–38°C), and this is reflected in their thermoreceptor function. For example, the TRPV1 channel in chickens is activated at 46–48°C, while in mammals, it is activated at around 42°C, demonstrating an adaptation to the higher core temperatures of birds (Cao et al., 2013; Jordt &

Julius, 2002). Additionally, TRPV3 channels, which typically sense warm temperatures in mammals, show reversed functionality in some species. In western clawed frogs, TRPV3 is activated by low temperatures (~16°C), enabling these amphibians to detect harmful cold rather than heat, a reversal from its typical role in mammals (Rosenblum et al., 2009).

The TRPA1 channel also exhibits considerable variation across vertebrate species. In zebrafish, however, TRPA1 is insensitive to temperature stimuli altogether (Prober et al., 2008; Viswanath et al., 2003). This divergence in TRPA1 function likely stems from the emergence of the TRPV1 gene, which plays a dominant role in heat sensation in vertebrates (Cao et al., 2013). The evolutionary transition from invertebrates to vertebrates marked the appearance of TRPV1, a homolog of TRPA1, which may have allowed TRPA1 to specialize in cold detection in mammals. In invertebrates such as fruit flies (*Drosophila melanogaster*), TRPA1 channels are activated at around 27°C, highlighting their primordial role in thermosensation (Okamura et al., 2005). This co-evolution of TRPV1 and TRPA1 in vertebrates suggests a conserved mechanism for temperature sensing and nociception across species, with notable adaptations that reflect the thermal demands of different habitats (Zhang et al., 2022).

1.4 The transient receptor potential melastatin 8 sturcture

As highlighted earlier, TRPM8 represents the primary receptor for cold sensation, is highly expressed in a subset of DRG neurons and is activated at temperatures of 26°C or lower (Bautista et al., 2007; McKemy, 2018; McKemy et al., 2002; Reimúndez et al., 2018; Zakharian et al., 2010). Initially cloned in 2000, TRPM8 was later characterized in 2007 as a receptor responsive to both cold and menthol in murine DRG and trigeminal neurons (Bautista et al., 2007). Subsequent studies confirmed that TRPM8 serves as the major transducer for mild cooling stimuli in physiological environments.

In mice, TRPM8 channels are present in certain Aδ fibers and C-fibers, which play a critical role in cold detection (Milenkovic et al., 2014; Simone & Kajander, 1997; Zimmermann et al., 2009). Mice lacking TRPM8 expression exhibit significantly reduced sensitivity to cold, particularly at temperatures down to 5°C, and show impaired performance in temperature preference tests. While these mice have a diminished response to mild cooling, their response to noxious cold stimuli is only partially reduced, indicating primary role of TRPM8 in mild cold sensation (González-Muñiz et al., 2019; Zakharian et al., 2010).

Recent findings from our lab suggest that TRPM8 may also play a role in detecting innocuous warm temperatures (Paricio-Montesinos et al., 2020). Our research indicates that detecting warmth might require lower spike activity in TRPM8-expressing cold-sensitive C-fibers. In *Trpm8*$^{-/-}$ mice, the absence of these spikes, due to the lack of functional TRPM8 channels, impairs their ability to sense warm temperatures (Paricio-Montesinos et al., 2020). Additionally, many cooling substances including menthol and icilin (Figure 7A), chemically activate TRPM8 channels and can induce painfulness in high doses (González-Muñiz et al., 2019; Zakharian et al., 2010).

TRPM8 is the most well-characterized cold receptor, and significant progress has been made in understanding its structure and activation mechanism in response to cold stimuli. The *Trpm8* gene in most rodents, as well as in humans, encodes a protein consisting of 1,104 amino acids. TRPM8 exists in a functional homotetrameric form, akin to the topological structure of other TRP channels, featuring six transmembrane segments with a pore-forming loop between S5 and S6. Both the amino- and carboxy-terminals of TRPM8 are located intracellularly. Functional TRPM8 channels are formed by the tetramerization of these subunits, a process that has been confirmed through techniques such as Atomic Force Microscopy (AFM) and cryo-electron microscopy (Dragoni et al., 2006; Yin et al., 2018, 2024).

Each part of the TRPM8 protein has its own specific functional role (Figure 7B). The N-terminal domain, which consists of 693 amino acids, includes four regions known as melastatin homology regions (MHR). These regions are thought to help in stabilizing the tetrameric structure of the channel (Pedretti et al., 2009). Research in mice has showed that the deletion of up to 39 amino acids from the N-terminus does not affect channel function, but deleting 86 amino acids will render the channel nonfunctional (Phelps & Gaudet, 2007). This indicates the importance of the N-terminal region in the proper folding and assembly of TRPM8. Further studies by Pertusa et al. 2014 identified specific mutations within the N-terminal region that enhance channel sensitivity to cold and menthol, highlighting the role of the N-terminal region in modulating the channel response to stimuli (Pertusa et al., 2014).

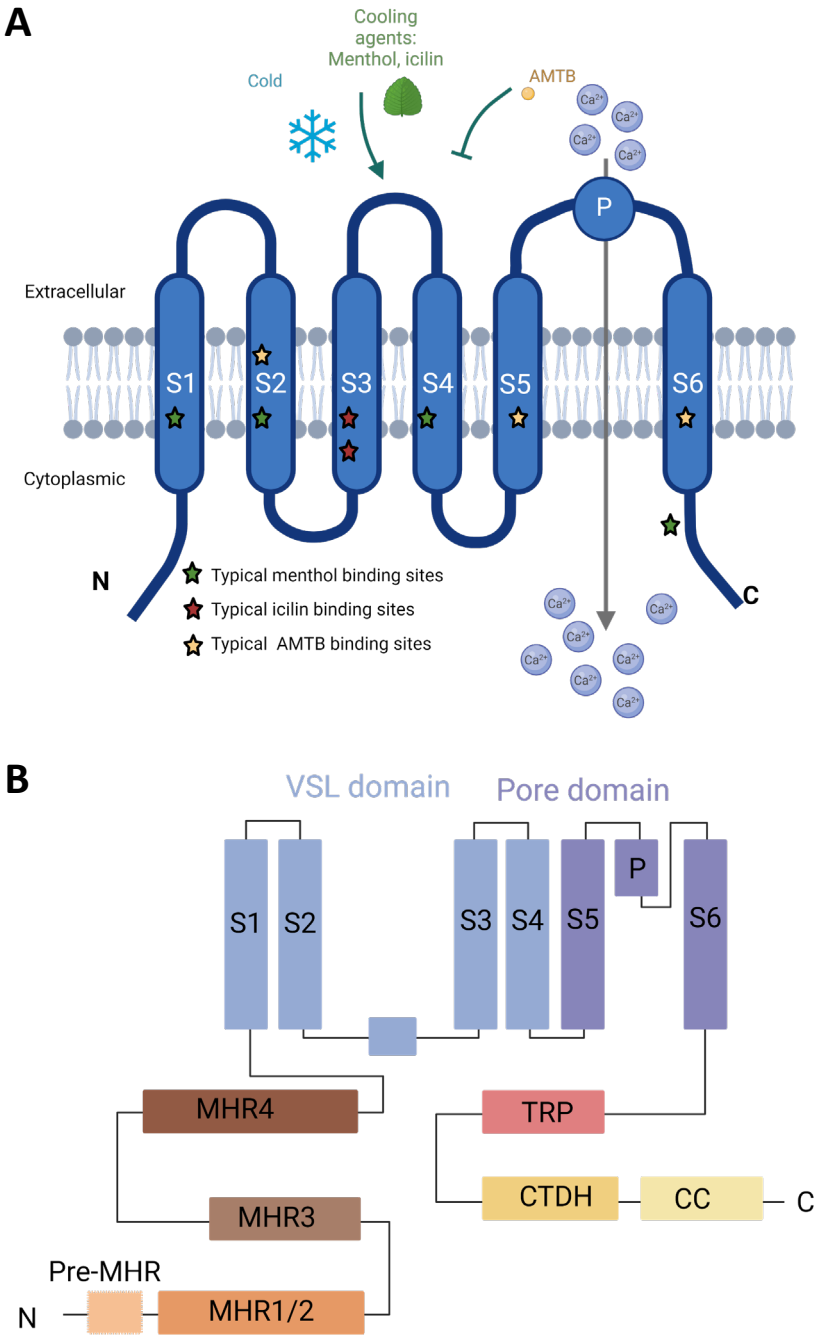

Figure 7. TRPM8 structure with ligand and cooling agents binding sites.
(A). The image depicts the TRPM8 channel with the six transmembrane domains (S1-S6) of the channel, the cytoplasmic N-terminal region and the C-terminal region. Specific binding sites for the cooling agents menthol and icilin, as well as the TRPM8-specific antagonist AMTB, are located within the transmembrane domains and are indicated by green, red, and yellow stars, respectively. A green leaf represents cooling agents: Menthol and Icilin. The small blue spheres denote calcium ions (Ca^{2+}), which are pivotal in the function of channel in TRPM8 channel cellular signaling. (B). Topology diagram delineating the protein domains with secondary structure elements. VSL domain: a voltage-sensor–like domain, CTDH: the C-terminal domain helix, MHR: melastatin homology region, TRP: Transient receptor potential, CC: coiled coil, P: the pore helix, S: transmembrane segment. Modified from Yin et al., 2009. Figures were drawn with biorender.

The C-terminal domain of TRPM8, which is relatively short at 120 residues, contains a crucial coiled-coil motif involved in the tetramerization process (Erler et al., 2006). However, even without this domain, TRPM8 can still form tetramers, despite being non-functional. The C-terminal domain also includes the TRP domain which is essential for the activation of TRPM8 and its interaction with phosphoinositides, such as PI (4, 5) P2 (Izquierdo et al., 2021; Rohács et al., 2005).

The first four transmembrane domains (S1-S4) of TRPM8 form the voltage sensor-like (VSL) domain, whereas the last two (S5 and S6) transmembrane contribute to the pore domain which harbor a highly conserved hydrophobic stretch and a crucial aspartate residue essential for ion selectivity (Latorre et al., 2007). Notably, the ankyrin repeat domain (ARD) which is widely present in majority of the TRP channels and considered related to channel temperature sensitivity, has not been identified in the amino end of TRPM8. Instead, the carboxyl-terminal domain (CTD) which contains the TRP structure domain (comprising 25 amino acids) has been found crucial for TRPM8 cold sensitivity. In fact, introduction of this region into TRPV1 induces cold sensitivity in TRPV1 (Díaz-Franulic et al., 2020; Xu et al., 2020).

The activation and desensitization of TRPM8 by intracellular signals, particularly Ca^{2+} and PIP2, demonstrate a complex regulation mechanism that is crucial for its role as a cold sensor and facilitator of cold-induced reactions (Latorre et al., 2007). Menthol, icilin, and WS-12 are all natural and synthetic cooling substances which have the ability to activate TRPM8 (Izquierdo et al., 2021; Yin et al., 2018). This activation triggers various physiological responses including cold-induced pain and reflexive actions to seek warmth. AMTB (*N-(3-aminopropyl)-2-[(3-methylphenyl)methoxy]-N-(2-thienylmethyl)benzamide*) is a potent and selective antagonist of TRPM8 that binds to the specific sites within TRPM8 channel and inhibits its activation triggered by cold and cooling agents (Yin et al., 2024). Recent studies using cryo-electron microscopy have successfully identified these binding sites, adding to our knowledge of how TRPM8 is modulated and how its activity can be targeted for therapeutic purposes (Palchevskyi et al., 2023).

1.5 Current state of knowledge on thermoregulation in Naked mole-rat

As previously mentioned, NM-R has a remarkable characteristic known as thermal lability which makes them a poikilothermic mammal due to their lost ability to regulate Tb (Buffenstein, Amoroso, et al., 2021). NM-Rs live in extensive burrow systems where they engage in social thermoregulation. By group huddling and shuttling between warmer and cooler parts of the burrow system, they can modulate their Tb in response to environmental changes (Buffenstein, Park, et al., 2021; Yahav & Buffenstein, 1991).

In addition to these behavioral adaptations, NM-Rs possess several physiological traits that aid in thermoregulation. For example, their lower basal metabolic rate compared to other rodents reduces their overall heat production and energy requirements, which is particularly beneficial in their hypoxic and hypercapnic subterranean environment. Furthermore, NM-Rs exhibit heterothermic capability, enabling them to tolerate a broader range of Tb and function efficiently under varying thermal conditions, thus minimizing the need for continuous thermogenesis (Buffenstein, Park, et al., 2021). A key feature of NM-R thermoregulation is their ability to adjust behavior according to environmental conditions. For instance, they are known to bask in shallow burrows to absorb heat from the sun during cooler periods, which helps them regulate Tb without expending significant metabolic energy. This behavioral flexibility is critical to their survival in extreme environments (Buffenstein, Park, et al., 2021).

Given these behavioral and physiological adaptations, it can be hypothesized that NM-Rs have developed specialized mechanisms to detect and respond to fluctuations in ambient temperature. Recent temperature preference behavior data from Dr. Jean-Sebastien Jouhanneau (James Poulet's Lab in MDC) suggests that NM-Rs prefer a higher temperature compared to mice (Figure 8). However, NM-Rs still require a system of peripheral thermoreceptors and central thermosensitive neurons to detect and respond to environmental temperature changes.

Since NM-Rs are rodents, their thermoregulatory system should, in theory, be similar to that of other mammals. However, being hairless, NM-Rs may be more vulnerable to damage or loss of peripheral thermoreceptors and central thermosensitive neurons, impacting their overall thermogenesis. What is known so far is that NM-R thermoregulatory profiles closely follow Ta in order to maintain their Tb, which is dependent on the Ta when exposed to temperatures outside their thermoneutral zone (31°C to 34°C).

Oiwa et al., 2020 suggested that NM-Rs are stenotherms since they can control Tb across a very small range of Ta. The fact that NM-Rs move to warmer or cooler areas of the burrow system or engage in huddling behaviors suggests that NM-Rs have similar ectothermic mechanisms. In addition, NM-Rs employ evaporative cooling and vasodilation to thermoregulate in normoxia at 25°C but that neither mechanism is involved in thermoregulatory changes during acute hypoxia (Vandewint et al., 2019).

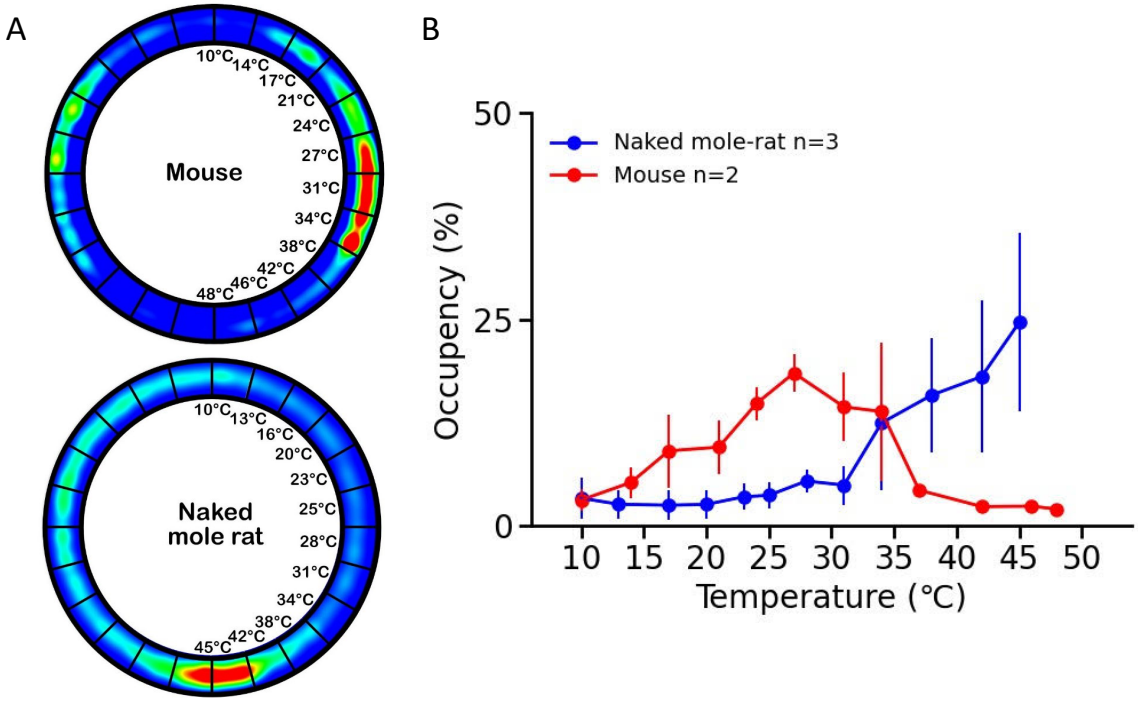

Figure 8. Temperature preference behavior in NM-R and mouse.
(A). Heat map showing temperature preference of mouse and NM-R in a temperature gradient ring (10–50°C). (B). Occupancy percentage of different temperatures for NM-R (n=3) and WT mouse (n=2), indicating NM-Rs prefer warmer temperatures compared to mice (Figures from Dr. Jean-Sebastien Jouhanneau, James Poulet's Lab in MDC).

NM-Rs reduce their Tb during low oxygen conditions, likely to conserve energy by diminishing non-shivering thermogenesis in BAT. This thermogenic activity is crucial for maintaining Tb in response to cold exposure. In NM-Rs, this thermogenic activity is particularly intriguing. A rapid decrease in UCP1 protein expression in BAT is observed during hypoxia, which correlated with the cessation of interscapular thermogenesis and a subsequent drop in Tb (Cheng et al., 2021). This finding demonstrates that the thermogenic response of NM-Rs is highly sensitive to oxygen levels, with the rapid downregulation of UCP1 suggesting an evolved mechanism to conserve oxygen by reducing energy expenditure during hypoxic conditions. Further complicating the thermogenic dynamics, Oiwa et al. 2020 demonstrated that

NM-R queens possess BAT with thermogenic activity. However, this BAT is insufficient to prevent a decline in Tb. Surprisingly, subordinate NM-Rs exhibit BAT but are unable to control their Tb as the queens. The differential ability of NM-R queens and subordinates to utilize BAT for thermoregulation may reflect an adaptation to their strict hierarchical social structure.

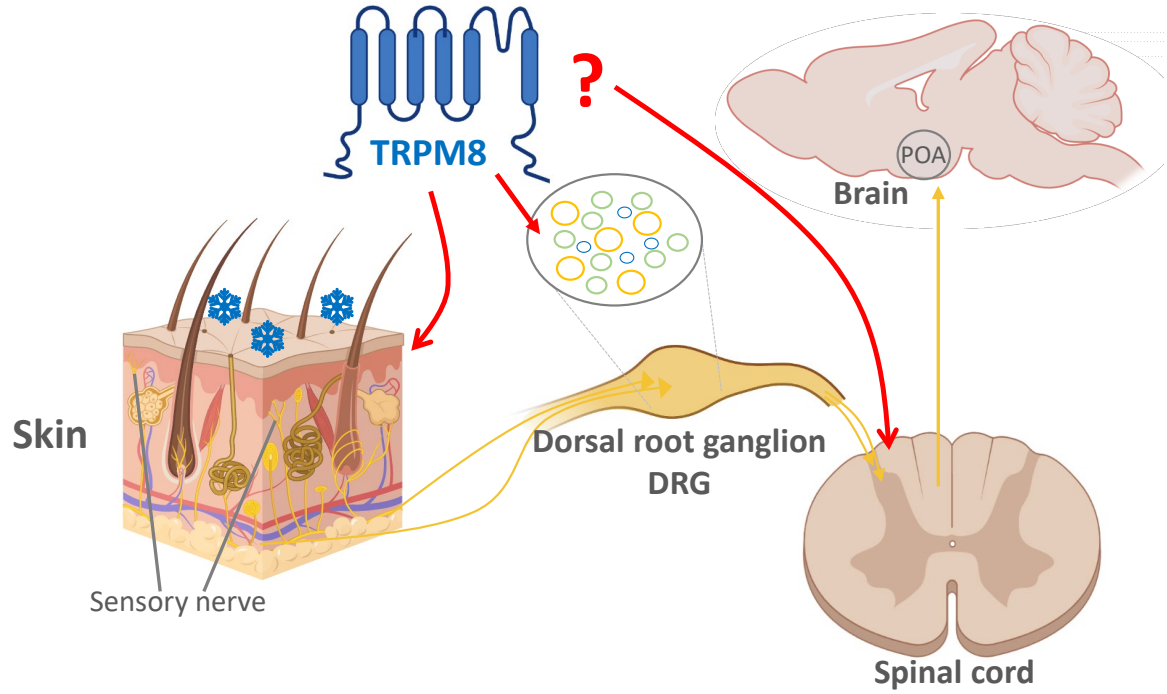

Figure 9. Investigating the role of TRPM8 in cold thermosensation in the NM-R.
This schematic explores whether the TRPM8 channel is involved in the cold thermosensation process in NM-Rs. Cold stimuli are detected by temperature-sensitive receptors in the skin, which transmit signals through sensory nerves to the DRG. From the DRG, signals travel to the spinal cord and are relayed to the POA of the brain for processing. The figure poses the question of whether TRPM8 contributes to this sensory pathway in NM-Rs, as its precise role remains uncertain. Drawn with BioRender.

It is known that the functional properties of TRPM8 are not static through evolution, and the cold sensitivity of TRPM8 seems to follow the core Tb of different species such as the lower cold sensitivity in frogs and higher sensitivity in birds (Myers et al., 2009). The TRPM8 orthologs of squirrels and hamsters are both out of trend, bolstering the hypothesis that the apparent cold tolerance among animals has evolved as a component of the sophisticated physiological system that promotes hibernation (Matos-Cruz et al., 2017). According to Poulson et al., 2020, *Trpm8* is expressed in NM-R DRGs, but at a reduced level compared to mice. Transcriptomic analysis carried out in our group has revealed that *Trpm8* gene expression pattern was similar in the DRGs of mice and NM-Rs but is greater in the spinal cord of NM-R compared to mouse.

The question remains as to why NM-R showed poor thermoregulation compared to other mammals, such as humans and mice. Therefore, we hypothesized that the protein of TRPM8 is less expressed or not expressed in tissues involved in thermosensation within NM-Rs (Figure 9). Our lab previously analyzed the RNAseq data acquired from the tissues of NM-R and C57BL/6 mice. The results suggested an increased *Trpm8* mRNA expression in the brain, spinal cord, and BAT of NM-Rs compared to mouse (Figure 10).

These contradictory results lead us to make the following hypotheses: (i) either TRPM8 expression levels in NM-R sensory tissues and non-sensory tissues might be lost or (ii) the sensitive temperature range of thermoreceptor TRPM8 changes in NM-Rs and affects their thermogenesis. These should help to clarify the role of TRPM8 in thermosensation and impaired thermoregulation in NM-Rs.

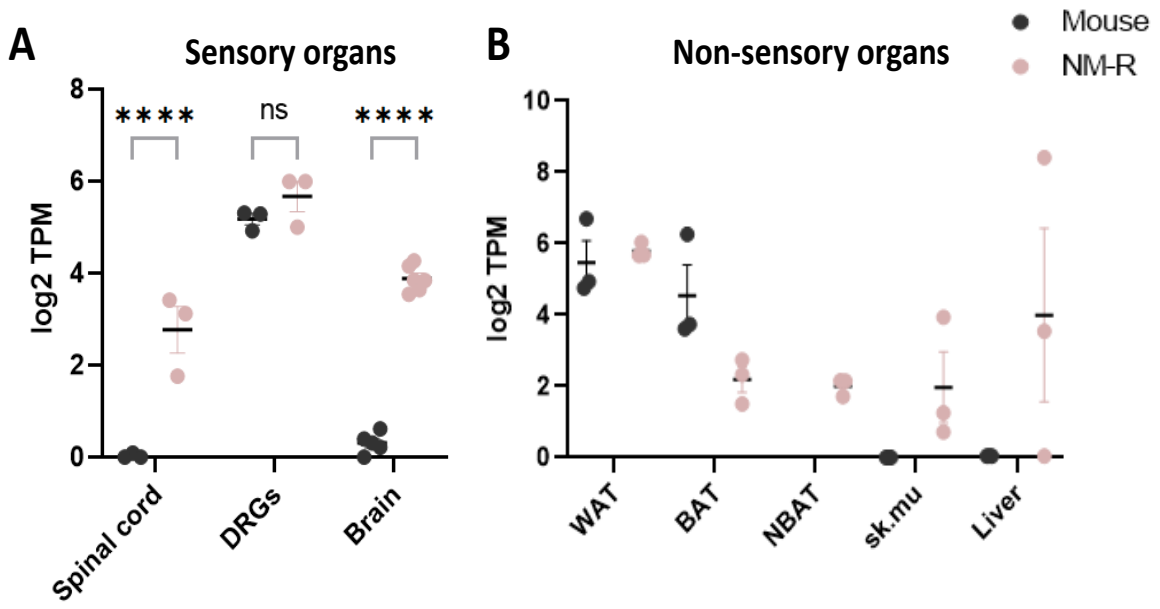

Figure 10. Transcriptomic analysis of sensory organs and non-sensory organs of NM-R. Transcriptomic analysis of various tissues of NM-R showing *Trpm8* mRNA levels in (A) spinal cord, dorsal root ganglia (DRG) and whole brain of the mouse and NM-R. (B) white adipose tissue (WAT), brown adipose tissue (BAT), neck brown adipose tissue (NBAT), skeletal muscle (sk.mu) and liver of mouse and NM-R. Data from Dr. O Eigendbrod, Dr. V. Bégay, unpublished.

2 Objectives of this study

The aim of this thesis is to unravel the paradox of cold sensation in NM-R. Additionally, NM-Rs lack thermoregulatory behaviors typical of poikilothermic mammals, hence prompting the hypothesis that the mechanisms underlying cold perception are unique in this species. This study will primarily focus on the TRPM8 ion channel which is recognized as the principal mediator of cold sensation in mammals. By probing the molecular and functional dynamics of TRPM8 in the NM-R, this can shed light on the unique cold sensation mechanisms and evolutionary adaptations of TRPM8.

The objectives are structured as follows:

1. To delineate the expression and localization pattern of TRPM8 within the sensory tissues of NM-Rs utilizing RNAScope and immunofluorescence techniques. This will include a comparative analysis with wild type to discern species-specific distribution patterns, particularly in the DRGs, spinal cord and skin.

2. To examine the specific structural features of NM-R TRPM8. This involves the use of sequence blast methods to compare the TRPM8 of NM-R with other mammalian TRPM8 variants and examine the known mutation sites associated with cold, menthol, and icilin sensitivity. Additionally, this study also aims to verify the presence of the extended N-terminal sequence in NM-R TRPM8.

3. To assess the functional capacity of NM-R TRPM8 in response to cold, menthol, and icilin stimuli through calcium imaging. Besides, this thesis also aims to investigate the impact of the extended N-terminal sequence on the function of TRPM8 in NM-R.

4. To investigate the native cold sensation in NM-Rs using calcium imaging of cultured NM-R DRGs and *ex vivo* skin nerve experiments. This involves the application of TRPM8-specific inhibitor and agonist to determine the specific role of TRPM8 in cold perception.

Objectives of this study

3 Materials and Methods

3.1 Materials

3.1.1 Chemicals and kits

Table 2. List of chemicals and reagents.

Name	Supplier	Catalog number
2'2-thiodiethanol (TDE)	Sigma Aldrich	88559
Agarose	Sigma Aldrich	A9414
Bovine serum albumin (BSA)	Sigma Aldrich	A2153-100G
CAL520® AM	Abcam	ab171868
CAL590® AM	AAT Bioquest	20510
Calcium chloride ($CaCl_2$)	Sigma Aldrich	C4901
Carbencillin	Carl Roth	6344.2
Collagenase D	Roche	1108888 2001
Dako Mounting Medium	Agilent Technologies	S3023
Dimethyl sulfoxide (DMSO)	PanReac AppliChem	A3672,0100
Disodium hydrogen phosphate (Na_2HPO_4)	Carl Roth	4984.1
Ethanol	Carl Roth	1HPH.1
Ethylenediaminetetraacetic acid (EDTA)	Carl Roth	8043.2
Fetal bovine serum (FBS)	PAN-Biotech GmbH	P40-37500
Fetal calf serum (FCS)	Sigma Aldrich	S2000-500
Fugene	Promega	E2311
Glucose	PanReac AppliChem	A1422,0500
Goat serum	Thermo Scientific	31872
HEPES	Roth	9105.4
Horse serum	Thermo Scientific	26050088
Ionomyin, calcium salt	Thermo Fisher Scientific	I24222
Lysogeny broth (LB)	Sigma Aldrich	L3022-1KG
Potassium chloride (KCl)	Carl Roth	7986.1
Magnesium chloride ($MgCl_2$)	Merck	105.833
Menthol	Sigma	M2772-100g-a
Methanol	Chem solution	14.372.511
NEB 5-alpha Competent E. coli	New England Biolabs GmbH	C2987H
OCT Tissue Tek	Sakura, Alphen aan den Rijn	4583
Opal 520	Perkin Elmer	FP1487001KT
Opal 570	Perkin Elmer	FP1488001KT
Opal 690	Perkin Elmer	FP1497001KT
Opti-MEM	Thermo Fisher Scientific	31985054
Pap Pen (Liquid Blocker)	Science Services GmbH	N71310

Paraformaldehyde (PFA)	Sigma-Aldrich	16005
Penicillin/Streptomycin	Sigma Aldrich	P4333
Phosphate-buffered saline (PBS)	Gibco	14190169
Poly-L-lysine (PLL)	VWR	P1524-25mg
PureYield Plasmid Midiprep System	Promega	A2495
RNAscope® Multiplex Fluorescent Kit v2	ACDBio	323100
Sodium chloride (NaCl)	Carl Roth	3957.1
Sodium diphosphate (Na_3PO_4)	Carl Roth	0269.3
Sodium hydroxide (NaOH)	Carl Roth	P031.1
Tissue-Tek® O.C.T Compound	Sakura Finetek	sa-4583
Tris-HCl	Tris-HCl	Tris-HCl
Triton X-100	Sigma Aldrich	X-100-500ML
Trypsin	Sigma Aldrich	T4174
Trypsin-EDTA (0.05% Trypsin, 0.02% EDTA in PBS without Ca^{2+}, Mg^{2+})	PAN-Biotech	P10-023100

3.1.2 Buffers and solutions

Table 3. List of buffers and solutions.

Name	Composition
Phosphate-buffered saline (PBS)	137 mM NaCl, 2.7 mM KCl, 10 mM Na_2HPO_4, and 1.8 mM KH_2PO_4
Blocking buffer for immunostaining	1× PBS with 5% serum and 0.1% TritonX-100
Blocking for DRGs	5% of normal goat/donkey serum, 95% PBS
Blocking for skin	5% of Invitrogen normal goat serum, 20% DMSO, 75% PBS
DMEM+glutaMAXTM	Dublecco's modified eagle medium high glucose GlutaMAX Supplpyruvate
DRG neurone growth medium	DMEM medium, 100 units/ml penicillin, 100 µg/ml streptomycin, 4 mM L-glutamine, glucose, 10% FBS
Extracellular solution for whole-cell patch clamp	140 mM NaCl, 4 mM KCl, 2 mM $CaCl_2$, 1 mM $MgCl_2$, 4 mM glucose, 10 mM HEPES; adjusted to pH 7.4 with NaOH
HEK293 growth medium	DMEM, 100 units/ml penicillin, 100 µg/ml streptomycin, 4 mM Lglutamine, 10% FBS
High K^+ solution	100 mM KCl
LB Agar	LB-medium + 1.5% (w/v) agar
LB medium	10g tryptone, 5g yeast extract, 10g NaCl in 1L H_2O
Paraformaldehyde solution (PFA 4%)	4% paraformaldehyde in 0.1M PBS, adjusted to pH 7.2 – 7.4 with NaOH and HCl

SIF (synthetic interstitial fluid)	2 nM $CaCl_2$, 5.5 mM glucose, 10 mM Hepes, 3.5 mM KCl, 0.7 mM $MgSO_4$, 123 mM NaCl, 1.5 mM NaH_2PO_4, 7.4 mM saccharose, set to pH 8.4 with NaOH
Washing buffer	0.1% Triton X-100 in 1x PBS

3.1.3 Plasmids

Table 4. List of plasmids.

Name	Obtained/Constructed from
ΔN-1-71 NM-R Trpm8-pRK9-IRES-EGFP	Dr. Valérie Bégay
NM-R Trpm8-pRK9-IRES-EGFP	Dr. Valérie Bégay
NM-R Nter-mTrpm8-pRK9-IRES-EGFP	Dr. Valérie Bégay
mTrpm8-pRK9-IRES-EGFP	Dr. Valérie Bégay
pRK9-IRES-GFP	Dr. Mirko Moroni
mCherry-tagged mouse TRPM8	Prof. Félix Viana

3.1.4 Antibodies

Table 5. List of antibodies.

Name	Supplier
First antibody	
Anti-CGRP rabbit	Immunostar, 24112
Anti-NF200 chicken	Abcam, AB72998
Anti-TRPM8 rabbit	Alomone, ACC-049, Lot ACC049AN1602
Anti-TRPV1 guinea pig	Novus Biologicals, NB300-122
Second antibody	
Alexa Fluo Anti-chicken 488	Invitrogen, A11039, 2420700
Alexa Fluor Anti-rabbit 555	Invitrogen, A21429, 2549401
Alexa647 donkey anti-guinea pig	Abcam, ab150075
Alexa488-conjugated IB4	Thermo Fisher Scientific, I21411
DAPI	Thermo Fisher Scientific, 62248

3.1.5 RNAScope probes

Table 6. List of RNAScope probes.

Name	Supplier
RNAscope™ Probe- Hg-Trpm8, for canonical Trpm8	ACD Bio, Cat No. 537651-C1
RNAscope™ Probe- Hg-Trpm8-O1-C2, for extended N-terminal Trpm8	ACD Bio, Cat No. 1280181-C2

3.1.6 Equipments

Table 7. List of equipments.

Name	Specifications	Supplier
Calcium imaging_DRG neurons		
Fixed stage microscope	BX51WI	Olympus Europa GmbH, Hamburg, Germany
CCD camera	CoolSNAP HQ2	Visitron Systems GmbH, Puccheim, Germany
Illumination System	pE-340fura	CoolLED, UK
Objective	UMPLFLN 10x/0.3W	Olympus Europa GmbH, Hamburg, Germany
Perfusion system	ValveLink 8.2	AutoMate Scientific by Science Products, Hofheim, Germany
Vacuum waste kit	ALA-VWK 2	ALA Scientific Instruments, Inc. UK
Temperature Controller CS-1	Co-CS-1	AutoMate Scientific
Calcium imaging_HEK cells		
Microscope	DMIRES-2	Leica Microsystems GmbH, Wetzlar, Germany
Cameras	Imago-QE Sensicam	PCO AG, Kelheim, Germany
Cameras	Retiga R3 CCD Camera	QImaging, a Photometrics Brand, Surrey, BC, Canada
Light Sources	LED light source Lambda 421	Sutter Instrument Company, Novato, CA, USA
RNAscope and IHC imaging		
Confocal laser scanning Microscope	Inverted Axio Observer Z1 LSM 700	Carl Zeiss AG, Oberkochen, Germany
Stage controller	XY Step SMC 2009	Carl Zeiss AG, Oberkochen, Germany
Objective	40x/1.3Oil	Carl Zeiss AG, Oberkochen, Germany
Illumination System	HXP 120C and HAL 100 halogen illuminator	Carl Zeiss AG, Oberkochen, Germany
Spining disk confocal	IX83 and CSU-W1	Olympus
Cryostat	Cryostar nx70	Thermo Fisher Scientific

3.1.7 Softwares

Table 8. List of software used for data analysis.

Name	Supplier
Adobe	CS v5.5
Fiji (ImageJ)	Open source
Fitmaster	HEKA Elekectronik
GraphPad Prism 9	Graphpad Software
LabChart 8 (including Spike Histogram extension)	ADInstruments Ltd
MatLab (R2022b, R2023b)	The MathWorks, Inc.
R (version 4.4.1)	The R Foundation for Statistical Computing
R Studio	Posit Software, PBC
Metafluor	Molecular Devices LLC, San Jose, CA, USA
Office 365	Microsoft
Origin 2024	OriginLab
QuPath	QuPath
SnapGene	GSL Biotech LLC, Chicago, IL, USA
Serial Cloner	Developed by Franck Perez
Zen	Carl Zeiss AG, Oberkochen, Germany
Adobe Illustrator	Adobe
BioRender	Science Suite Inc.

3.2 TRPM8 protein blast

3.2.1 Analysis of protein sequences

The Basic Local Alignment Search Tool (BLAST) was used to find similarities between the TRPM8 protein sequence of interest and a large library of known sequences. BLAST enables the identification of proteins that have similarities with a certain query sequence by comparing it to a database. The flexibility of this technique is shown in its ability to be used to both nucleotide and protein sequences. By employing the BLAST algorithm, we can identify homologous proteins of TRPM8 in different species.

3.2.2 Multiple sequence alignment

After identifying homologous sequences, the CLUSTALW was employed for multiple sequence alignment. CLUSTALW generates an alignment file that is essential for further studies using HMMER, a collection of tools based on Hidden Markov Models (HMMs) as described by Durbin et al., 1998. More precisely, the hmmemit function in HMMER was used

to produce a consensus sequence based on the aligned input sequences. In addition, the bioinformatics data alignments produced by CLUSTALW were interpreted and improved using Jalview, a software platform specifically designed for visualization and analysis. This enabled a more detailed comprehension of the structural and functional patterns seen in the TRPM8 protein sequences.

3.2.3 TRPM8 protein sequence data

The protein sequence data for the TRPM8 protein used in this work was obtained from the National Center for Biotechnology Information (NCBI) and an internal lab database.

TRPM8 sequences from human (*Homo sapiens*, NP_001384535.1), mouse (*Mus musculus*, NP_599013.1), rat (*Rattus norvegicus*, NP_599198.2), thirteen-lined ground squirrel (*Ictidomys tridecemlineatus*, XP_005326460.1), golden hamster (*Mesocricetus auratus*, XP_040608998.1), Chinese hamster (*Cricetulus griseus*, XP_007653247.1), brandt's bat (*Myotis brandtii*, XP_014399646.1), chicken (*Gallus gallus*, NP_001007083.2), African clawed frog (*Xenopus laevis*, NP_001155066.1), tropical clawed frog (*Xenopus tropicalis*, NP_001155105.1), domestic guinea pig (*Cavia porcellus*, NP_001166561.1), European rabbit (*Oryctolagus cuniculus*, XP_017193019.1), Wild yak (*Bos mutus*, XP_005902661.2), cattle (*Bos taurus*, XP_005205017.1), dog (*Canis lupus familiaris*, NP_001104239.1), rhesus monkey (*Macaca mulatta*, XP_028687091.1), chimpanzee (*Pan troglodytes*, XP_024210920.1), Sumatran orangutan (*Pongo abelii*, XP_024099164.1), aardvark (*Orycteropus afer afer*, XP_007941877.1), Yangtze River dolphin (*Lipotes vexillifer*, XP_007463971.1), sperm whale (*Physeter catodon*, XP_023980419.1), Cape golden mole (*Chrysochloris asiatica*, XP_006866830.1), Cape elephant shrew (*Elephantulus edwardii*, XP_006893517.1), crab-eating macaque (*Macaca fascicularis*, XP_015288477.2), long-tailed chinchilla (*Chinchilla lanigera*, XP_005395389.1), prairie vole (*Microtus ochrogaster*, XP_005361774.1), star-nosed mole (*Condylura cristata*, XP_004674816.1), degu (*Octodon degus*, XP_004637389.1), killer whale (*Orcinus orca*, XP_049568349.1), small-eared galago (*Otolemur garnettii*, XP_023364519.1) and Tasmanian devil (*Sarcophilus harrisii*, XP_012405546.3) were aligned and compared to NM-R TRPM8 (*Heterocephalus glaber*, XP_021102976.1).

3.3 Animals

All animal experiments were carried out according to the German and EU animal protection laws and were approved by the Berlin Animal Ethics Committee (Landesamt fur Gesundheit und Soziales). All efforts were made to minimize animal suffering.

3.3.1 Naked mole-rat (*Heterocephalus glaber*)

Non-reproductive healthy adult NM-Rs (aged between 2 and 10 years, from both sex) used in this study, were housed in humidified incubator (50–60% humidity, 28–30°C) with heated cables placed beneath at least one cage per colony to enable behavioral thermoregulation. A diet of sweet potato, banana, apple, cucumber, celery root, and carrot was available ad libitum. NM-Rs were sacrificed by decapitation.

3.3.2 Mouse lines

C57BL/6N (referred to as C57BL/6 in this study) and *Trpm8* knockout (KO) (Bautista et al., 2007) mice (aged between 2 and 8 months, from both sex) used in this study were maintained under pathogen-free conditions in a fixed 12-hour light-dark cycle (45–65% humidity, 20–24°C) and provided with ad libitum food in addition to water. Mice were killed by cervical dislocation.

3.4 Molecular biology

3.4.1 Construction of expression vectors for cell biology experiments

The following plasmids were used in this study: ΔN-1-71 NM-R Trpm8-pRK9-IRES-EGFP (ΔN-1-71 NM-R TRPM8), NM-R Trpm8-pRK9-IRES-EGFP (NM-R TRPM8), NM-R Nter-mTrpm8-pRK9-IRES-EGFP (Nter-mTRPM8), mTrpm8-pRK9-IRES-EGFP (mTRPM8), pRK9-IRES-GFP and mCherry-tagged mouse TRPM8 (mTRPM8_cherry) plasmids.

3.4.2 Plasmid DNA extraction

Plasmid DNA was extracted from bacterial cultures using the PureYield™ Plasmid Miniprep/Midiprep system (Promega GmbH). NEB 5-alpha Competent E. coli (New England Biolabs GmbH) were transformed with the plasmid, and ampicillin-resistant colonies were selected for further analysis. These colonies were then grown in large-scale bacterial cultures for plasmid production. Following bacterial growth, plasmid DNA extraction was carried out

according to the manufacturer's protocol. DNA concentrations were measured using the GeneQuant 1300 photometer (GE Healthcare), and all DNA preparations were stored at -20°C.

3.4.3 DNA Sequencing

Sequencing of DNA samples was done by LGC Genomics, Berlin.

3.5 Cell biology

3.5.1 Cell line culture

In our study, Human Embryonic Kidney 293 (HEK293) cells served as a heterologous expression system, facilitating the isolated study of our TRPM8 protein. This approach allowed for an in-depth exploration of its functional characteristics and regulatory mechanisms. Originating from the renal tissue of an aborted human embryo in 1973, HEK293 cells have become a staple in cell biology and biotechnology due to their robust growth and high transfection efficiency as described in Russell et al., 1977. Besides, we employed the HEK293T variant, an extension of the HEK293 line, which includes the SV40 T-antigen for enhanced transfection capability.

HEK293 and HEK293T cell lines were employed as an exogenous platform for the augmented expression of mechanosensitive ion channels. These cells were cultivated and sustained at 37°C within a moisture-controlled incubator, which was continuously infused with 5% CO_2, across 25 cm^2 culture dishes. The HEK293 and HEK293T cell lines were propagated in DMEM medium, enriched with 10% fetal bovine serum (FBS) and 1% mixture of penicillin and streptomycin. When the cell cultures reached approximately 70% confluency, the old growth medium was discarded. The cultures were then briefly rinsed with PBS at room temperature (RT), followed by the removal of PBS. Subsequently, the cells underwent 3 minutes incubation with 1ml of Trypsin-EDTA solution. The trypsinization process was stopped by adding growth medium fortified with 10% serum. Afterward, the cells were centrifuged at 1,000 rpm, and typically reseeded at a dilution ratio of 1:5 to ensure continuous culture propagation.

3.5.2 Poly-L-Lysine application for cell seeding

Poly-L-Lysine (PLL) was utilized to prepare surfaces for the seeding of primary chondrocytes and HEK293T cells. Both round coverslips, measuring 15mm in diameter, and pillar arrays were treated with PLL to enhance cell adhesion. Initially, the coverslips and pillar arrays,

following cleansing and plasma treatment, respectively, were immersed in a 10 µg/ml solution of PLL. This coating procedure was conducted within a laminar flow cabinet to maintain sterility, lasting for one hour. Subsequent to the PLL application, the items were thoroughly rinsed with sterile water and left to air-dry under sterile conditions. Post-drying, the PLL-treated coverslips underwent ultraviolet (UV) illumination for an overnight period to ensure complete sterilization and to enhance the efficacy of coating for cell attachment.

3.5.3 HEK293 and HEK293T cells transfection

The HEK293 and HEK293T cells were seeded onto PLL-coated glass coverslips or onto arrays covered with PLL in serum-free medium, ensuring adherence for a minimum duration of four hours. The introduction of plasmid DNA into HEK293 cells was achieved through transient transfection, employing lipofection to facilitate nucleic acid entry via lipid vesicles that merge with the cellular membrane. This method enabled the temporary expression of our proteins of interest without genomic integration, using mammalian expression vectors (Kim & Eberwine, 2010). For transfection in HEK293 cells, 50,000 cells per well were seeded in 6-well plates. Cells were transfected using Lipofectamine 2000 according to the protocol of manufacturer. For transfection in HEK293T cells, 10,000 cells were seeded per well in 24-well plates one day before transfection with a mixture containing 1 µg of plasmid DNA with 3 µl of FuGene 6D reagent and 100 µl of Opti-MEM. This mixture was allowed to incubate at RT for 20 minutes before being applied to the cells in each well. Transfection efficiency was assessed by the presence of fluorescence signaling from a marker (either EGFP or mCherry). Then, cells were prepared for immunostaining and calcium imaging analyses to examine protein function between 24-48 hours post-transfection.

3.5.4 Culturing of dorsal root ganglion neurons

DRG neurons were meticulously harvested from L3-L5 lumbar dorsal segments of mice and NM-Rs and immediately submerged in a chilled plating medium. This medium comprised DMEM-F12 (Invitrogen), enriched with L-Glutamine (2 µM, Sigma-Aldrich), Glucose (8mg/ml, Sigma-Aldrich), Penicillin (200 U/mL)-Streptomycin (200 µg/mL) antibiotic mix, and 10% fetal horse serum. For the disaggregation of neuronal tissue, Collagenase IV (1mg/ml, Sigma-Aldrich) treatment was applied for 1 hour. The DRGs were then rinsed thrice in PBS devoid of Ca^{2+} and Mg^{2+} ions. This step was followed by 15 minutes incubation with trypsin (0.05%, Invitrogen) at 37°C to further dissociate the cells. After enzymatic processing, the tissue was gently triturated with a pipette tip, then strategically positioned in a coverslip,

previously coated with PLL and laminin (4 μg/cm^2, Invitrogen), following the methodology by Poole et al., 2014. After overnight incubation, calcium imaging assessments were performed between 18-36 hours post-seeding.

3.6 Immunostaining protocol for cultured cells

Only HEK293T-transfected cells were utilized for this experiment. The cells were gently rinsed with PBS and subsequently fixed with 4% PFA for 10 minutes at RT. Following fixation, the cells underwent three PBS rinses. For intracellular staining, the cells were permeabilized with 0.1% Triton X-100 in PBS for 5 minutes. To block non-specific binding, cells were them incubated in 0.1% Triton X-100 in PBS containing 5% serum for one hour at RT. For antibody staining, cells were incubated with the primary antibody diluted in 0.1% Triton X-100 in PBS containing 5% serum at 1:1000 for two hours at RT. After primary antibody incubation, the coverslips were washed three times for 20 minutes each in 0.1% Triton X-100 in PBS with 5% serum. Subsequently, the secondary antibody and DAPI (diluted at 1:2000) were applied to the cells and incubated for one hour at RT. Finally, the coverslips were washed three times for 10 minutes each in PBS, mounted onto glass slides using ProLong Gold antifade mountant, and allowed to dry.

3.7 Histology

3.7.1 Animal organ harvesting

NM-Rs and mice were sacrificed as described in Section 3.3. DRGs, spinal cord and skin were collected and fixed at 4°C in 4% PFA overnight. Second, DRGs, and spinal cord were kept in 30% sucrose after three times 15 minutes wash with cold PBS. Skin was kept in 15% sucrose after three times 30 minutes wash with cold PBS for one day, another one day of 20% sucrose, finally 3-4 days of 30% sucrose.

3.7.2 Preparation of histochemical slices

Tissue samples were embedded in O.C.T. Tissue-Teks, frozen on dry ice and stored at -80C° prior use. For further histochemical experiments frozen embedded tissues were sectioned on Cryostat (Thermo Fisher Scientific) on to slides and dried at RT. The thickness of sections was dependent on tissue type and the type of staining used.

3.7.3 Immunofluorescence

DRGs sections with 10 µm, skin with 30 µm, and spinal cord sections with 14 µm were used for immunofluorescence. OCT tissue sections were washed three times with PBS and then blocked with a mixture of 0.1% Triton X-100 in PBS (0.1% PBST) and 5% serum for 2 hours at RT. The primary antibodies were diluted in a mixture of 0.1% PBST and 5% serum and applied to the sections, which were incubated overnight at 4°C. Following primary antibody incubation, slides were washed three times in 0.1% PBST for 20 minutes each, then incubated with secondary antibodies and DAPI, also prepared in a mixture of 0.1% PBST and 5% serum, for 2 hours at RT. After secondary antibody application, slides underwent three additional 0.1% PBST washes before being mounted with Dako Mounting Medium. Simplified workflow immunofluorescence is summarised in Figure 11.

3.7.4 Combined RNAscope with Immunofluorescence in tissues

As before, DRGs sections of 10 µm, skin of 30 µm and spinal cord sections of 14 µm were used for RNAscope. RNAscope in-situ hybridization was performed according to the instructions of manufacturer (ACDbio).

The RNAscope Multiplex Fluorescent Kit v2 was employed, with adjustments made to the protocol of manufacturer. Sections were washed with PBS for 2 minutes, and dry for 30 min at 40°C. Then sections were exposed to hydrogen peroxide for 15 minutes at RT to inhibit endogenous peroxidase activity, followed by 5 minutes wash in 100% ethanol. Protease III was subsequently applied for 30 minutes at 40°C. After rinsing thrice with PBS, *Trpm8* and *Ex-trpm8* probes (Figure 12) were applied, and hybridization was performed in a humidified oven at 40°C for 2 hours. Amplification involved sequential 30 minutes incubations with Amp1, Amp2, and Amp3 at 40°C. Detection was achieved by applying channel-specific horseradish peroxidase (HRP) (HRP-C1, HRP-C2, HRP-C3) for 15 minutes each, followed by TSA-mediated fluorophore binding for 30 minutes and final HRP deactivation for 15 minutes at 40°C.

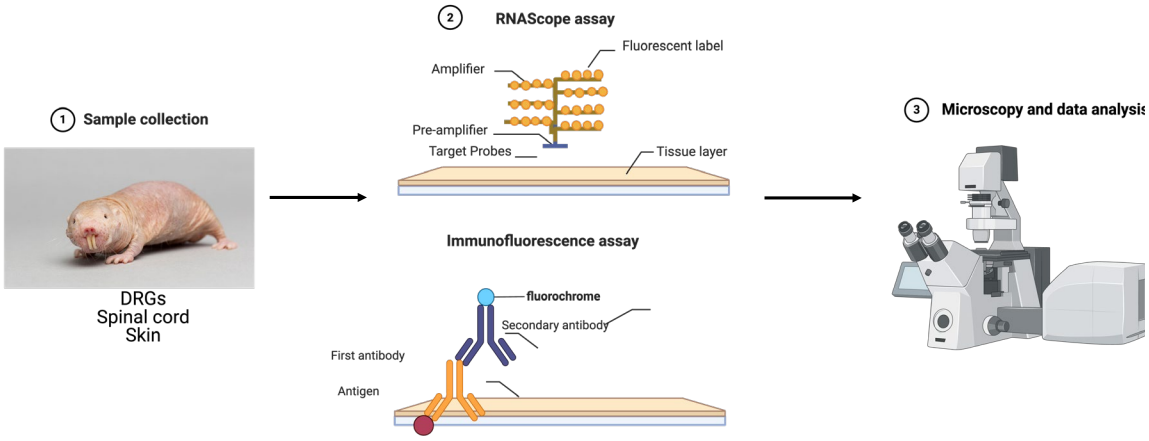

Figure 11. Workflow of NM-R tissues collection, assay, and analysis of RNAscope staining and immunofluorescence.
① Sample Collection: tissue samples are collected from various regions including DRGs, spinal cord, nerve and skin. A naked mole-rat is shown as the sample source. ② RNAscope assay: tissue samples are prepared and specific RNA targets within the tissue are labeled using RNAscope technology. Target Probes bind to the RNA of interest. Pre-amplifier and amplifier sequences increase the signal. Fluorescent labels are attached to the amplified signal to visualize the RNA. Immunofluorescence assay: Tissue sections are incubated with a primary antibody that binds to a specific antigen. A secondary antibody, which binds to the primary antibody, is tagged with a fluorochrome to produce fluorescence. ③ Microscopy and data analysis: The prepared tissue samples are examined under a microscope to visualize the fluorescent signals. Drawn with biorender.

Then, the sections were blocked with a mixture of 0.1% PBST and 5% serum for 1 hours at RT. The primary antibodies were diluted in 0.1% PBST and 5% serum, applied to the sections, and incubated overnight at 4°C. Following primary antibody incubation, the slides were washed three times in 0.1% PBST for 20 minutes each, then incubated with secondary antibodies and DAPI, diluted in 0.1% PBST and 5% serum, for 2 hours at RT. After secondary antibody application, the slides underwent three additional washes with 0.1% PBST before being mounted with Dako Mounting Medium. Simplified workflow immunofluorescence is summarised in Figure 11.

3.7.5 Confocal imaging and data processing

Imaging was performed by confocal 700LSM Zeiss and spining disk (Olympus) and analysed by FIJI Software.

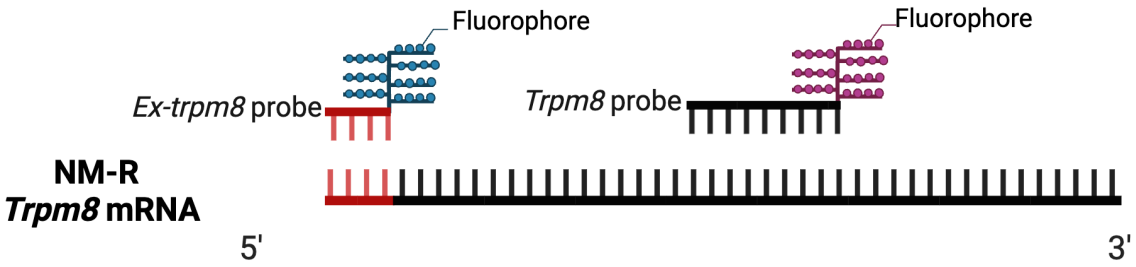

Figure 12. Schematic of RNAScope probes targeting NM-R *Trpm8* mRNA.
NM-R *Trpm8* probes design was base on XM_021247317.1 from NCBI. *Trpm8* probe was designed from 1510 – 2485 bp, and *Ex-trpm8* probe was designed from 415 – 854 bp.

3.8 Calcium Imaging

Simplified workflow of Calcium Imaging is summarised in Figure 13. Calcium imaging in TRPM8 transfected HEK 293 cells were done in collaboration with the Prof. Félix Viana (IN, Alicante) and calcium imaging in cultured DRG neruons were done in Berlin.

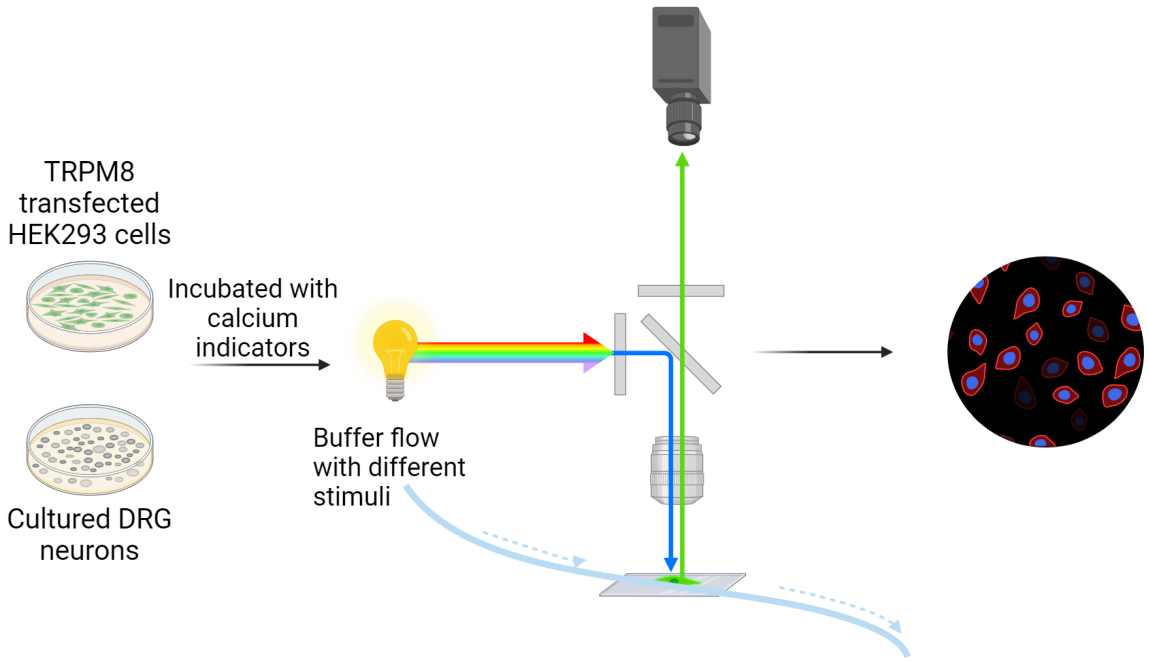

Figure 13. Workflow of calcium imaging of HEK293 cells and cultured DRG neurons.
TRPM8-transfected HEK293 cells and cultured DRG neurons are incubated with calcium indicators 1h before experiments. The samples are exposed to buffer flow with different stimulations while being illuminated by light of needed wavelengths. Fluorescence signals are captured using a microscope to visualize and analyze calcium influx in the cells. Drawn with biorender.

3.8.1 Fluorescence indicators

Fluorescence calcium indicators were employed to monitor fluctuations in intracellular calcium levels. In HEK 293 cells, the Fura-2 acetoxymethyl (AM) calcium indicator from Invitrogen, a probe that permeates cell membranes, was employed. Upon incubation, this indicator diffuses into cells where intracellular esterases cleave its AM ester group, effectively trapping Fura-2 within the cell. Fluorescence of Fura-2 excitation peak shifts in response to calcium binding: from 362 nm when unbound to 335 nm upon binding. The emission spectra remain unchanged, enabling the calculation of free intracellular calcium concentration through fluorescence intensity ratio at 340 nm and 380 nm (F340/380).
For calcium imaging in cultured DRG neurons, the Cal-520 AM indicator (Invitrogen) was employed, offering a different excitation/emission profile suitable for these neurons.

3.8.2 Experimental setup

HEK 293 cells: calcium imaging experiments conducted in HEK 293 cells were performed using a Leica DMIRES-2 microscope equipped with a 20x objective lens. Two camera models were employed: the Imago-QE Sensicam (PCO) and the Retiga R3 CCD Camera (Qimaging). For illumination, a rapid switching monochromator (TILL Photonics) and an LED light source Lambda 421 (Sutter Instruments) were used to excite the fluorescent indicators. Data acquisition and analysis were facilitated by TillVision (TILL Photonics) and Metafluor (Molecular Devices) software, with images captured at 2-3 second intervals.

DRG neurons: calcium imaging in cultured DRG neurons was conducted using a BX51WI fixed-stage microscope (Olympus Europa GmbH, Hamburg, Germany) paired with a CoolSNAP HQ2 CCD camera (Visitron Systems GmbH, Puccheim, Germany). The illumination was provided by a pE-340fura system (CoolLED, UK), and imaging was performed using a UMPLFLN 10x/0.3W objective (Olympus Europa GmbH, Hamburg, Germany). The setup included a ValveLink 8.2 perfusion system (AutoMate Scientific by Science Products, Hofheim, Germany) and a vacuum waste kit ALA-VWK 2 (ALA Scientific Instruments, Inc., UK) for fluid management during experiments.

3.8.3 Cell preparation and imaging protocol

HEK 293 Cells: cells were transfected with GFP-reporter plasmids and pre-incubated with 5 µM Fura-2 AM and 0.02% Pluronic for 45 minutes at 37°C. Following incubation, the cells were transferred to the microscope chamber. Initially, transmitted light images and 460 nm

excitation images were captured to identify GFP-expressing cells. Subsequently, fluorescence imaging commenced with the application of various stimuli or drugs.

DRG neurons: cultured DRG neurons were similarly prepared and incubated with 5 µM Cal-520 AM for 45 minutes at 37°C. After incubation, neurons were placed under the microscope, and fluorescence imaging was conducted.

3.8.4 Experimental conditions

In the HEK 293 cell experiments, the cells were exposed to several stimuli to assess intracellular calcium responses. These stimuli included thermal stimulation at 40°C (warm) and 16°C (cold), as well as chemical stimulation with 200 µM menthol and 10 µM icilin. Additionally, a combined stimulus of 10 µM icilin with cold was applied to evaluate the synergistic effects of cold and icilin. For the DRG neurons, the experiments involved exposure to cold, 200 µM menthol, and 10 µM AMTB to investigate the response of neurons to these specific conditions.

3.9 Skin-nerve preparation

Electrophysiological assessments were conducted on cutaneous sensory fibers originating from the tibial and saphenous nerves, utilizing an *ex vivo* skin-nerve preparation technique. This methodology aligns with the procedures detailed in prior studies by Milenkovic et al., 2014 and Walcher et al., 2018. Simplified workflow of skin-nerve preparation is summarised in Figure 14.

3.9.1 Hairy skin and saphenous nerve sample preparation

The experimental subjects were euthanized through cervical dislocation. Post-euthanasia, and the saphenous nerve, along with the associated hindpaw skin, was meticulously dissected. This complex was then inverted and positioned within a chamber designed for perfusion. This chamber was continuously infused with interstitial fluid, warmed to a temperature of 32°C and saturated with oxygen. The saphenous nerve was delicately extended via a slender passage to a recording section, which was isolated within mineral oil. Here, individual fibers were spread out for single-unit electrophysiological recordings, employing a platinum wire electrode for the purpose of monopolar recording, complemented by a reference electrode.

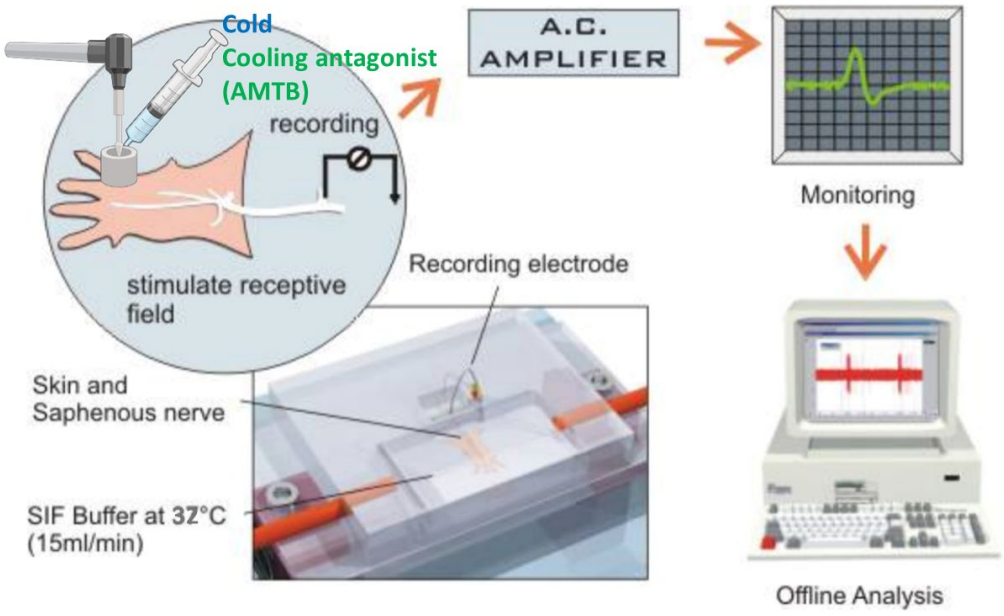

Figure 14. Workflow of skin-nerve preparation.
The figure depicts the process used for skin-nerve preparation and recording. The skin is stimulated at the receptive field with cold or cooling antagonist (such as AMTB), and saphenous nerve will transmit electrical responses. Electrical responses are recorded using an electrode connected to an A.C. amplifier. The amplified signals are monitored in real-time. Data is collected and analyzed offline using Labchart software. The experiment is performed in a chamber with SIF buffer maintained at 32°C (15 ml/min). Image modified from Paul Heppenstall.

3.9.2 Isolating single sensory units

To isolate single units, the perineurium was gently stripped using fine forceps, and individual nerve bundles were teased apart before being placed atop a platinum wire electrode for recording. Initial identification of mechanosensitive units was performed using non-sharp stimulation via a glass rod. The classification of each unit was based on the analysis of their firing patterns and their response to the velocity of the applied stimulus, adhering to criteria established in previous works (Walcher et al., 2018).

3.9.3 Conduction velocity measurements

Conduction velocity (CV) was determined using the equation CV = distance/time delay. Velocities exceeding 10m/s were attributed to rapidly adapting mechanoreceptors (RAMs) or slowly adapting mechanoreceptors (SAMs), denoted as Aβ fibers. Velocities less than 10m/s were categorized as Aδ fibers, and velocities below 1.5m/s were indicative of C-fibers. To ensure accuracy, all recorded responses, whether mechanical or thermal were adjusted for

latency delays from the electrical stimulus to the action potential detection at the recording electrode.

3.9.4 Thermal sensitivity testing

To evaluate the thermal sensitivity of cutaneous sensory afferents, both cold and warm SIF buffers were applied directly to the receptor fields using a 1 ml pipette. The temperature of the SIF buffer was adjusted in advance to the desired temperature using an external water bath or a heating/cooling system. The specific application protocols were as follows:

For cold stimulation, SIF buffer pre-cooled to 10°C was pipetted directly onto the receptor fields in 1 ml aliquots. For warm stimulation, SIF buffer heated to 45°C was applied in the same manner, directly using a pipette. The application was performed manually, and temperature readings were monitored with a thermocouple near the skin surface to confirm that the receptor field was exposed to the desired temperature.

The initial basal skin temperature was maintained at approximately 32°C by the SIF buffer in the chamber before each thermal stimulus was applied. Although temperature control was conducted manually, a fine thermocouple (Temperature Controller CS-1, AutoMate Scientific) was placed near the receptor fields to ensure accurate monitoring of the temperature at the site of SIF buffer application. The thermocouple recorded the real-time temperature change during each application. Temperature data were collected continuously using Labchart 8 software, enabling the correlation of afferent responses with specific temperature changes.

3.9.5 Compound stimulation protocol

To assess the role of specific thermoreceptors, such as TRPM8 channels, a compound stimulation protocol was employed using cold and AMTB (TRPM8 inhibitor) combined stimuli. This protocol included the following experimental conditions:

Cold SIF buffer (10°C) was applied directly as described above, to activate cold-sensitive afferents. Warm SIF buffer (40°C) was used to activate warm-sensitive afferents, following the same procedure. To assess the modulation of cold-sensitive TRPM8 channels, AMTB (10 μM) was added to the cold SIF buffer (10°C) and warm SIF buffer (40°C). The AMTB solution was freshly prepared and pre-cooled or pre-warmed before direct application to the receptor fields using the same pipette method. After each stimulus application, the receptor fields were allowed to recover for 2 minutes before the next stimulus was applied.

3.9.6 Electrophysiological recording and analysis

The acquisition of raw neural data was facilitated by an analog signal derived from a Neurolog amplifier, which amplified the extracellular recordings of action potentials from the sensory afferents. The amplified signal was filtered to remove noise and then digitized using a Powerlab 4/30 system (ADInstruments Ltd., Dunedin, New Zealand). The digitized signals were processed and recorded using LabChart 8 software.

Post-experiment analysis was performed using R software. The instantaneous firing rate (IFR) was plotted as a function of time and temperature to visualize the dynamic response of the afferents to thermal stimuli. Temperature data were synchronized with neural recordings to correlate specific temperature changes with the onset of neural activity.

4 Results

4.1 The expression of TRMP8 mRNA and protein in sensory tissues of Naked mole-rat

We hypothesized that the cold-sensitive TRPM8 channel is either absent or expressed less in the crucial temperature sensing organs of NM-Rs. This section focuses on investigating the presence of TRPM8 channels in NM-R sensory tissues using RNAscope (*in situ* hybridization technique that allows precise visualization of RNA molecules within intact cells) and immunofluorescence techniques. We examined various sensory tissues, such as the DRGs, the spinal cord, and skin.

4.1.1 TRPM8 mRNA and protein expression and localization in DRGs of Naked mole-rat

To elucidate the expression of *Trpm8* in this tissue, we employed RNAscope with a *Trpm8*-specific probe. To further characterize the specific types of TRPM8-positive neurons within the DRGs, we examined the co-expression of these *Trpm8*$^{+}$ neurons with several other sensory neuron-specific markers to gain a more detailed insight into the *Trpm8*$^{+}$ neuron subtypes. For example, the heavy neurofilament protein, NF200, is a neurofilament protein essential for maintaining neuronal structure, particularly in the axons of both central and peripheral neurons. Being found predominantly in the larger, myelinated A-fiber sensory neurons, NF200 acts as a biomarker for neurons which are involved in rapid signal transmission including proprioception and tactile sensation (L. Li et al., 2011; Usoskin et al., 2015).

Additionally, TRPV1 is a distinctive marker for neurons responsive to noxious stimuli which plays a vital role in pain sensation and is predominantly localised in small to medium-sized neurons. While IB4 selectively labels a distinct subset of non-peptidergic nociceptive neurons, aiding the identification of pain pathways. Furthermore, calcitonin gene-related-peptide (CGRP) is commonly used as a marker for peptidergic nociceptive neurons which are responsible for the transmission of acute pain signals (Li et al., 2011; McCoy et al., 2012; Molliver et al., 1997).

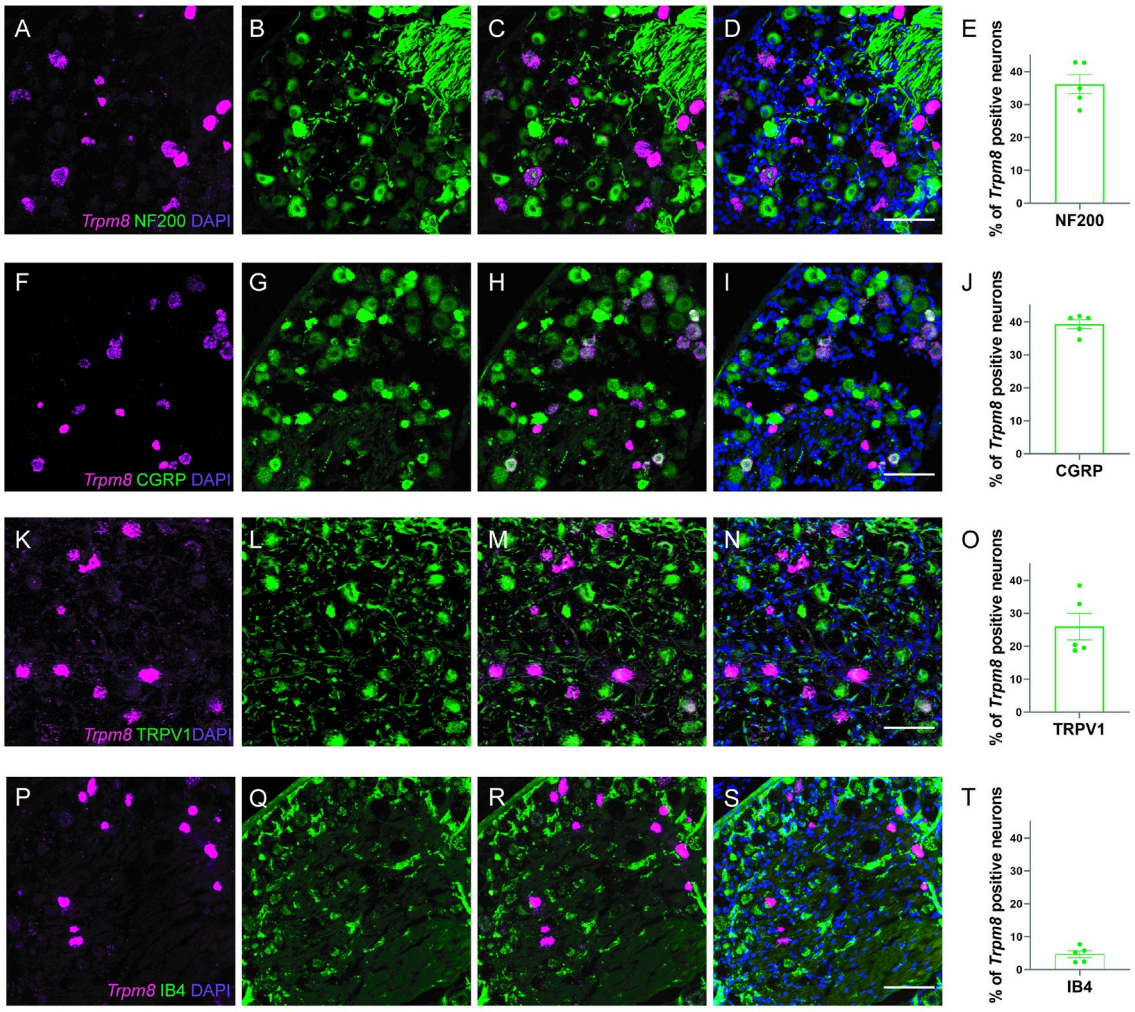

Figure 15. Representative images of adult NM-R L3-L5 lumbar DRGs stained with combined immunofluorescence markers and RNAscope for *Trpm8*.
(A-D). The DRGs stained with an NF200 antibody and *Trpm8* probe. (E). Quantification of the percentage of *Trpm8*-expressing neurons that also express the NF200 marker within the DRGs of NM-Rs. (F-I). NM-R DRGs stained with CGRP antibody and *Trpm8* probe. (J). Quantification of the proportion of *Trpm8*-positive neurons expressing CGRP within the DRGs through a graphical analysis. (K-N). These images present the DRGs stained for TRPV1 alongside *Trpm8* probe. (O). This barplot displays a graphical analysis of the percentage of *Trpm8* neurons expressing TRPV1 in the DRGs. (P-S). NM-R DRGs stained with IB4 antibody and *Trpm8* probe. (T). Quantification of *Trpm8* neurons expressing IB4 in DRGs. NM-R probe *Trpm8* is lablled in magenta. Neuronal markers NF200, IB4, TRPV1 and CGRP are indicated in green. Nuclei are stained with DAPI (blue). Data are presented as mean ± SEM from 5 NM-Rs (more than 2000 neurons were counted for each group). NM-R *Trpm8* probe design was base on XM_021247317.1 (1510 – 2485) from NCBI. Scale bar: 30 µm.

This section presents a comprehensive analysis showing the co-localization of *Trpm8* with neuronal markers NF200, IB4, CGRP, and TRPV1, in the DRG neurons of NM-Rs (Figure 15). Figure 15A-D depict the co-localization of *Trpm8* probe with NF200 which marks myelinated

neurons. Quantitative analysis presented in Figure 15E indicated approximately 36.17% of TRPM8-positive neurons that also co-expressed NF200, suggesting an abundance of myelinated neurons which were *Trpm8*$^{+}$. This finding hints at a potential role of TRPM8 in the normal function of myelinated sensory fibers, potentially through involvementg in mechanical stimuli perception or body position and movement awareness. Furthermore, the co-localization of *Trpm8* with CGRP (Figure 15F-J) and TRPV1 (Figure 15K-O) showed a high expression of TRPM8 in sensory neurons responsible for nociception and temperature sensitivity. Quantitative analysis in Figure 15J and Figure 15O revealed that 39.33% and 25.99% of *Trpm8*$^{+}$ neurons expressed CGRP and TRPV1, respectively. The presence of IB4, a marker for non-peptidergic neurons, implies a potential role of TRPM8 in a specific subset of these neurons since only a low co-expression level was detected (4%).

Since mRNA levels do not always correlate with protein expression, we extended our investigation to include immunofluorescence staining with antibody. A commercial antibody targeting TRPM8 was utilized and its specificity was rigorously assessed through extensive validation based on comparisons of their expression level between *Trpm8* KO and wild-type (WT) mouse tissues (Figure 16A). In the DRG sections from C57BL/6 mice, TRPM8 (red) was expressed in a subset of neurons. As expected, no TRPM8 signal was detected in theDRG sections from TRPM8 KO mice, confirming the specificity of this antibody. TRPM8 expression was observed in the DRG sections from NM-Rs. Interestingly, in NM-R DRGs, TRPM8 expression was not limited to only smaller neurons but was also prominently observed in larger diameter neurons (Figure 16B).

Subsequently, we investigated the co-localization of TRPM8 with various types of neuronal markers in NM-R DRGs (Figure 17). We utilized PGP9.5, a marker presents in all NM-R DRG neurons, to ascertain the proportion of TRPM8-positive neurons within the entire DRG population (Figure 17A-E). Quantitative analysis revealed that TRPM8 expression was present in approximately 16% of the DRG neurons, as indicated by co-localization with PGP9.5. Consistent with the previously conducted RNAscope experiments, we examined the co-localization of TRPM8 with NF200, TRPV1, and IB4. Figure 17F-J, K-O, and P-T illustrate the concurrent presence of TRPM8 with NF200, TRPV1, and IB4, respectively. These visual representations provided compelling evidence that various neuronal subtypes were positive for TRPM8 expression. Detailed analysis showed that 33.70%, 19.45%, and 1.1281% (almost none) of TRPM8-positive neurons exhibited the presence of NF200, TRPV1, and IB4, respectively

(Figure 17J-T). Due to species incompatibility, the co-staining of TRPM8 and CGRP was not feasible.

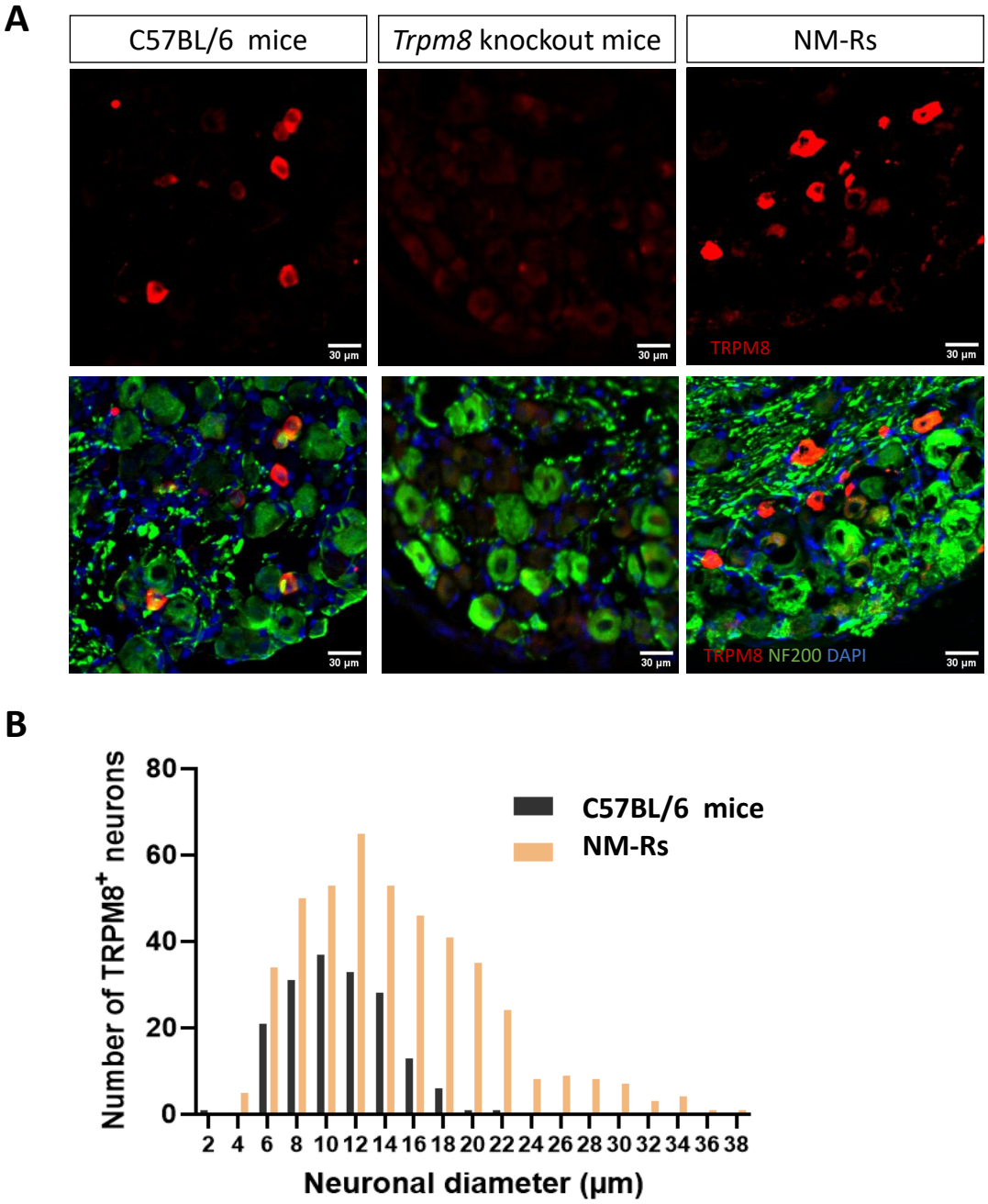

Figure 16. TRPM8 expression in L3-L5 lumbar DRGs of adult C57BL/6 mice, *Trpm8* knockout mice, and NM-Rs.
(A). Representative images of TRPM8 expression in the DRG neurons shows clear labelling in C57BL/6 mice and NM-Rs, but no detectable signal in TRPM8 KO mice. TRPM8 is indicated in red. Neuronal markers NF200 is indicated in green in all images. Nuclei are stained with DAPI (blue). Scale bar: 50µm. (B). Histograms show the distribution of TRPM8-positive neurons by neuronal diameter in C57BL/6 mice and NM-Rs. Notably, larger diameter neurons also expressed TRPM8 in NM-Rs, indicating a broader range of sensory neurons expressing TRPM8 in this group. C57BL/6 mice: n=3, 172 neurons, NM-Rs: n=3, 447 neruons.

In conclusion, both the RNAscope and immunofluorescence data show consistent patterns of TRPM8 expression and distribution in DRG neurons of NM-R.

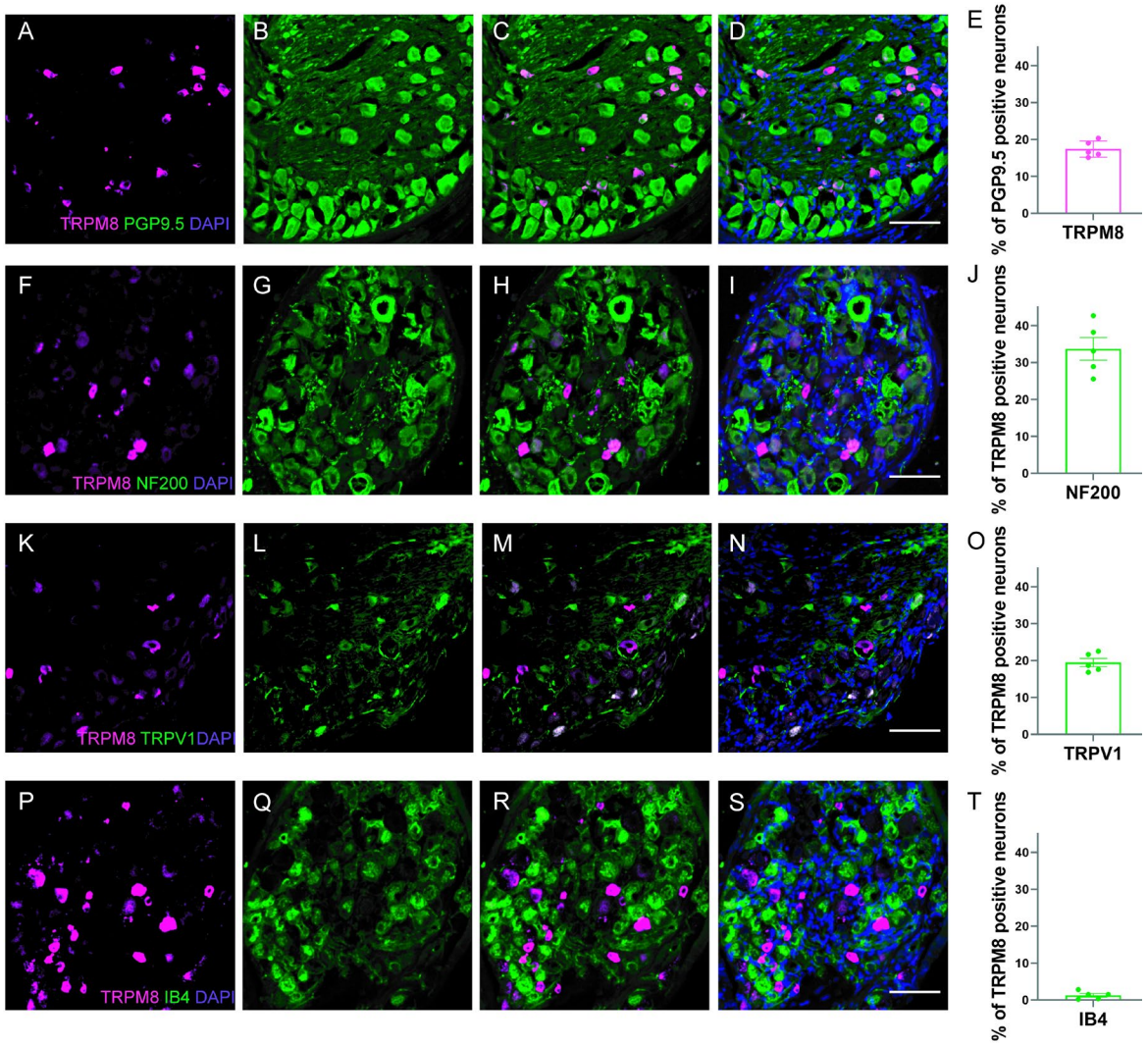

Figure 17. Representative images of adult NM-R L3-L5 lumbar DRGs stained with various neuronal markers and TRPM8 antibody.
(A-D). NM-R DRGs stained with NF200 antibody and TRPM8. (E). Graphical representation of the pencentage of neurons expressing TRPM8 in the whole DRGs. (F-I). NM-R DRGs stained with CGRP antibody and TRPM8 antibody. (J). Graphical representation of the proportion of TRPM8 neurons expressing NF200 in NM-R DRGs. (K-N). NM-R DRGs stained with TRPV1 and TRPM8. (O). Graphical representation of the proportion of TRPM8 neurons expressing TRPV1 in NM-R DRGs. (P-S). NM-R DRGs stained with IB4 antibody and TRPM8. (T). Graphical representation of the proportion of TRPM8 neurons expressing IB4 in NM-R DRGs. NF200, IB4, TRPV1 and PGP9.5 labeling are shown in green whereas TRPM8 is shown in magenta. Nuclei are stained with DAPI (blue). Quantitative analysis showing the percentage of TRPM8 positive neurons in each group from 5 NM-Rs (more than 2000 neurons were counted for each group). Scale bar: 30 μm.

4.1.2 TRPM8 mRNA and protein expression in the spinal cord of Naked mole-rat

It is well-established that the sublayers of layer I and layer II of the spinal cord collectively form the dorsal horn (DH) which receives input from the Aδ and C primary afferent thermoreceptors and nociceptors, which then relay this information to the brain (Basbaum et al., 2009). Electrophysiological studies have demonstrated that the neurons in layer I of cats respond exclusively to innocuous cooling (Craig & Dostrovsky, 2001). Furthermore, TRPM8 immunofluorescence staining has shown that TRPM8-positive neurons project to the superficial layer I of the DH in the mouse spinal cord, with no significant overlapping at the single fiber level between TRPM8 and CGRP (Dhaka et al., 2008). The primary question for this investigation is whether TRPM8 is expressed in the NM-R spinal cord and, if so, whether its projections are predominantly localized to layer I or layer II. To accomplish this, we examined the spatial distribution of *Trpm8* based on the comparison with well-characterized neuronal markers such as CGRP and Isolectin B4 (IB4). CGRP was predominantly localized to the outer regions of Lamina I and Lamina II in the dorsal horn, as illustrated by the cyan region (Figure 18A). IB4 was primarily projected to the inner part of Lamina II, corresponding to the green region (Figure 18A). Similar staining was observed in NM-R, although a thicker lamina II gave rise to increased IB4 staining (Park et al., 2008).

In this section, we employed RNAscope and immunofluorescence techniques to examine TRPM8 expression in the spinal cord of NM-Rs. In adult NM-R, a lot of *Trpm8* mRNA could be observed in spinal cord (Figure 18B). To further detail the *Trpm8* mRNA distribution in the dorsal horn of the spinal cord, we co-stained with IB4 and CGRP (Figure 19A). The merged image illustrated the presence of both *Trpm8* and CGRP in layer I of the spinal cord. In contrast, within the ventral horn area (Figure 19B), the absence of IB4 and CGRP was accompanied by a subtle presence of *Trpm8*. Additionally, *Trpm8* in the NM-R spinal cord seemed to be present in a subset of neurons that has not been previously characterized in mice.

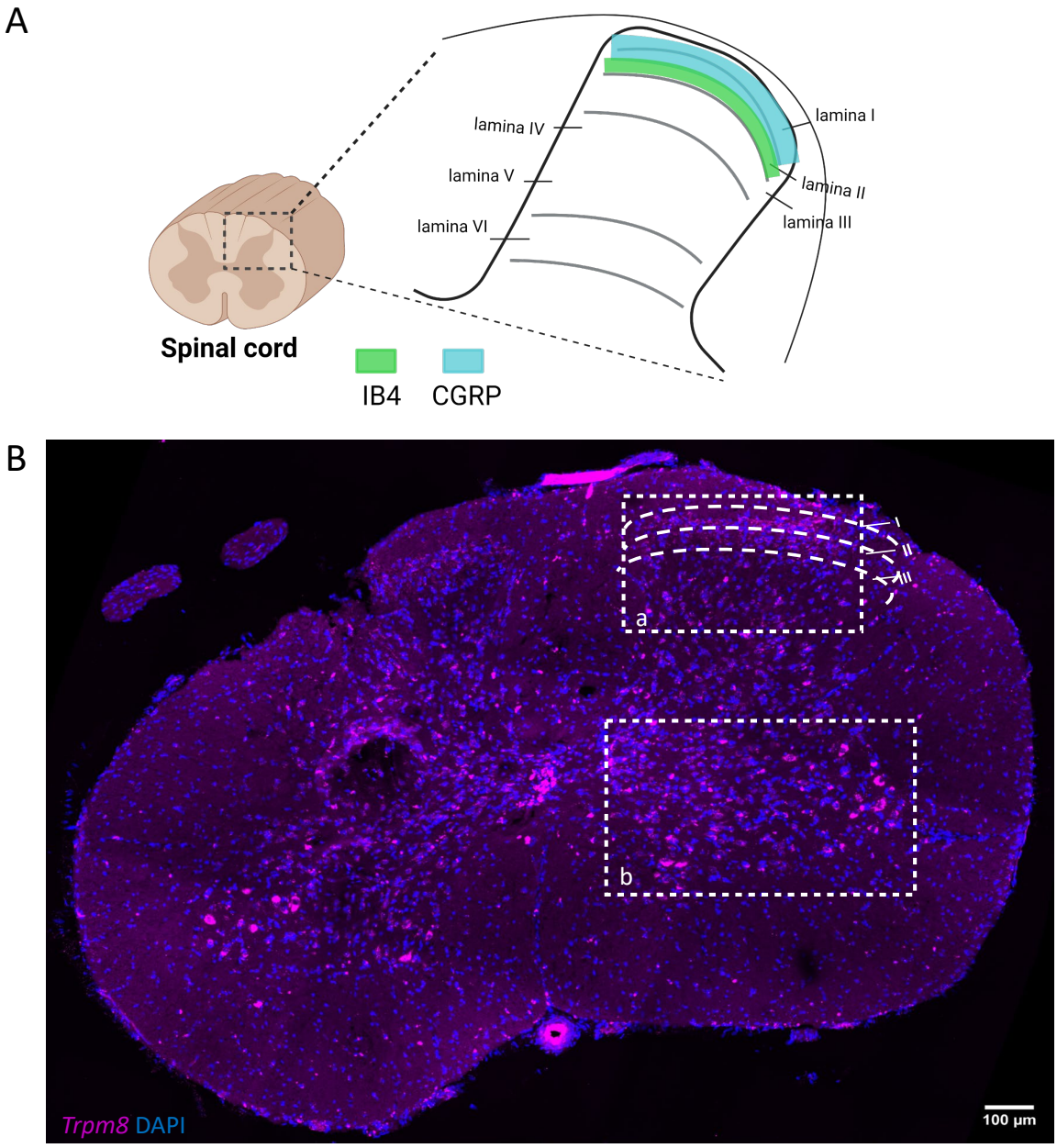

Figure 18. Representative image of *Trpm8* RNAscope staining of the adult NM-R lumbar spinal cord.
(A). Laminar distribution in the spinal cord dorsal horn and distribution of sensory fibers stained with IB4 (green) and CGRP (cyan). Drawn with biorender. (B). An overview of the NM-R spinal cord with *Trpm8* mRNA. The dashed lines demarcate the anatomical boundaries of the spinal cord layers, labeled as I, II, and III, to guide the assessment of markers co-localization within specific neuronal populations. Each magenta puncta indicates one RNA molecule bound to the *Trpm8* probe. Nuclei are stained with DAPI (blue). Scale bar: 100 µm. NM-R *Trpm8* probe design was base on XM_021247317.1 (1510 – 2485) from NCBI.

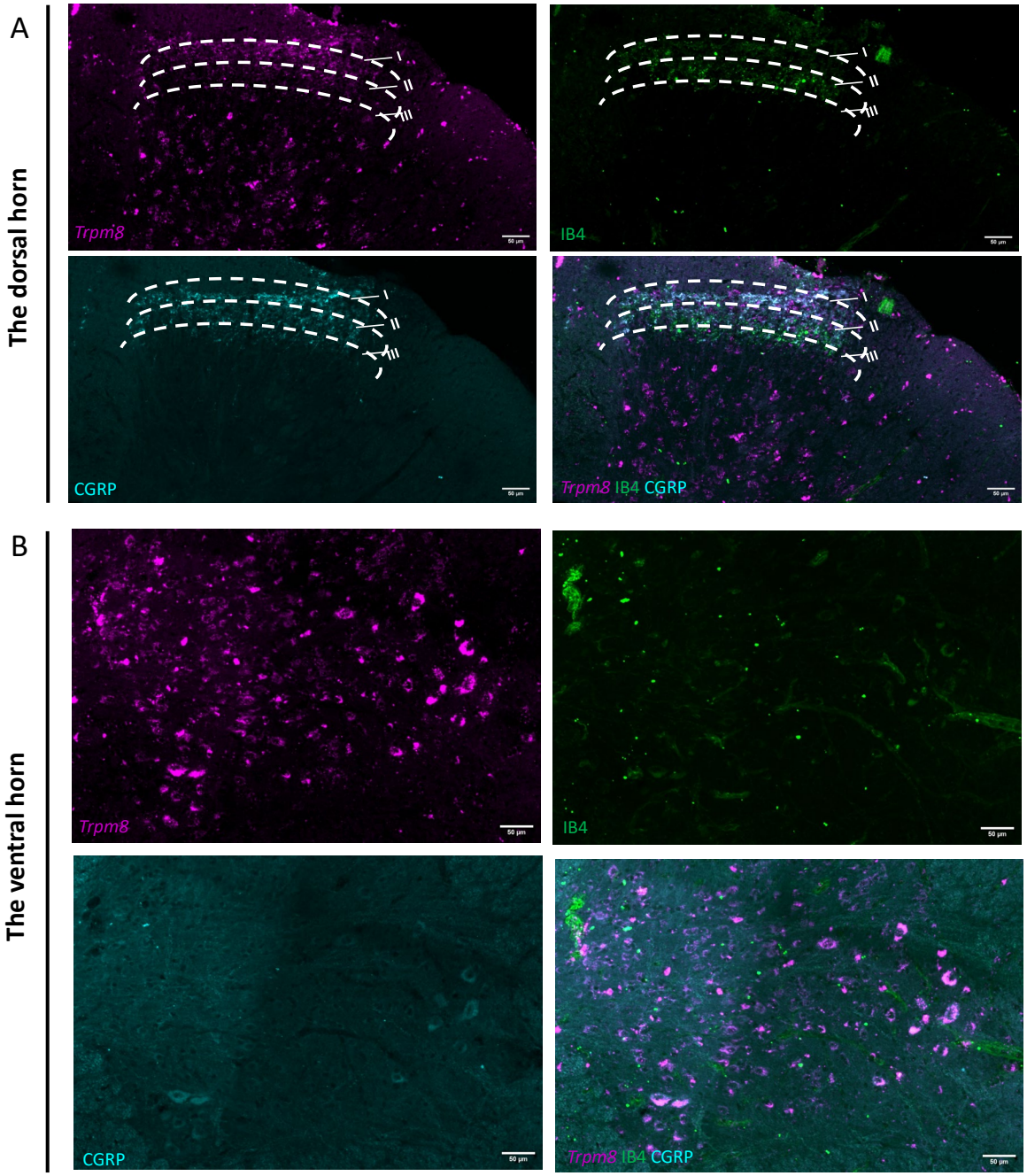

Figure 19. Combined *Trpm8* RNAscope and IB4, CGRP immunofluorescence staining of adult NM-R lumbar spinal cord.
(A). Zoomed in images from the 'a' area in Figure 18 show stainings of *Trpm8*, IB4 and CGRP in the dorsal horn. (B). Images from the 'b' area in Figure 18 show stainings of *Trpm8*, IB4 and CGRP in the ventral horn. The spinal cord layer markers IB4, CGRP are labeled in green and cyan, respectively. Each magenta puncta indicates one RNA molecule bound to the *Trpm8* probe. Nuclei are stained with DAPI (blue). NM-R *Trpm8* probe design was base on XM_021247317.1 (1510 – 2485) from NCBI. Scale bar: 50 µm.

To validate the data obtained at the *Trpm8* mRNA using RNAScope, we performed immunofluorescence staining with an antibody directly against TRPM8 in combination with IB4. Representative images from the lumbar segments 3 and 4 of the adult NM-Rs spinal cord are shown in Figure 20. In these images, TRPM8 protein was visualized in magenta, while IB4 staining was shown in cyan (Figure 20A and B). We observed a low level of TRPM8 expression, predominantly localized in Laminae I, with no overlap between TRPM8 and IB4, consistent with findings previously reported in mice, and the TRPM8 staining appeared to be restricted to the sensory endings (Takashima et al., 2007).

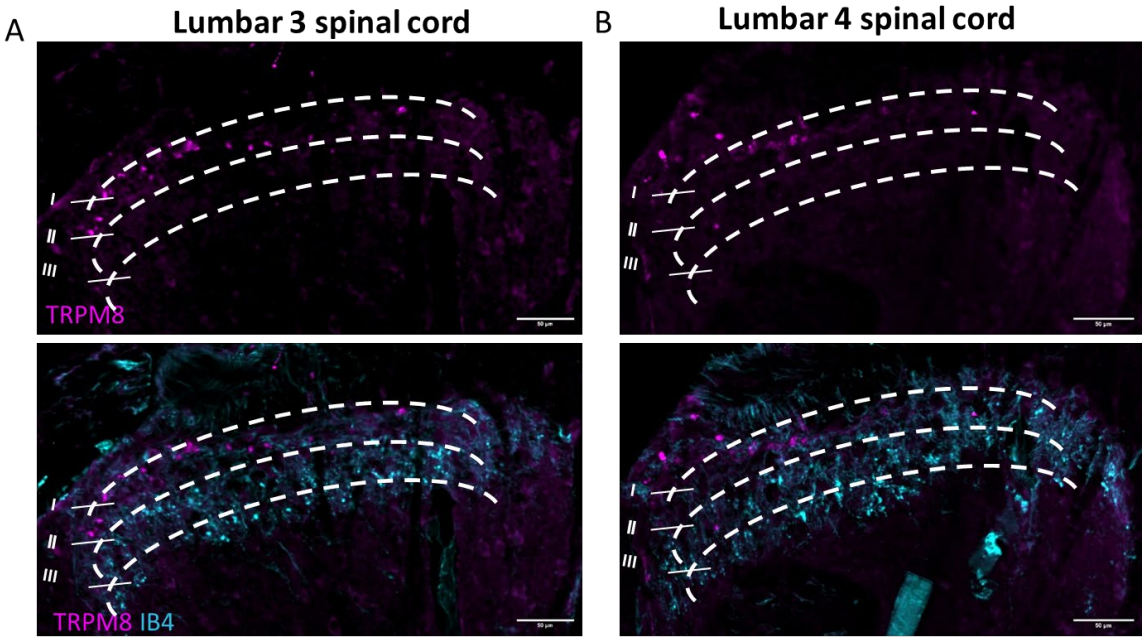

Figure 20. Representative immunofluorescence images of combined TRPM8 and IB4 of adult NM-Rs lumbar spinal cord.
(A). Lumbar 3 spinal cord section from adult NM-Rs satined with TRPM8 and IB4. (B). Lumbar 4 spinal cord section from adult NM-Rs satined with TRPM8 and IB4. The dashed lines demarcate the anatomical boundaries of the spinal cord layers, labeled as I, II, and III. TRPM8 expression is shown in magenta, and the spinal cord layer marker IB4 is shown in cyan. Scale bar: 50 µm

4.1.3 TRPM8 protein expression in the skin of Naked mole-rat

In the exploration of sensory mechanisms, the skin is of paramount importance, serving as the primary interface between external stimuli and our sensory nerves. In mice, it has been observed that nerve endings expressing TRPM8 receptors extend into various regions of the superficial layers of hairless skin, including the mystacial pad (Dhaka et al., 2008). While RNAscope has been previously applied in skin studies, it has not yet been used to investigate *Trpm8* expression (Bonnet et al., 2021). Prior studies have demonstrated the presence of *Trpm8* RNA and TRPM8

protein in the NM-R DRGs and spinal cord. The objective of our study was to delineate the presence of *Trpm8* RNA and TRPM8 protein in the NM-R skin. The findings from our RNAscope analysis revealed that while the markers NF200 and CGRP effectively delineated specific nerve fibers within the skin, *Trpm8* mRNA positive nerves or corpuscles were not discernible (Figure 21). However, an interesting observation such that a limited number of cells within the epidermal layer consistently exhibited *Trpm8* staining was noted, as highlighted by the arrow in the upper right image of Figure 21. Notably, a similar staining pattern was observed in a previous study investigating TRPM8 expression in mouse skin (Dhaka et al., 2008), though the exact identity and function of these TRPM8-positive cells remain unclear.

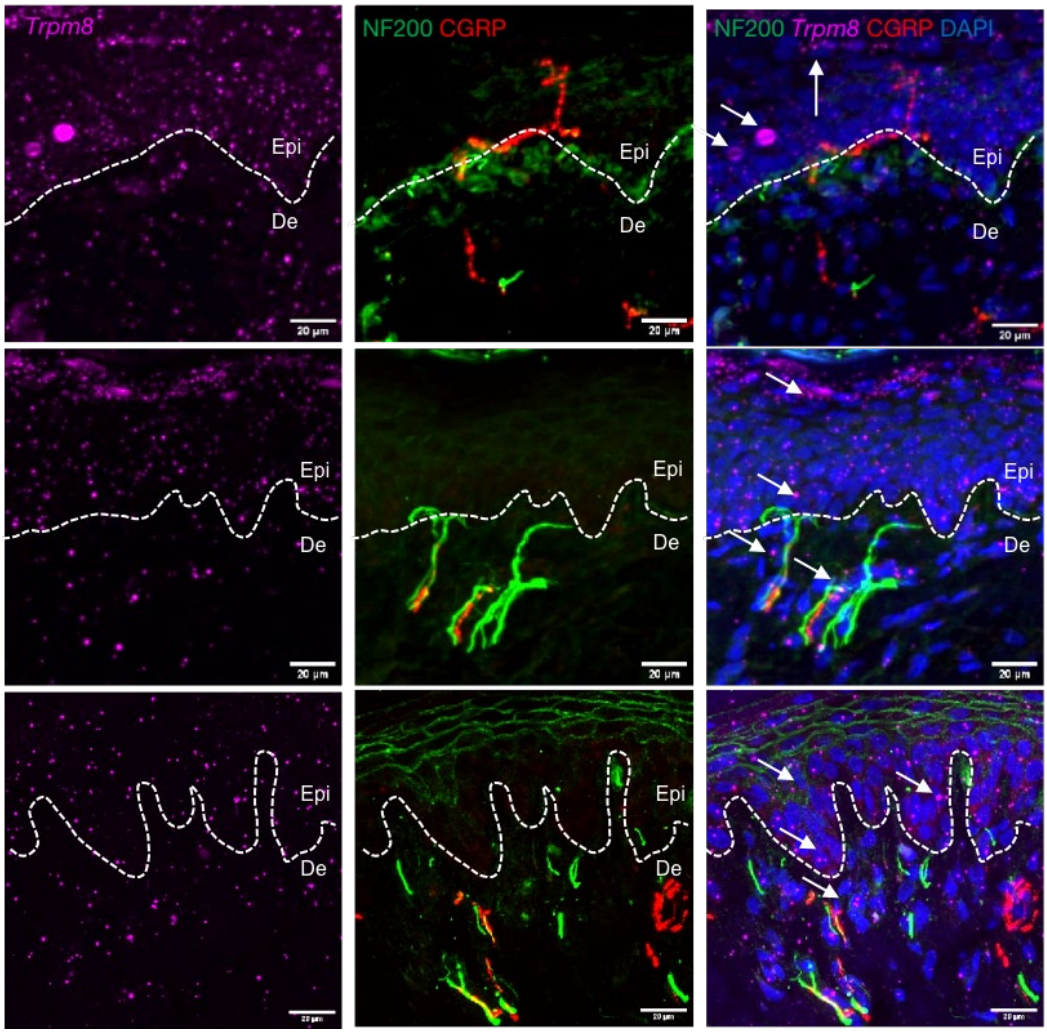

Figure 21. Representative *Trpm8* RNAScope staining images of adult NM-R glabrous skin. High-resolution RNAScope staining images reveal the expression patterns of *Trpm8* mRNA within the NM-R skin. Each magenta puncta (white arrow) may indicate one RNA molecule bound to the *Trpm8* probe. Nuclei are stained with DAPI (blue). Two nerve markers NF200 and CGRP are indicated in green and red, respectively. The dashed white line delineates the boundary between the epidermis and dermis, serving as a reference for the anatomical context of the molecular signals. Epi: Epidermis, De: Dermis. NM-R *Trpm8* probe design was base on XM_021247317.1 (1510 – 2485) from NCBI. Scale bar: 20 µm.

To extend these findings, we performed immunofluorescence staining with NF200 (Figure 22). These images clearly demonstrated that certain nerve fibers within the skin exhibited double expression of TRPM8 (in red) and NF200 (in green). The zoomed-in view revealed a specific structure labeled for TRPM8 protein in NM-R glabrous skin (Figure 22G-I). The co-expression of NF200 and TRPM8 was not uniformly distributed across all nerve fibers, as highlighted by the arrows.

Trpm8-positive epidermal cells observed with RNAscope were not detected in antibody-based immunofluorescence, while TRPM8-labeled structures identified by immunofluorescence were absent in RNAscope. This suggests that although some epidermal cells express *Trpm8* RNA, they may not produce detectable protein levels. Conversely, nerve fibers expressing TRPM8 protein were not identified by RNAscope, indicating a lack of RNA transport to the nerve endings, which is considered normal.

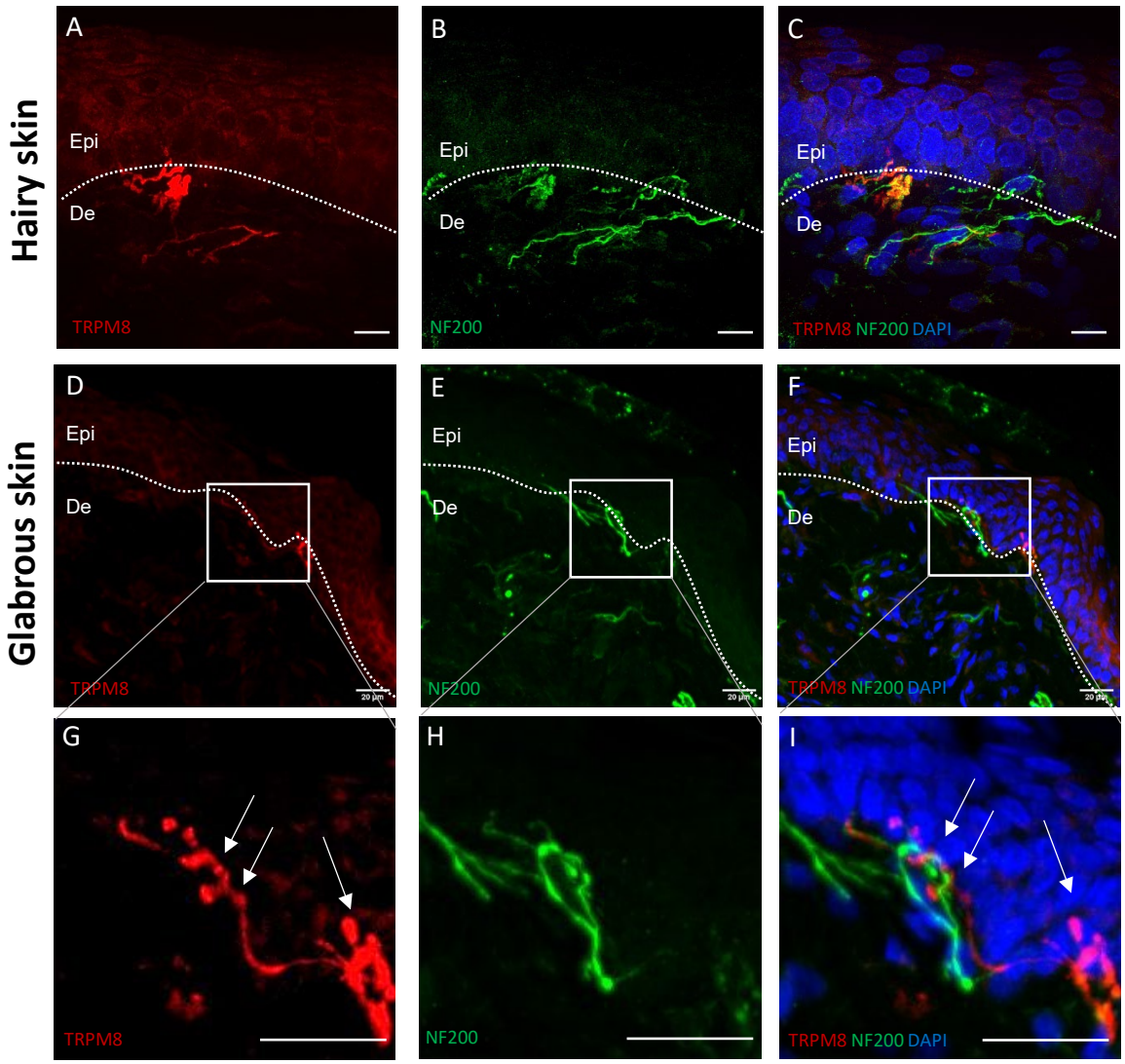

Figure 22. Representative immunofluorescence staining of TRPM8 and NF200 in NM-Rs hairy and glabrous skin.
(A, D). Staining of TRPM8 in the NM-Rs hairy and glabrous skin, respectively. (B, E) NF200 delineates the structure of myelinated nerve fibers in the skin. (C, F) Composite images showing TRPM8 and NF200 co-expression. (G-I). High magnification of the selected region in D-F, as indicated by the white box, providing a closer inspection of the labeling. Presence of TRPM8, as denoted by the white arrows, suggests specific loci of TRPM8 within the NM-R skin. TRPM8 and NF200 are indicated in red and green, respectively. The dashed white line delineates the boundary between the epidermis and dermis. Epi: Epidermis, De: Dermis. Scale bar: 20 µm.

4.2 Comparative analysis of NM-R TRPM8 and its functional sites

NM-R represents a unique species in the context of mammalian thermoregulation, largely due to its apparent inability to perform thermogenesis. This raises questions about the sensory mechanisms underlying this trait, particularly the role of TRPM8 protein, which is known to be a critical sensor for cold stimuli. Section 3.1 have confirmed the expression of TRPM8 in the DRGs, spinal cord, and skin of NM-R, indicating that TRPM8 is present in the peripheral and central nervous system (CNS).

4.2.1 Comparison of Naked mole-rat TRPM8 protein with its orthologs

To elucidate the functional role of TRPM8 in NM-R, we conducted a comprehensive analysis of the TRPM8 protein sequence in NM-R and compared it to data from over thirty species, including cold-blooded species such as fish and frog, available in the NCBI protein database. TRPM8 sequences from human (*Homo sapiens*), mouse (*Mus musculus*), rat (*Rattus norvegicus*), thirteen-lined ground squirrel (*Ictidomys tridecemlineatus*), golden hamster (*Mesocricetus auratus*), Chinese hamster (*Cricetulus griseus*), brandt's bat (*Myotis brandtii*), chicken (*Gallus gallus*), African clawed frog (*Xenopus laevis*), tropical clawed frog (*Xenopus tropicalis*), domestic guinea pig (*Cavia porcellus*), European rabbit (*Oryctolagus cuniculus*), Wild yak (*Bos mutus*), cattle (*Bos taurus*), dog (*Canis lupus familiaris*), rhesus monkey (*Macaca mulatta*), chimpanzee (*Pan troglodytes*), Sumatran orangutan (*Pongo abelii*), aardvark (*Orycteropus afer afer*), Yangtze River dolphin (*Lipotes vexillifer*), sperm whale (*Physeter catodon*), Cape golden mole (*Chrysochloris asiatica*), Cape elephant shrew (*Elephantulus edwardii*), crab-eating macaque (*Macaca fascicularis*), long-tailed chinchilla (*Chinchilla lanigera*), prairie vole (*Microtus ochrogaster*), star-nosed mole (*Condylura cristata*), degu (*Octodon degus*), killer whale (*Orcinus orca*), small-eared galago (*Otolemur garnettii*) and Tasmanian devil (*Sarcophilus harrisii*) were aligned and compared to NM-R TRPM8 (*Heterocephalus glaber*). This comparative approach revealed a notable extension in the N-terminal region (1-71 amino acids) of the NM-R TRPM8 protein, which showed no homologs in the corresponding region of other species (Figure 23). NM-R specific sequence extended-N-terminal part is highlighted in red). Interestingly, similar N-terminal extensions were also observed in the star-nosed mole, wild yak, frogs, and Brandt’s bat, although the amino acid sequences across these species.

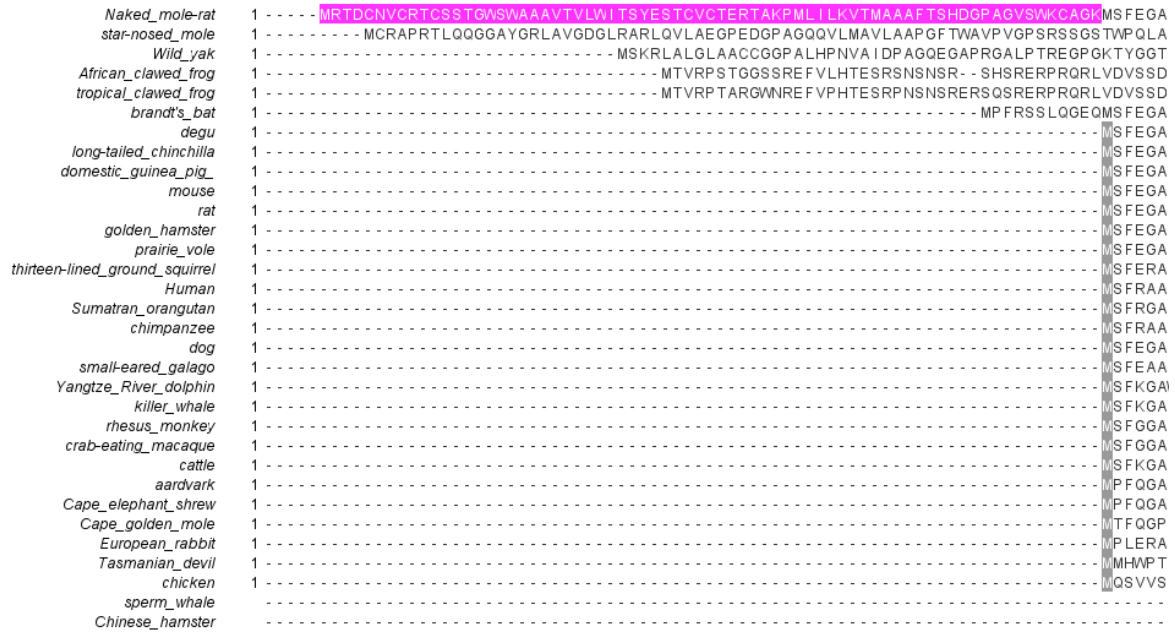

Figure 23. Comparative analysis of TRPM8 extended N-terminal sequences across diverse mammalian.
This figure illustrates a multiple sequence alignment of the extended N-terminal regions of the TRPM8 protein from 31 mammalian species, with a focus on the NM-R. The NM-R specific sequence extended-N-terminal part is highlighted in purple. The consensus start codon, a feature predominantly conserved among the examined mammals, is highlighted in gray. Sequences were aligned using Serial Cloner software.

To further investigate this, we constructed an evolutionary tree of full length TRPM8 proteins across different species, utilizing CLUSTALW. While the comparative analysis of TRPM8 revealed that several species also possess an extended N-terminal region, our evolutionary tree analysis (Figure 24) demonstrates that these species are not closely related.

NM-R belongs to the *Bathyergidae* family which comprises six genera, each showcasing distinct social structures and ecological niches (Begall et al., 2015; Cox et al., 2020; Faulkes & Bennett, 2013; Montoya-Sanhueza, Šaffa, et al., 2022). Our investigation into the TRPM8 protein sequences across various members of the *Bathyergidae* family revealed a significantly extended N-terminal region in its TRPM8 protein compared to other mole-rat species within the same family. While an extended N-terminal region is a feature shared by most *Bathyergidae* species analyzed, the length and specific amino acid composition of this region in NM-R are uniquely distinct and this extended N-terminal region in NM-R is encoded by an additional exon (Data available in NCBI: PRJNA394865). In contrast, other species, such as those from the genera *Fukomys*, *Cryptomys*, and *Georychus*, exhibit

shorter N-terminal extensions with less variation in amino acid sequences (Data available in NCBI: PRJNA394865).

4.2.2 Comparative analysis of TRPM8 functional sites in the Naked mole-rat

Following the structural overview of TRPM8 provided in the introduction (Figure 7), we performed a detailed comparative analysis to assess the conservation of functionally significant amino acids within the TRPM8 protein across multiple species, including NM-

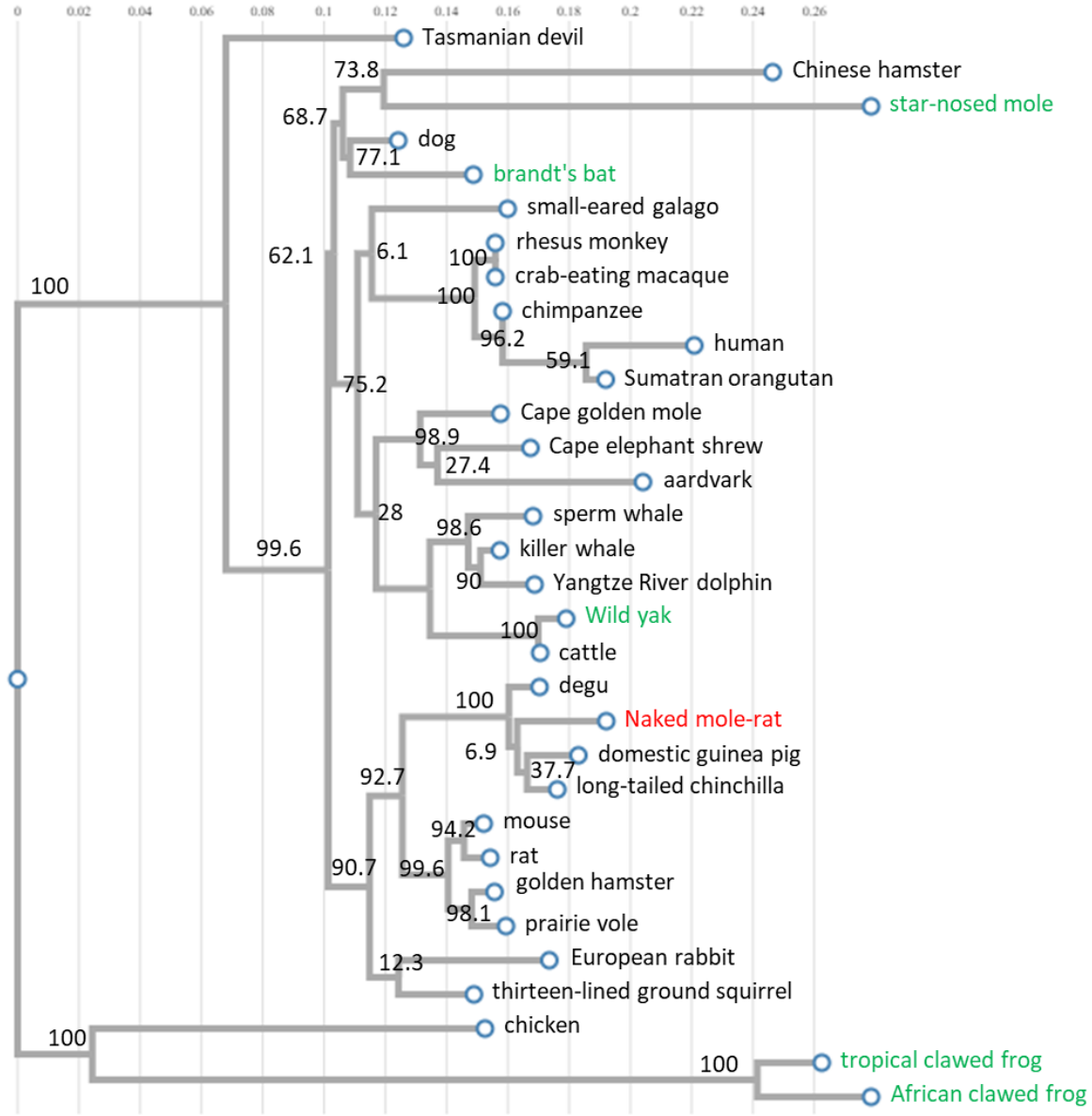

Figure 24. Phylogenic analysis of TRPM8 proteins between different species.
This tree illustrates the evolutionary relationships among TRPM8 protein sequences from various species, with branch lengths representing genetic distances. NM-R is highlighted in red. Species with extended N-terminal sequences of TRPM8, as identified in Figure 23, are marked in green. Bootstrap values at branch points indicate the statistical support for each cluster. The tree was generated using CLUSTALW.

R and other thermogenic animals. This analysis highlights the key conserved amino acids associated with the sensitivity of TRPM8 to cold, icilin, menthol, and AMTB, as well as other residues critical for its function (Plaza-Cayón et al., 2022; Yin et al., 2018, 2019, 2024) (Figure 25).

Our alignment of the TRPM8 protein sequences from NM-R, domestic guinea pig, mouse, rat, and human reveals that amino acids critical for TRPM8 function are highly conserved across all species examined (Figure 25). This is particularly evident in the following functional contexts: amino acids essential for the cold-induced activation of TRPM8 are uniformly conserved among the species studied (in blue). These residues are predominantly localized within the VSL domain (ice blue box), encompassing the S2, S3, and S4 transmembrane segments. The amino acids involved in mediating sensitivity of TRPM8 to icilin are also highly conserved across species (in pink). Similarly, amino acids responsible for the sensitivity of TRPM8 to menthol are conserved across species, with these residues being primarily localised within the TRP domain (in green).

In addition to the residues critical for cold and menthol sensitivities, amino acids associated with AMTB sensitivity, a known antagonist of TRPM8, are marked in orange. These residues are located within the VSL domain and pore region, areas essential for the interaction of TRPM8 channel with AMTB. Amino acids highlighted in red are crucial for maintaining the structural integrity and proper activation of TRPM8 channel. These residues are located primarily within the S4 and S5 transmembrane segments. Notably, these residues are not only essential for TRPM8 response to a single type of stimulus but are also critical for multiple channel functions. For instance, the serine residues S26, S27, and S29, are critical for both cold and menthol sensitivities (Rivera et al., 2021). Another key residue is tyrosine Y745, which plays a pivotal role in response to cold, menthol, and AMTB (Malkia et al., 2009). The fact that these amino acids are highly conserved across NM-R and other species examined indicates that the fundamental mechanisms by which TRPM8 responds to various stimuli may be preserved throughout evolution (Plaza-Cayón et al., 2022).

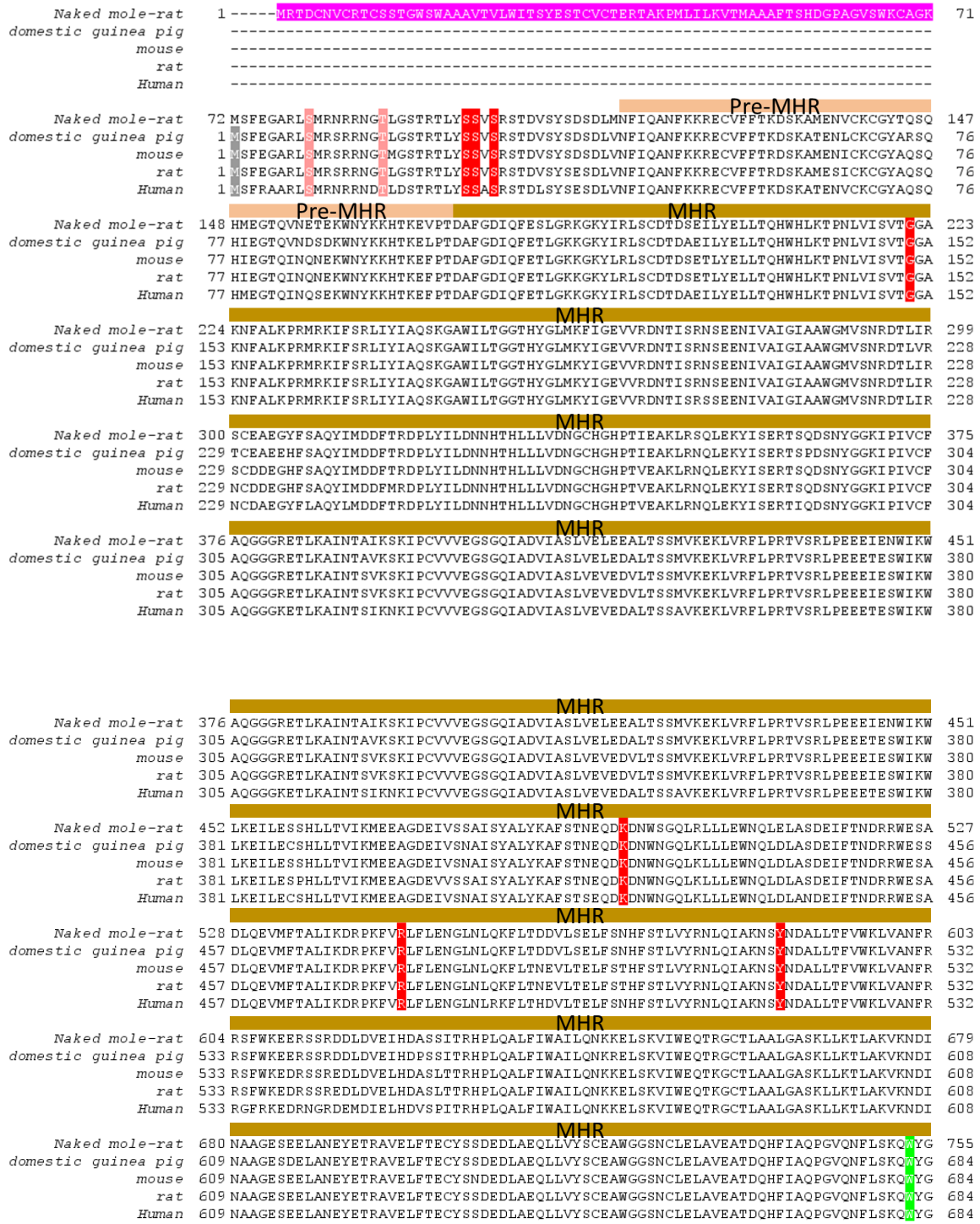
Naked mole-rat
domestic guinea pig
mouse
rat
Human
Pre-MHR
MHR

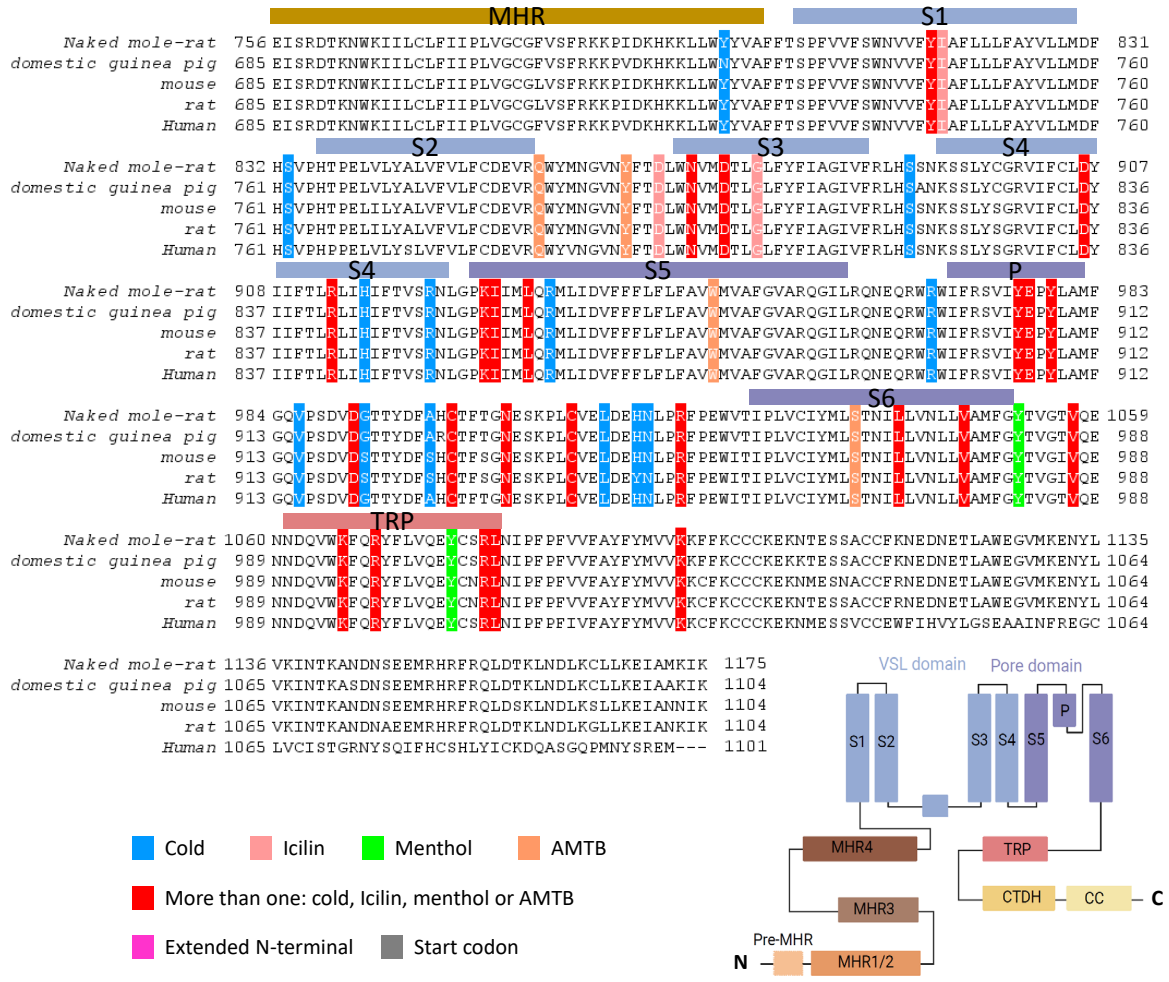

Figure 25. Comparative sequence alignment of TRPM8 channels across five species.
This figure presents a multiple sequence alignment of TRPM8 channels from five species: NM-R, domestic guinea pig, mouse, rat, and human. The alignment is color-coded to depict the conservation and variation of amino acid residues across these species. The uniquely extended N-terminal region of the NM-R TRPM8 is highlighted in purple, while the consensus start codon is marked in gray. Residues critical for TRPM8 function are color-coded based on their involvement in different sensory responses: blue for cold sensitivity, green for menthol sensitivity, pink for icilin sensitivity, and orange for AMTB sensitivity. Residues that are crucial for more than one of these functions are highlighted in red. In the lower right corner, a reduced version of Figure 7B is included for reference, illustrating the structural domains of TRPM8 to facilitate comparison with the aligned sequence segments. VSL domain: a voltage-sensor–like domain, CTDH: the C-terminal domain helix, MHR: melastatin homology region, TRP: Transient receptor potential, CC: coiled coil, P: the pore helix, S: transmembrane segment.

Although the functionally critical regions of TRPM8 are highly conserved across species, TRPM8 protein in NM-R exhibits a unique, extended N-terminal region which is absent in other species analyzed (in purple, Figure 25). The precise role of this extended N-terminal segment remains unknown since no existing studies have explored its potential influence on the functionality of TRPM8 or its contribution to the sensory adaptations observed in

NM-R. Given the distinctive nature of this N-terminal extension, further investigation is necessary to better understand its impact on the overall function of TRPM8 and to assess whether it plays a role in the thermosensory capabilities of NM-R.

4.3 Characterization of Naked mole-rat TRPM8 extended-N terminal part

In this section, we examined the presence and potential functional significance of the extended N-terminal sequences in the TRPM8 channel of NM-R. Our data have revealed that TRPM8 is more abundantly expressed in the DRGs, spinal cord, and other sensory tissues of NM-R compared to murine models. Given the critical role of TRPM8 in mediating cold sensation, we hypothesized that the extended N-terminal region of NM-R TRPM8 may enhance its cold sensitivity, thereby contributing to thermosensory adaptations.

4.3.1 Confirmation of the presence of extended N-terminal part of Naked mole-rat *Trpm8*

To confirm the presence of the extended N-terminal variant of TRPM8 in NM-R, we performed reverse transcription polymerase chain reaction (RT-PCR) using mRNA extracted from various tissues. Primers used for DNA amplification were designed to specifically target the extended N-terminal region, with forward primer 3 and reverse primer 2 (Figure 26A) chosen to generate an amplicon co-staining the extended sequence.

RT-PCR analysis successfully detected an amplicon of the expected size in multiple sensory tissues, including POA of the hypothalamus, DRG, and spinal cord (Figure 26B). Interestingly, the presence of this TRPM8 variant was also observed in non-sensory tissues such as interscapular BAT (iBAT) and skeletal muscle, suggesting a broader expression pattern of the extended TRPM8 variant than initially anticipated. In contrast, no amplification was detected in the liver or spleen, thereby confirming the tissue-specific expression of the extended N-terminal TRPM8 variant in NM-R.

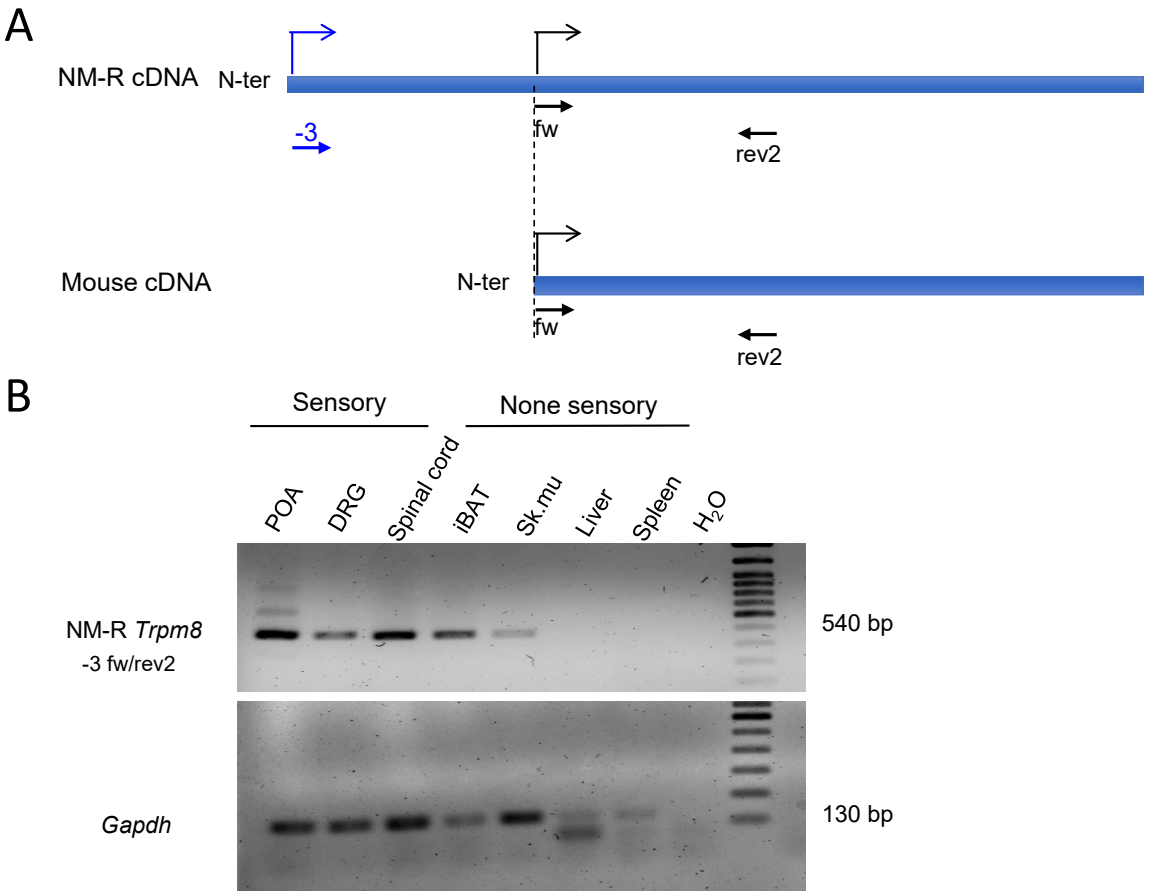

Figure 26. Expression of the extended mRNA of *Trpm8* in both sensory and none sensory tissues of NM-Rs.
(A). Primers designed for confirming the presence of the extended N-terminal part of NM-R *Trpm8*. Blue primer (-3) is specific for NM-R, black primers are common for both species (fw and rev2). (B). RT-PCR results shown for PCR run with forward primer -3 and reverse primer rev2 on sensory and none sensory tissues. Gapdh was used as housekeeping gene. DRG: dorsal root ganglion, POA: the preoptic area of the hypothalamus, iBAT: interspacular BAT, Sk.mu: skeletal muscle, fw: forward, rev: reverse. Data from Dr. V. Bégay.

4.3.2 Validation of the extended N-terminal *Trpm8* expression in Naked mole-rat DRGs

To further confirm whether the 1-71 amino acid N-terminal region exists in NM-Rs, we designed the *Ex-trpm8* probe. This probe targets the 415 – 854 bp region of NM-R *Trpm8* mRNA which only includes the 1-71 amino acid N-terminal region (Figure 12). To accurately assess the presence and distribution of this extended sequence in NM-R DRGs, we employed the *Ex-trpm8* probe with the canonical *Trpm8* probe (called *Trpm8*$^{+}$) annealing *Trpm8* mRNA downstream of the common start codon found in all species.

The staining patterns in the DRGs revealed a robust expression of *Trpm8* transcripts, consistent with our earlier observations (Section 3.1.1). Red color marks the presence of the canonical *Trpm8* mRNA as detected by the *Trpm8*, while cyan color corresponds to the *Ex-trpm8*. Overlay of these images demonstrates co-localization of the two signals (Figure 27A and B, right panel), where neurons expressing both the canonical and extended *Trpm8* transcripts appear in a light purple. However, distinct populations of neurons expressing either only $Trpm8^{+}$ or $Ex\text{-}trpm8^{+}$ were also observed.

Quantitative analysis revealed two distinct populations of neurons based on their probe labeling. On average, 62.81% of neurons expressed both *Trpm8* and *Ex-trpm8* forming the largest subpopulation across all three neuron types (Figure 27C, in light pink). $Trpm8^{-}$ $Ex\text{-}trpm8^{+}$ neurons (expressing only the extended variant) represented the second-largest group, comprising an average of 28.09% of neurons (Figure 27C, in cyan). $Trpm8^{+}$ $Ex\text{-}trpm8^{-}$ neurons (expressing only the canonical *Trpm8*) were the smallest group, constituting only 9.1% of the total neuron population (Figure 27C, in red). These data confirm the existence of the extended N-terminal RNA variant in NM-R DRG neurons. Surprisingly, $Trpm8^{-}$ $Ex\text{-}trpm8^{+}$ neruons were found, suggesting the presence of an isoform missing the sequence recognised by the canonical *Trpm8* probe. Note that $Trpm8^{+}$ $Ex\text{-}trpm8^{+}$ neurons express either the canonical *Trpm8* isoform and the extended isoform or only the extended isoform.

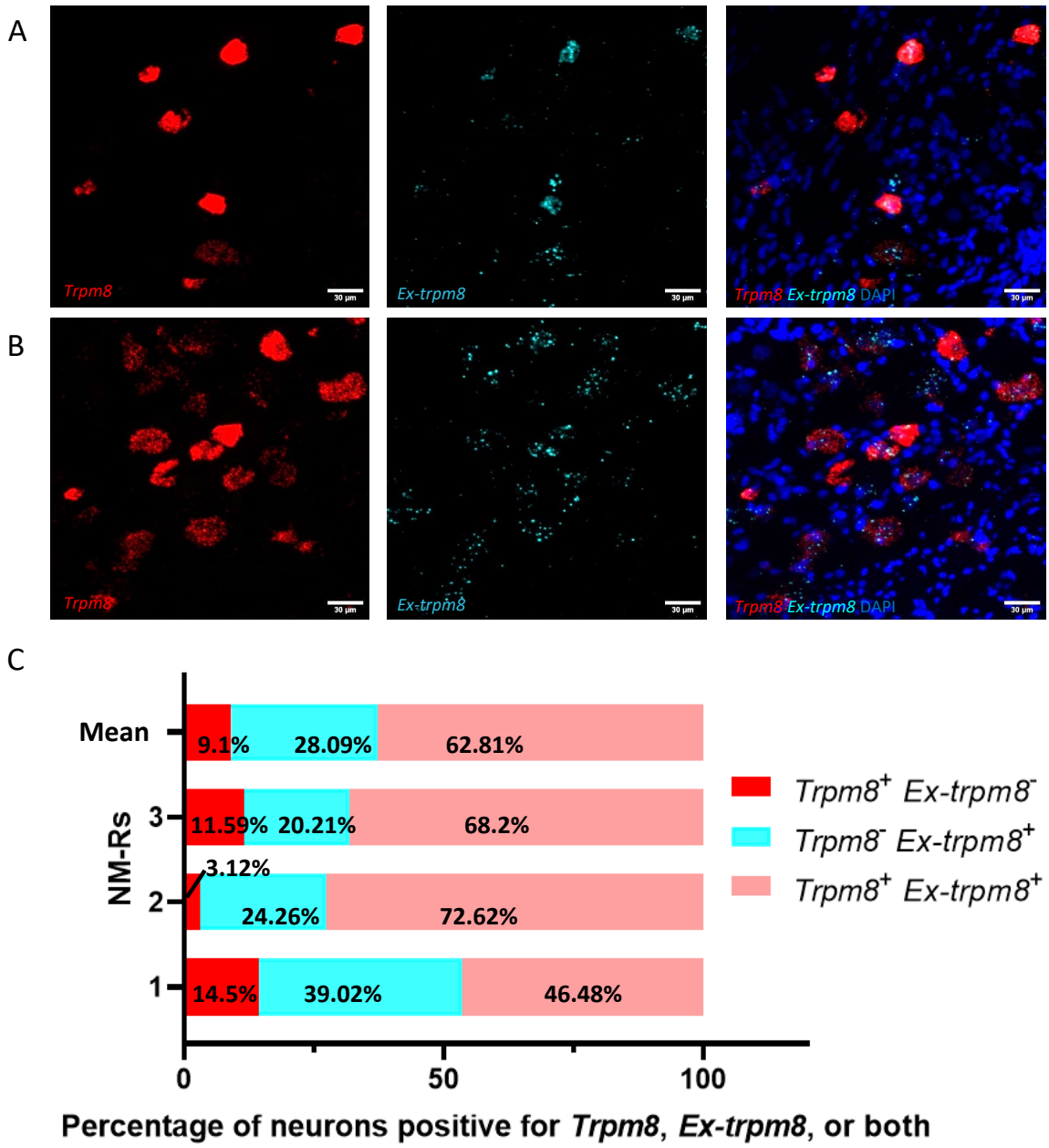

Figure 27. RNAScope staining of the NM-R lumbar DRGs with *Trpm8* and *Ex-trpm8*.
(A-B). Representative images of the different lumbar DRGs. *Trpm8* is indicated in red, and *Ex-trpm8* probe is indicated in cyan. Nuclei are stained with DAPI (blue). Scale bar: 30 µm. (C). Bar graph displaying the percentage of neurons positive for *Trpm8*, *Ex-trpm8*, or both in NM-R lumbar DRGs. The red portion represents neurons positive for *Trpm8* but negative for *Ex-trpm8* (*Trpm8*$^{+}$ *Ex-trpm8*$^{-}$), the cyan portion represents neurons positive for *Ex-trpm8* but negative for *Trpm8* (*Trpm8*$^{-}$ *Ex-trpm8*$^{+}$), and the light pink portion represents neurons positive for both probes (*Trpm8*$^{+}$ *Ex-trpm8*$^{+}$). In the mean analysis across three NM-R samples, 62.81% of neurons co-labeled both *Trpm8*$^{+}$ *Ex-trpm8*$^{+}$, 28.09% expressed only *Ex-trpm8*$^{+}$, and 9.1% expressed only *Trpm8*$^{+}$. More than 2000 neurons were counted across three NM-R samples.

4.3.3 Assessment of the extended N-terminal of Naked mole-rat TRPM8 in HEK293T cells via RNAscope

To investigate the potential functional implications of the extended N-terminal region in NM-R TRPM8, we hypothesized that this extended region might modulate the channel's cold sensitivity, thus potentially altering the temperature range for cold perception or even diminishing the cold-sensing capability of NM-R. To test this hypothesis, full length NM-R TRPM8 and mouse TRPM8 were ectopically expressed in HEK293T cells. Each construct had an IRES followed by a Enhanced Green Fluorescent Protein (EGFP) sequence included to facilitate the visualization of transfection efficiency and confirm protein expression through fluorescence imaging. Successful expression of the NM-R TRPM8 construct was indicated by green fluorescence from the EGFP tag which confirmed an effective transfection. Red fluorescence signal marked the presence of TRPM8 protein, as detected by a specific antibody target TRPM8. Co-localization of GFP and TRPM8 signals, along with DAPI-stained nuclei, confirmed that NM-R TRPM8 was successfully expressed in the transfected cells (Figure 28A). A similar pattern was observed in HEK293T cells transfected with mouse TRPM8, providing a further validation about the transfection and expression of the mouse TRPM8 construct (Figure 28B).

Next, we utilized *Trpm8* and *Ex-trpm8* probe, on HEK293T cells transfected with full length NM-R TRPM8 and mouse TRPM8 to detect the presence of the extended sequence *in vitro*. Although the specificity of this probe had not been fully validated in NM-R DRGs, the strong expression of TRPM8 in NM-R sensory tissues warranted its application in this context. Cyan staining from the *Ex-trpm8* probe in HEK293T cells transfected with NM-R TRPM8 confirmed the presence of the extended N-terminal region. No *Ex-trpm8* signal was detected in cells transfected with mouse TRPM8, demonstrating the specificity of the probe for the NM-R TRPM8 extended N-terminal sequence (Figure 28C and D).

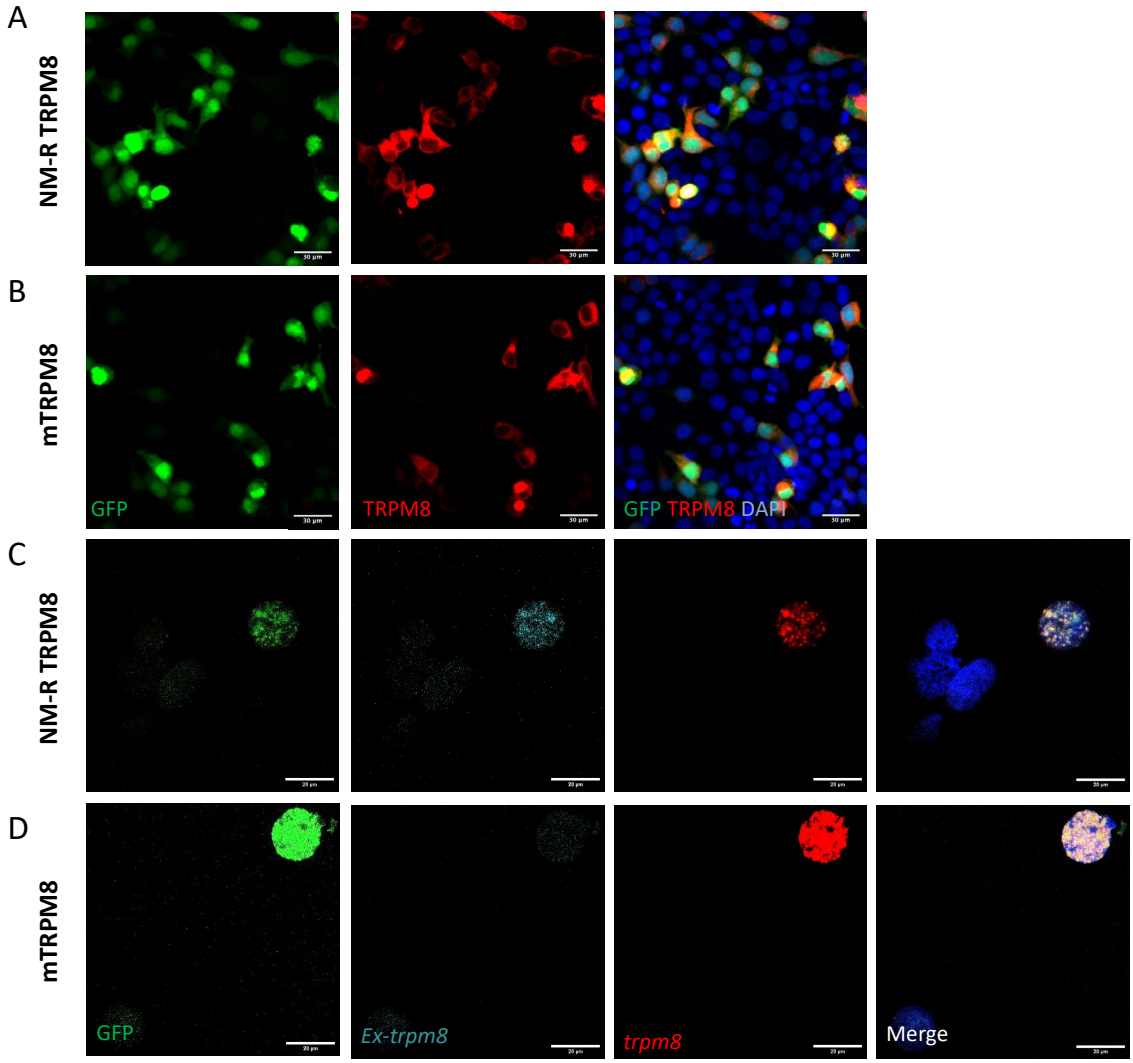

Figure 28. Expression of TRPM8 and the extended N-terminal in HEK293T cells transfected with the NM-R TRPM8 and mouse TRPM8 construct.
(A-B). HEK293T cells transfected with NM-R TRPM8 (NM-R full length TRPM8) and mouse TRPM8 constructs, with GFP (green) indicating successful transfection, TRPM8 protein (red), and DAPI-stained nuclei (blue). Merged images demonstrate co-localization of these signals. (C-D). HEK293T cells transfected with NM-R TRPM8 and mouse TRPM8 constructs, with *Trpm8* (red) identifying *Trpm8* and *Ex-trpm8* (cyan) identifying the extended N-terminal region specifically in NM-R TRPM8-transfected cells, while *Trpm8* (red) marks *Trpm8* mRNA. (C). GFP confirms transfection, with no *Ex-trpm8* signal detected in mouse TRPM8-transfected cells (D). The merged images include all markers: GFP, *Ex-trpm8*, *Trpm8*, and DAPI. Scale bars: 20 µm (C, D); 30 µm (A, B).

4.4 The physiological properties of Naked mole-rat TRPM8 using calcium imaging

Before conducting functional analysis of TRPM8 constructs, we assessed the transfection efficiency across the different plasmids used in HEK293 cells. Transfection efficiency was found to be comparable across all constructs, with no significant variation in the efficiency of TRPM8 expression. Notably, NM-R full length TRPM8 consistently demonstrated slightly higher transfection efficiency compared to the other constructs. This observation was consistent across multiple independent transfection experiments, ensuring that the subsequent functional assays were not biased by differences in expression levels between the constructs.

In the subsequent experiments, HEK293 cells transfected successfully with TRPM8 constructs were examined using calcium imaging assays. These assays elucidate the physiological functions of TRPM8 under various experimental conditions. Calcium imaging serves as an invaluable methodology for assessing the activation of ion channels like TRPM8, wherein activation is marked by a calcium ion influx that can be detected through fluorescent calcium indicators. Upon channel activation by cold temperatures or specific chemical agonists, a notable augmentation in the intracellular calcium levels will be observed, manifesting as an enhanced fluorescence signal. Given the critical role of TRPM8 in mediating cold sensation, we propose that the extended N-terminal region may affect the cold sensitivity of NM-R TRPM8, potentially contributing to specialized thermosensory adaptations in NM-Rs. By exposing the transfected HEK293 cells to different stimulations and monitoring the subsequent calcium influx under these different conditions, we evaluated the sensitivity and functional thresholds of the various TRPM8 constructs.

4.4.1 The physiological properties of mouse TRPM8 in HEK293 cells

Being a control construct, mouse TRPM8 is known for its distinct activation threshold, therefore providing comparative data to evaluate species-specific differences in channel behavior. The structure of mouse TRPM8 highlights its transmembrane domains and intracellular regions, and this is shown in the first panel of the figure (Figure 29A). This schematic serves as a reference for understanding the functional regions of the channel.

Dynamic calcium responses in cells expressing mouse TRPM8 when subjected to varying temperature conditions are depicted in the subsequent panel (Figure 29A). Fluorescence intensity over time in HEK293 cells expressing mouse TRPM8 is shown when exposed to a

series of temperature changes, along with the applications of 200 μM menthol and 10 μM icilin, both of which are agonists of TRPM8. The colored traces represent individual cells and display a marked increase in the intracellular calcium levels, as indicated by the Fura-2 ratio upon stimulation. This phenomenon is consistent with the activation of TRPM8 channels in response to the temperature drop and the application of TRPM8 agonists. The temperature profile, represented by the lower black trace, is synchronized with the fluorescence data, demonstrating that TRPM8 channel activation is tightly coupled with temperature shifts within the defined activation threshold of mouse TRPM8 (< 26°C).

Quantification of the intracellular calcium responses under different conditions is provided in the final panel (Figure 29A). In this analysis, the ΔFura-2 ratio, representing the change in fluorescence intensity, was plotted for various experimental conditions: baseline (Base), cold stimulation (Cold), menthol stimulation (Menthol), icilin stimulation (Icilin), and a combination of icilin with cold (Icilin+cold). Analysis showed that all stimuli (Cold, Menthol, Icilin, and Icilin+cold) resulted in significantly higher ΔFura-2 ratios compared to the baseline condition (Figure 29A). Moreover, comparison between the cold stimulation alone and the combination of cold and icilin also revealed significant difference ($p < 0.001$), indicating a potent synergistic effect when these stimuli were combined. Additionally, the condition involving icilin alone was significantly different compared to the combination of icilin and cold ($p < 0.01$), further emphasizing the enhanced activation of mouse TRPM8 when both thermal and chemical stimuli were applied together.

The robust increase in intracellular calcium levels upon menthol and icilin application confirms the functionality of mouse TRPM8 in the HEK293 cells. This control experiment establishes a baseline for comparison with NM-R TRPM8, allowing for the identification of any unique activation characteristics that may be present in the NM-R TRPM8.

4.4.2 The physiological properties of NM-R TRPM8 in HEK293 cells

Next, we characterized the functional properties of NM-R full length TRPM8. The structure of the NM-R full length TRPM8 is presented to illustrate the functional regions of the channel (Figure 29B, left panel). Calcium imaging results provide insight into channel activation by thermal and chemical stimuli (Figure 29B, middle panel). Compared to mouse TRPM8, NM-R TRPM8 exhibited a notably blunted response to cold, 200 μM menthol, and 10 μM icilin stimulations. The colored traces represent individual cells and display minimal increases in intracellular calcium levels, as indicated by the Fura-2 ratio, upon stimulation. However, a

subtle response could be observed when 10 μM icilin was applied in combination with cold, though it remained markedly weaker than that of mouse TRPM8.

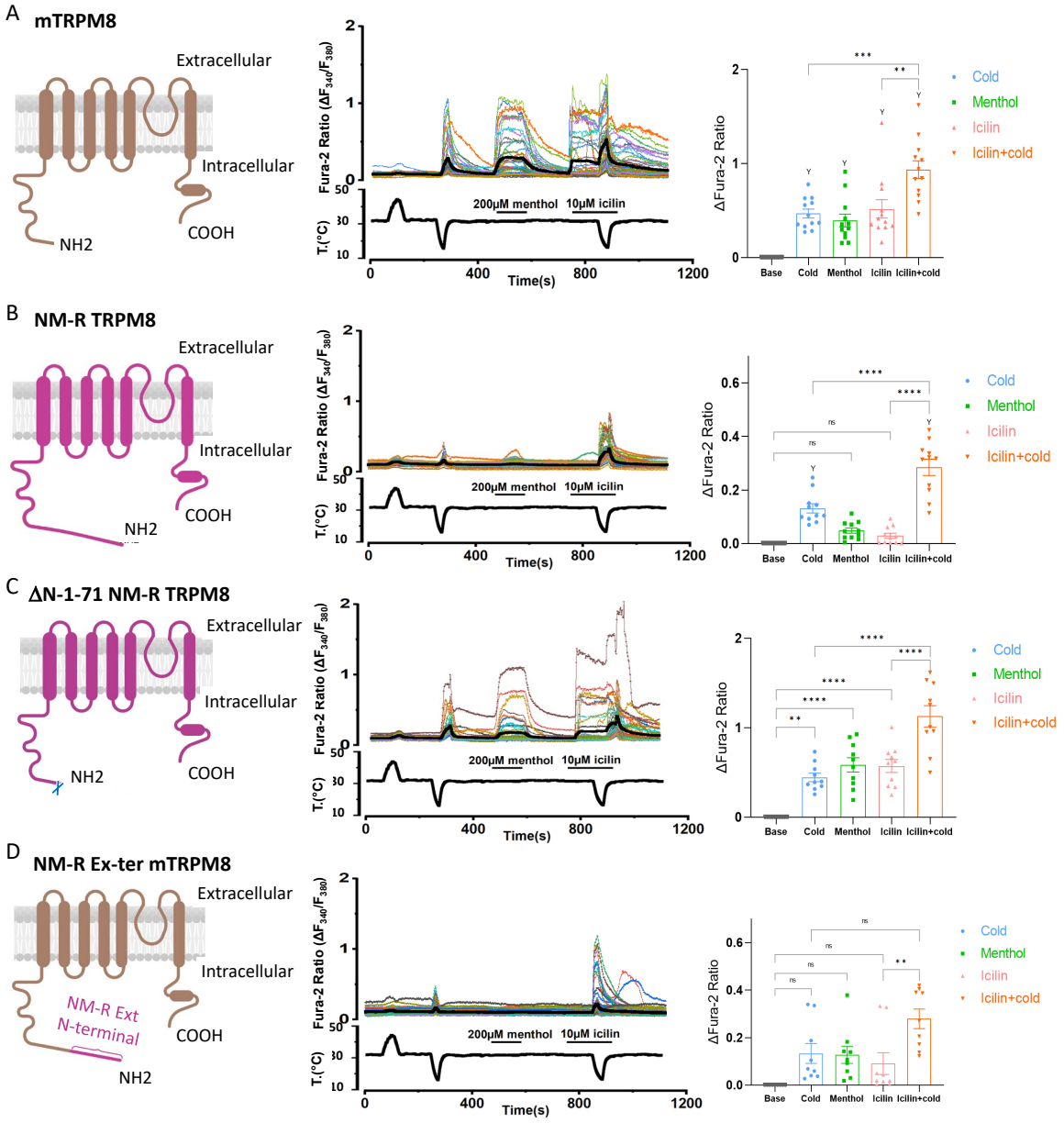

Figure 29. Functional calcium imaging shows calcium responses to cold and chemical stimuli within HEK293 cells overexpressing various mouse and NM-R TRPM8 constructs.
(A). Schematic representation of the mouse TRPM8 channel is shown in the left panel. In the middle panel, traces illustrate intracellular calcium levels (Fura-2 ratio) from HEK293 cells overexpressing mouse TRPM8 and subjected to warm, cold, 200 μM menthol, 10 μM icilin and cold+icilin. Colored traces depict the temporal responses of individual GFP- positive cells, while the black line represents the mean response across all cells. Bar graph in the right panel summarizes ΔFura-2 ratios under the above-described stimuli. (B). Schematic representation of NM-R TRPM8 (NM-R full length TRPM8, left panel). Middle panel: calcium imaging data from HEK293 cells overexpressing NM-R TRPM8 treated as in (A). Right panel: bar graph summarizes ΔFura-2 ratios for each condition. (C). Left panel: schematic representation of the ΔN-1-71 NM-R TRPM8 construct missing the first 1-71 aa of the N-terminal regions. The accompanying trace illustrates intracellular calcium levels from HEK293 cells exposed to the same conditions as in (A). Bar histogram in the third column provides a summary of ΔFura-2 ratios for each stimulation condition. (D). Structure of the NM-R Nter-mTRPM8 construct, where the NM-R extended N-terminal is fused to the mouse TRPM8, is depicted. Calcium imaging results show intracellular calcium levels in HEK293 cells transfected

with Nter-mTRPM8 under identical conditions. Bar histogram in the third column summarizes ΔFura-2 ratios, reflecting the intracellular calcium responses under different stimulation conditions. All experiments included at least eight transfected coverslips per group (n > 8). Statistical significance levels are indicated as follows: $**p < 0.01$, $***p < 0.001$, $****p < 0.0001$. NS: non-significant. Symbol 'Y' indicates a significant difference ($p < 0.0001$) compared to the baseline. All statistical analyses were performed using Tukey's multiple comparisons test.

In the final panel (Figure 29B, right panel), quantification of these responses is presented as ΔFura-2 ratio under different conditions. NM-R TRPM8 exhibited a modest but statistically significant increase in the ΔFura-2 ratio under cold stimulation when compared to the baseline condition ($p < 0.0001$). However, neither menthol nor icilin application alone produced a significant increase in the intracellular calcium levels compared to the baseline (NS). The combination of icilin with cold, however, did result in a significant response, as illustrated by a marked increase in the ΔFura-2 ratio compared to both the baseline ($p < 0.0001$) and individual cold stimulation ($p < 0.0001$) and icilin stimulation ($p < 0.0001$).

Overall, compared to mouse TRPM8, NM-R full length TRPM8 shows a very poor response to cold, 200 μM menthol, or 10 μM icilin stimulation. However, responses can be observed when 10 μM icilin is combined with cold stimuli.

4.4.3 Investigating the impact of Naked mole-rat TRPM8 extended N-terminal

To further investigate whether the presence of the extended N-terminal region affects the functionality of NM-R TRPM8, we further expanded our earlier findings (Section 3.2). It has been suggested that this extended N-terminal region is unique to NM-R TRPM8, and aside from this extension, other amino acid sequences are highly conserved. We hypothesized that the extended N-terminal part can potentially have impact on the function of NM-R TRPM8 such as modifying the cold reception temperature range of NM-R or ablating NM-R TRPM8 cold activation. To address this question, we then created constructs: ΔN-1-71 NM-R TRPM8 and NM-R Nter-mTRPM8. The ΔN-1-71 NM-R TRPM8 construct involves the deletion of the extended N-terminal region from NM-R TRPM8, while NM-R Nter-mTRPM8 expresses the NM-R full length TRPM8 extended N-terminal (N-1-71) fused to the N-ter of the mouse TRPM8.

We proceeded with calcium imaging to evaluate the functional properties of the ΔN-1-71 NM-R TRPM8 and NM-R Nter-mTRPM8 constructs. These results were compared with those of NM-R TRPM8 and mouse TRPM8 to determine the role of the extended N-terminal region (N-

1-71). A schematic illustrating the deletion of the N-terminal region in ΔN-1-71 NM-R TRPM8 construct is provided (Figure 29C, left panel). The intracellular calcium levels, as indicated by the Fura-2 ratio, in HEK293 cells transfected with ΔN-1-71 NM-R TRPM8, are shown under various conditions (Figure 29C, middle panel). Fluorescence response in ΔN-1-71 NM-R TRPM8 transfected cells was markedly increased compared to the NM-R full length TRPM8 (Figure 29B).

In the final panel (Figure 29C, right panel), ΔFura-2 ratio was quantitatively analyzed under different conditions: baseline, cold stimulation, menthol stimulation, icilin application stimulation, and the combination of icilin with cold ($p < 0.001$). Besides, the figure revealed several significant findings compared to the NM-R full length TRPM8. Menthol stimulation resulted in a greater increase in the ΔFura-2 ratio compared to the baseline (Y, $p < 0.0001$; the symbol 'Y' indicates a significant difference compared to the baseline, with $p < 0.0001$). Icilin stimulation showed a similar response, with a significant increase in calcium influx compared to the baseline condition (Y, $p < 0.0001$). The combination of icilin with cold resulted in the greatest increase in the ΔFura-2 ratio which was significantly greater than icilin and cold stimulation alone ($p < 0.0001$).

Next, a schematic of the extended N-terminal from NM-R full length TRPM8 fused mouse TRPM8 is presented (Figure 29D, left panel). The intracellular calcium levels in HEK293 cells transfected with the NM-R Nter-mTRPM8 construct are shown (Figure 29D, middle panel). The response to cold and chemical stimuli was significantly reduced compared to the native mouse TRPM8, indicating that the addition of the NM-R extended N-terminal diminished channel sensitivity. This sensitivity reduction suggests that the NM-R N-terminal addition impairs the functional response of mouse TRPM8 to stimuli that normally elicit robust calcium influxes.

In the final panel (Figure 29D, right panel), ΔFura-2 ratio was quantitatively analyzed under different conditions. We found cold stimulation led to a slight increase in the ΔFura-2 ratio compared to baseline, but this change was not statistically significant (NS), indicating a reduced cold sensitivity in the NM-R Nter-mTRPM8 construct. Menthol stimulation similarly did not result in a significant increase in calcium influx compared to the baseline condition (NS). Icilin stimulation showed a small increase in the ΔFura-2 ratio, but this was also not statistically significant compared to baseline (NS). The combination of icilin with cold resulted in the most substantial response, with a significant increase in the ΔFura-2 ratio compared to baseline ($p <$

0.0001) and Icilin stimulation alone ($p < 0.01$). However, this response was still significantly lower than what is typically observed with native mouse TRPM8.

Overall, the deletion of the extended N-terminal restores the responsiveness of NM-R TRPM8 to cold and chemical stimuli, and the addition of the NM-R extended N-terminal to mouse TRPM8 diminishes its sensitivity.

4.4.4 Comparative analysis of TRPM8 constructs in HEK293 cells

To explore species-specific differences in TRPM8 function, we compared the responses of mouse TRPM8 and NM-R full length TRPM8 when subjected to thermal and chemical stimuli. ΔFura-2 ratio was analyzed under various conditions including cold stimulation, menthol application, icilin application, and a combination of icilin with cold (Figure 30A). The results revealed significant differences between the channels of both species for all conditions. For mouse TRPM8, a substantial increase in intracellular calcium levels was observed in response to cold, menthol, and icilin, with the response being most pronounced when icilin was combined with cold. In contrast, NM-R full length TRPM8 displayed a significantly blunted response, with only a minor increase in the ΔFura-2 ratio, primarily when icilin and cold were applied together. Statistical analysis confirmed these differences, highlighting the reduced sensitivity of NM-R TRPM8 compared to mouse TRPM8, with *p*-values indicating significant disparities (**$p < 0.01$, ****$p < 0.0001$).

To investigate the role of the extended N-terminal region in NM-R TRPM8, we compared the ΔN-1-71 NM-R TRPM8 construct, which lacks this region, to the full length NM-R TRPM8 (Figure 30B). ΔN-1-71 NM-R TRPM8 construct exhibited a significantly enhanced response to all stimuli compared to the full length version. This was particularly evident with icilin and the combination of icilin with cold, where the ΔN-1-71 NM-R TRPM8 showed a markedly higher increase in the intracellular calcium levels. Deletion of the extended N-terminal region restored channel responsiveness, bringing it closer to the levels observed in mouse TRPM8. Statistical analysis confirmed these findings, with highly significant differences observed across all conditions (***$p < 0.001$, ****$p < 0.0001$) that strongly hinted towards the critical role of the extended N-terminal region in NM-R TRPM8 in modulating channel sensitivity to thermal and chemical stimuli.

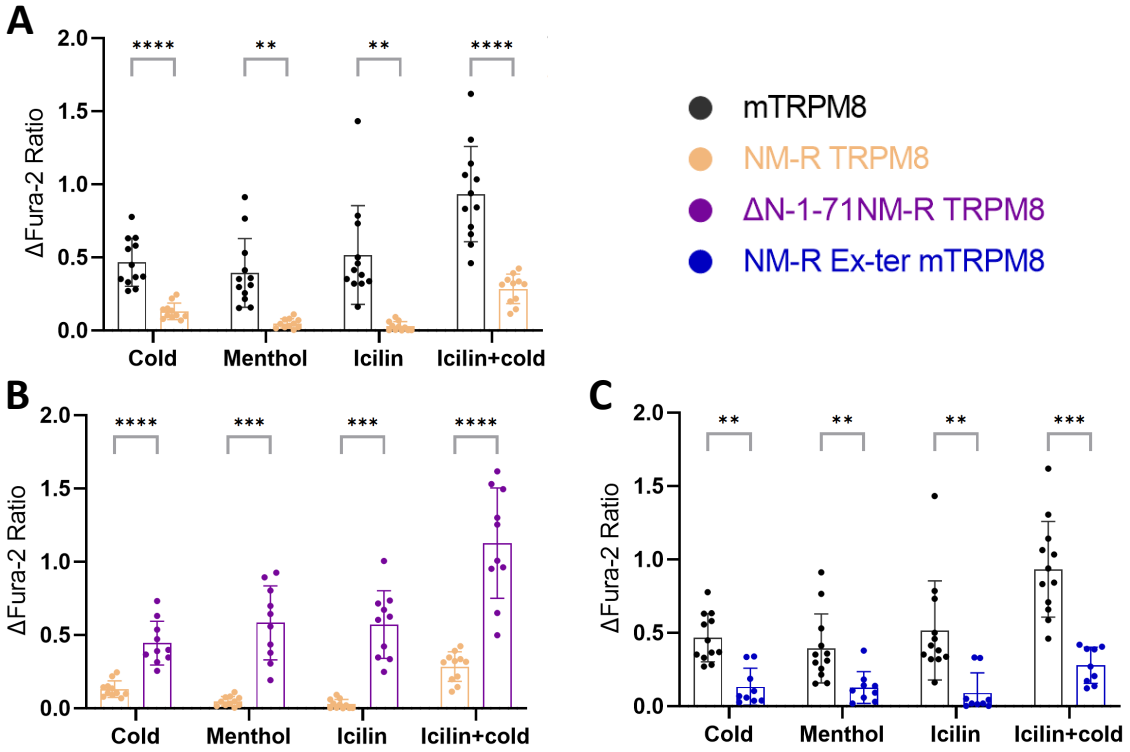

Figure 30. The unique N-terminal 1-71 aa of NM-R TRPM8 inhibits the function of mouse and NM-R TRPM8 channels,
(A-C). Comparative analysis of the ΔFura-2 ratio responses in HEK293 cells overexpressing different TRPM8 constructs. Constructs include mouse TRPM8 (black bar), NM-R TRPM8 (NM-R full length TRPM8, orange bar), ΔN-1-71 NM-R TRPM8 (purple bar), and NM-R Ex-ter mTRPM8 (blue bar). Cells were exposed to the following stimuli: cold, 200 µM menthol, 10 µM icilin, and a combination of 10 µM icilin with cold. (A). Comparison between mouse TRPM8 and NM-R TRPM8. ΔFura-2 ratios highlight significant differences in sensitivity between the two channels across all stimuli. (B). Comparison between ΔN-1-71 NM-R TRPM8 and NM-R TRPM8. Deletion of the extended N-terminal region (ΔN-1-71) significantly enhances the responsiveness of channel to all stimuli compared to the NM-R full length TRPM8. (C). Comparison between NM-R Ex-ter mTRPM8 and mouse TRPM8. Addition of the NM-R extended N-terminal to mouse TRPM8 (Ex-ter mTRPM8) results in a significantly diminished response to all stimuli compared to the native mouse TRPM8. All experiments included at least eight transfected coverslips per group ($n > 8$). Statistical significance is denoted as follows: $^{**}p < 0.01$, $^{***}p < 0.001$, $^{****}p < 0.0001$. All statistical analyses were performed using Tukey's multiple comparisons test.

Further analysis was conducted to determine the impact of adding the NM-R extended N-terminal to mouse TRPM8 (NM-R Nter-mTRPM8) compared to the native mouse TRPM8 (Figure 30C). NM-R Nter-mTRPM8 construct demonstrated a significantly blunted response to all stimuli compared to native mouse TRPM8. This reduction in responses was particularly pronounced during cold and icilin stimulation, in which the NM-R extended N-terminal substantially reduced the activity of channel. Statistical analysis confirmed significant differences between NM-R Nter-mTRPM8 and mouse TRPM8 under all conditions tested (**p

< 0.01, $***p < 0.001$). These findings suggest that the NM-R extended N-terminal, when fused to mouse TRPM8, impairs the normal functionality of channel, leading to diminished sensitivity to both thermal and chemical stimuli.

4.4.5 Percentage of TRPM8-transfected HEK293 cells responding to different stimuli

Following our experimental assays, it became evident that a significant proportion of HEK293 cells transfected with NM-R TRPM8 exhibited no detectable response to cold. This observation prompted a more detailed statistical analysis on the calcium imaging data, with a specific aim to quantify the proportion of GFP-positive cells that responded to each stimulus (Figure 31). This analysis provided a clearer understanding of the functional efficacy of each TRPM8 construct. The vertical axis represented the percentage of responding cells within the transfected HEK 293cells, thereby highlighting the relative activity of each construct under different conditions as previously shown.

Cold stimuli (Figure 31A) revealed that GFP-positive HEK293 cells transfected with mouse TRPM8 (48.22 ± 3.82%) and ΔN-1-71 NM-R TRPM8 (57.86 ± 5.19%) demonstrated significantly higher responses compared to cells expressing NM-R TRPM8 (15.32 ± 2.25%) and Nter-mTRPM8 (14.74 ± 1.10%). This suggests a robust cold sensitivity in the mouse TRPM8 and ΔN-1-71 NM-R TRPM8 constructs.

Mouse TRPM8 showed the highest response to menthol stimulation (48.51 ± 3.92%), and this aligned with its established activation profile. In contrast, NM-R TRPM8 exhibited a significantly diminished response (7.64 ± 1.52%). The ΔN-1-71 NM-R TRPM8 construct elicited a response similar to that of mouse TRPM8 (56.81 ± 6.11%), while the NM-R Nter-mTRPM8 construct showed a reduced response (9.99 ± 1.30%) (Figure 31B).

Icilin (10 μM) stimulation (Figure 31C) followed this trend, with transfection using mouse TRPM8 exhibited the highest responsiveness (39.85 ± 3.74%). NM-R TRPM8 demonstrated a markedly lower response (4.12 ± 0.93%), whereas ΔN-1-71 NM-R TRPM8 transfection showed a higher response (54.51 ± 7.20%). The NM-R Nter-mTRPM8 construct again showed a lower response than mouse TRPM8 (7.34 ± 1.56%).

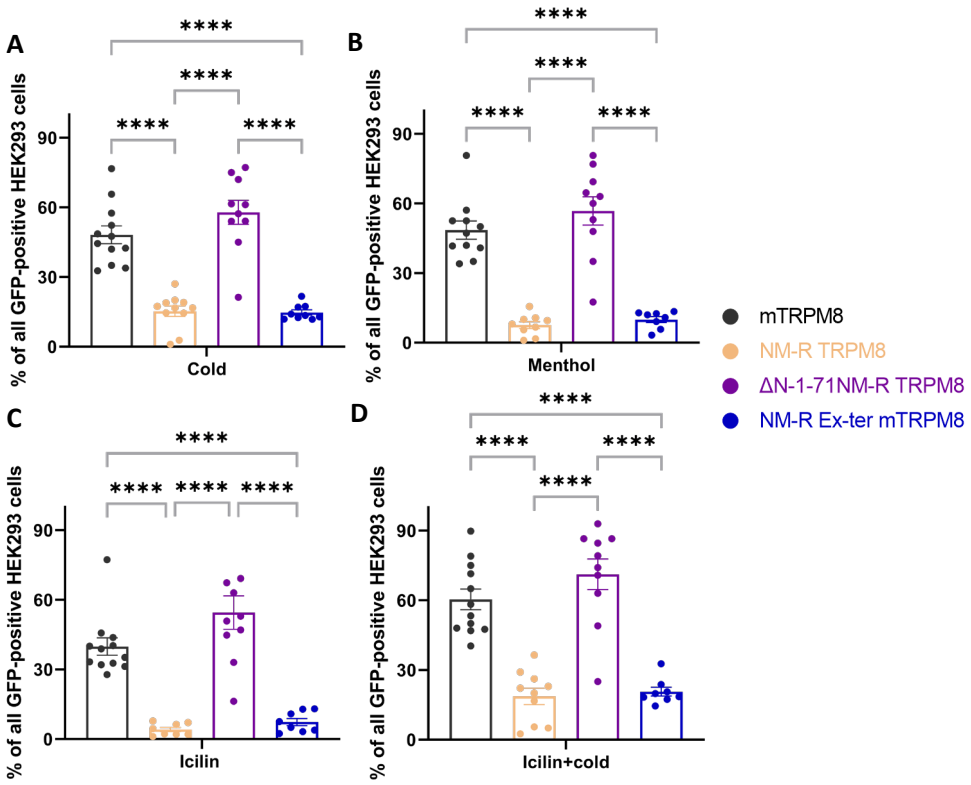

Figure 31. Percentage of GFP⁺ cells responding to cold and chemical stimuli depend on the presence of the unique 1-71 aa of NM-R TRPM8.
(A-D). Percentage of GFP-positive HEK293 cells overexpressing either mouse TRPM8 (black bar), NM-R TRPM8 (NM-R full length TRPM8, brown bar), ΔN-1-71 NM-R TRPM8 (purple bar), or NM-R Nter-mTRPM8 (blue bar) responding to cold exposure (A), 200 µM menthol (B), 10 µM icilin (C) and combined icilin and cold stimulation (D). Asterisks (*) indicate the level of statistical significance regarding the cellular response to stimuli. Transfection efficiency was similar independently of each construct used. Each TRPM8 construct is represented by a different colored bar, with groupings under each stimulus category. Above some bars, asterisks (*) signify the level of statistical significance regarding the cellular response to stimuli. Each group n>8 transfected coverslips, ****p<0.0001, with Tukey's multiple comparisons test, based on One-Way ANOVA.

Icilin (10 µM) + cold stimulation (Figure 31D) resulted ineven more drastic differences, with mouse TRPM8 showing robust activation (60.40 ± 4.46 %). In contrast, NM-R TRPM8 had a significantly lower response (18.67 ± 3.56 %) while ΔN-1-71 NM-R TRPM8 showed a response similar to mouse TRPM8 (71.19 ± 6.58 %). NM-R Nter-mTRPM8 displayed reduced sensitivity (20.71 ± 1.95 %).

Mouse TRPM8 transfection exhibited a vigorous response across all tested stimuli, confirming the functionality of the channel within the standard construct. In contrast, the NM-R TRPM8 with an extended N-terminal region showed a notably reduced proportion of cells that responded to stimuli, implying a detrimental effect of the N-terminal elongation on the channel

activity. The ΔN-1-71 NM-R TRPM8 construct which lacks the extended N-terminal region displayed a response pattern that aligned closely with that of the mouse TRPM8. This resemblance suggests that the deletion of the extended region may alleviate the inhibitory effect observed in the NM-R full length TRPM8 construct. Furthermore, the chimeric NM-R Nter-mTRPM8 construct, with the NM-R N-terminal fuses to the mouse TRPM8 sequence, resulted in a lower percentage of responsive cells compared to the mouse TRPM8. This finding indicates that the NM-R full length TRPM8 N-terminal might confer a structural alterationthat impacts the native function of TRPM8 channel in mice.

4.4.6 Evaluation of the effects of co-expression of Naked mole-rat TRPM8 and mouse TRPM8 isoforms in HEK293 cells

To explore the potential interaction between different TRPM8 isoforms in NM-R and mouse, HEK293 cells were co-transfected with varying amounts of EGFP-tagged NM-R TRPM8 plasmid alongside a constant amount of 0.25 μg mCherry-tagged mouse TRPM8 (mTRPM8) plasmid. This experimental design aimed to assess whether the different expression levels of NM-R TRPM8 would influence the functional activity of mTRPM8. Experiments was clustered into four distinct groups based on the amount of NM-R TRPM8 plasmid used in the co-transfection: Group 1: control group, only mTRPM8 was expressed, Group 2: 0.25 μg NM-R TRPM8, Group 3: 0.50 μg NM-R TRPM8, Group 4: 1.00 μg NM-R TRPM8. We show the experimental setup, which highlights the co-transfection strategy and illustrates how the GFP^+ (NM-R TRPM8) and RFP^+ (mTRPM8) cells were identified for analysis (Figure 32A). Specifically, cells that were double-positive for both GFP and RFP were selected to ensure the subsequent calcium imaging data was derived only from cells that co-express both TRPM8 isoforms.

Intracellular calcium responses were monitored using Fura-2 ratio metric imaging under four different conditions: cold exposure, 200 μM menthol application, 10 μM icilin application, and the combination of icilin with cold. Fluorescence traces from cells co-expressing GFP and RFP (Figure 32B) demonstrated robust and consistent responses across all experimental groups. Despite the varying amounts of NM-R TRPM8, the overall activity of mTRPM8 appeared unaffected, with the fluorescence traces showing similar patterns of calcium influx in response to the stimuli across all groups.

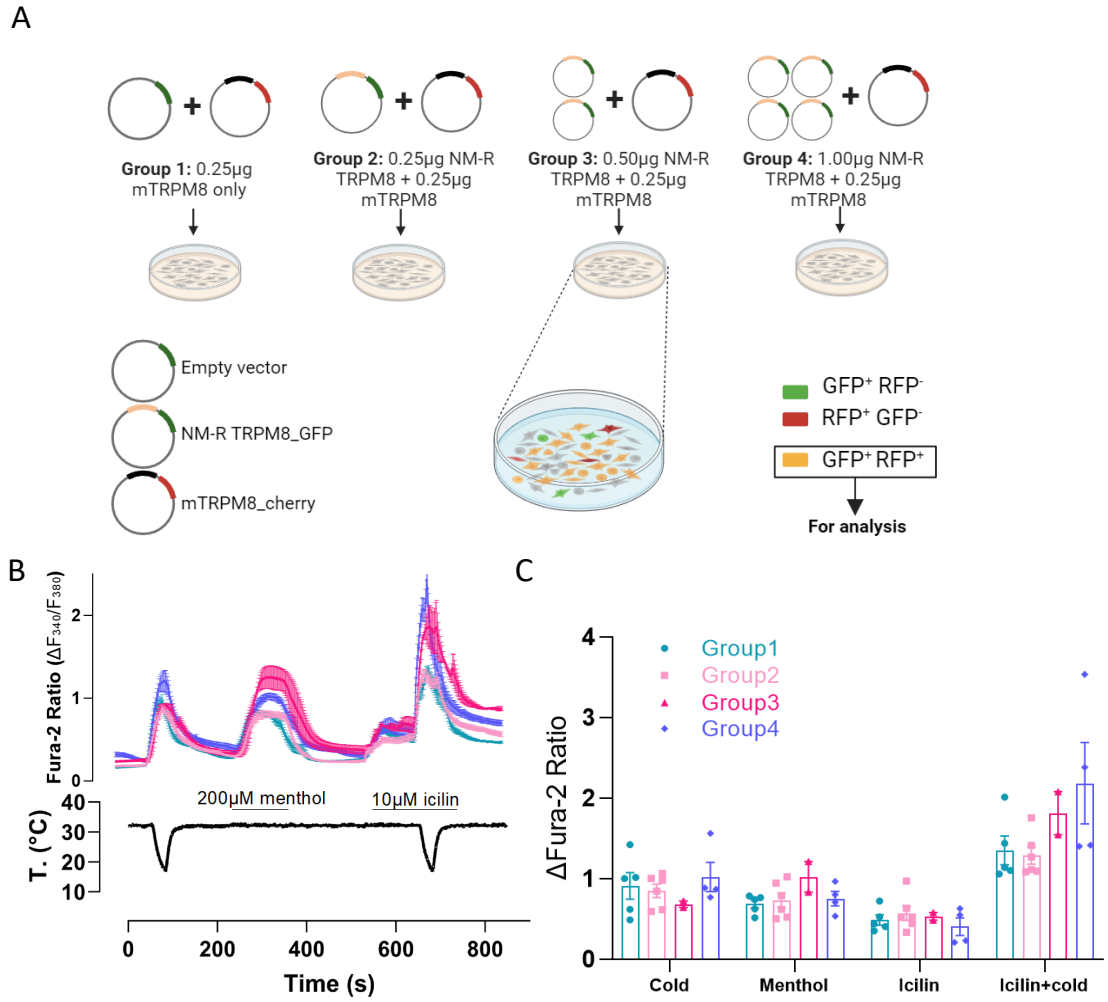

Figure 32. Calcium responses in HEK293 cells co-expressing NM-R TRPM8 and Mouse TRPM8.
(A). Traces of intracellular calcium levels, represented by Fura-2 ratio, in response to cold, 200 µM menthol, 10 µM icilin, and the combination of icilin with cold. HEK293 cells were co-transfected with a constant 0.25 µg of mTRPM8 plasmid and varying amounts of NM-R full length TRPM8 plasmid (Group 1 with 0.00µg; Group 2 with 0.25 µg; Group 3 with 0.50 µg; and Group 4 with 1.00µg). Drawn with biorender. (B). Taces of intracellular calcium levels, as indicated by Fura-2 ratio, in response to cold, 200 µM menthol, 10 µM icilin, and a combination of icilin with cold. (C). Quantitative analysis of ΔFura-2 ratio across different experimental conditions demonstrates no significant difference. Group 1, n = 5; Group 2, n = 6; Group 3, n = 2; and Group 4, n = 4). Data are presented as mean ± SEM. $p > 0.05$ for all comparisons, based on Tukey's multiple comparisons test.

To quantify these observations, ΔFura-2 ratios were calculated and analyzed for each group under the different experimental conditions (Figure 32C). The bar graph shows that there were no significant differences in calcium influx among the four groups studied, regardless of the NM-R TRPM8 concentration. Specifically, the responses to cold, menthol, icilin, and icilin

combined with cold were consistent across all groups, suggesting that the functional properties of mTRPM8 were not significantly altered by the co-expression of NM-R TRPM8.

4.5 Calcium imaging of DRG cultured neurons from Naked mole-rat and mouse

To determine the ability of NM-R DRG neurons in detecting cold, we conducted calcium imaging experiments comparing the responses of NM-R and mouse DRG neurons when exposed to cold stimuli, TRPM8 agonist menthol, and TRPM8 inhibitor AMTB. This investigation aimed to reveal any potential differences in cold sensitivity between the two species.

4.5.1 Calcium responses in mouse and Naked mole-rat DRG neurons

Representative calcium imaging results from the DRG neurons of C57BL/6 mice are presented in Figure 33A (top row). Under baseline conditions, DRG neurons exhibited minimal fluorescence, indicating a low intracellular calcium levels (Figure 33 A, leftmost panel). Upon exposure to cold (10°C), a subset of neurons (trace 1, 2 and 3) showed a marked increase in fluorescence signal, indicative of a significant calcium influx (Figure 33 A, second panel; corresponding traces below).

Subsequent application of menthol (200 μM) increased the calcium influx of some cells and this was consistent with cold activation (Figure 33A, third panel), confirming the role of TRPM8 in cold sensation (traces 1 and 2 below). The response to cold was notably diminished following pre-treatment with the TRPM8 inhibitor AMTB (10 μM), as evidenced by the reduced fluorescence intensity (arrows in Figure 33A, fourth panel) and the corresponding traces, underscoring the efficacy of inhibitor in suppressing TRPM8 activity. Upon repeated cold stimulation, no calcium influx was observed in the traces for cells 1 and 2 (below, trace arrows) until after washing for more than 3 minutes (Figure 33A, fifth panel; trace 2, arrows below). Finally, KCl (100 mM) was applied to depolarize the neurons. This resulted in a robust calcium influx across the neuronal population (cells indicated by arrow 4), confirming the general viability and excitability of neurons (Figure 33A, rightmost panel; corresponding traces for the four cells are shown below).

In contrast, the DRG neurons from NM-Rs exhibit distinct calcium responses, as shown in Figure 33B (bottom row). Baseline fluorescence was similarly low under resting conditions (Figure 33B, leftmost panel). Upon cold stimulation, a greater number of NM-R neurons (Figure 33B, third panel, shows the corresponding traces labeled 1-2, 4, and 6-7, as indicated by arrows in the figure) displayed an increase in fluorescence. When treated with menthol, a smaller number of NM-R neurons also exhibited a calcium influx, but the response was weaker than that observed in mouse neurons (Figure 33B, third panel; corresponding traces for cells, 1, 3, and 5, indicated by arrows). Interestingly, pre-treatment with AMTB altered the cold-induced calcium response in few NM-R neurons (Figure 33B, fourth and fifth panels, trances 2-3, indicated by arrows). Finally, the application of KCl induced a strong and widespread calcium influx within NM-R neurons, a response similar to those observed in mouse neurons, confirming that the NM-R neurons were viable and capable of generating action potentials (Figure 33B, rightmost panel; corresponding traces for the eight cells are shown below).

4.5.2 Proportion of cold-sensitive neurons within mouse and Naked mole-rat DRGs

We first quantified the proportion of cold-sensitive neurons within DRG cultures from both C57BL/6 mice and NM-Rs based on their responses to the first cold stimuli. Our analysis demonstrated a significant difference between the two species, with NM-Rs exhibiting a notably higher proportion of cold-sensitive neurons compared to mice ($p < 0.01$) (Figure 33E). Approximately 20.83% of NM-R DRG neurons were responsive to cold, while only 6.30 % of DRG neurons in C57BL/6 mice exhibited cold sensitivity.

4.5.3 Cell size of cold-sensitive neurons within mouse and Naked mole-rat DRGs

Next, to further investigate the potential differences underlying cold sensitivity, we analyzed the cell size of cold-sensitive neurons. The size of DRG neurons was measured by their cross-sectional area (in μm^2), and cold-sensitive neurons were plotted accordingly (Figure 33C and D).

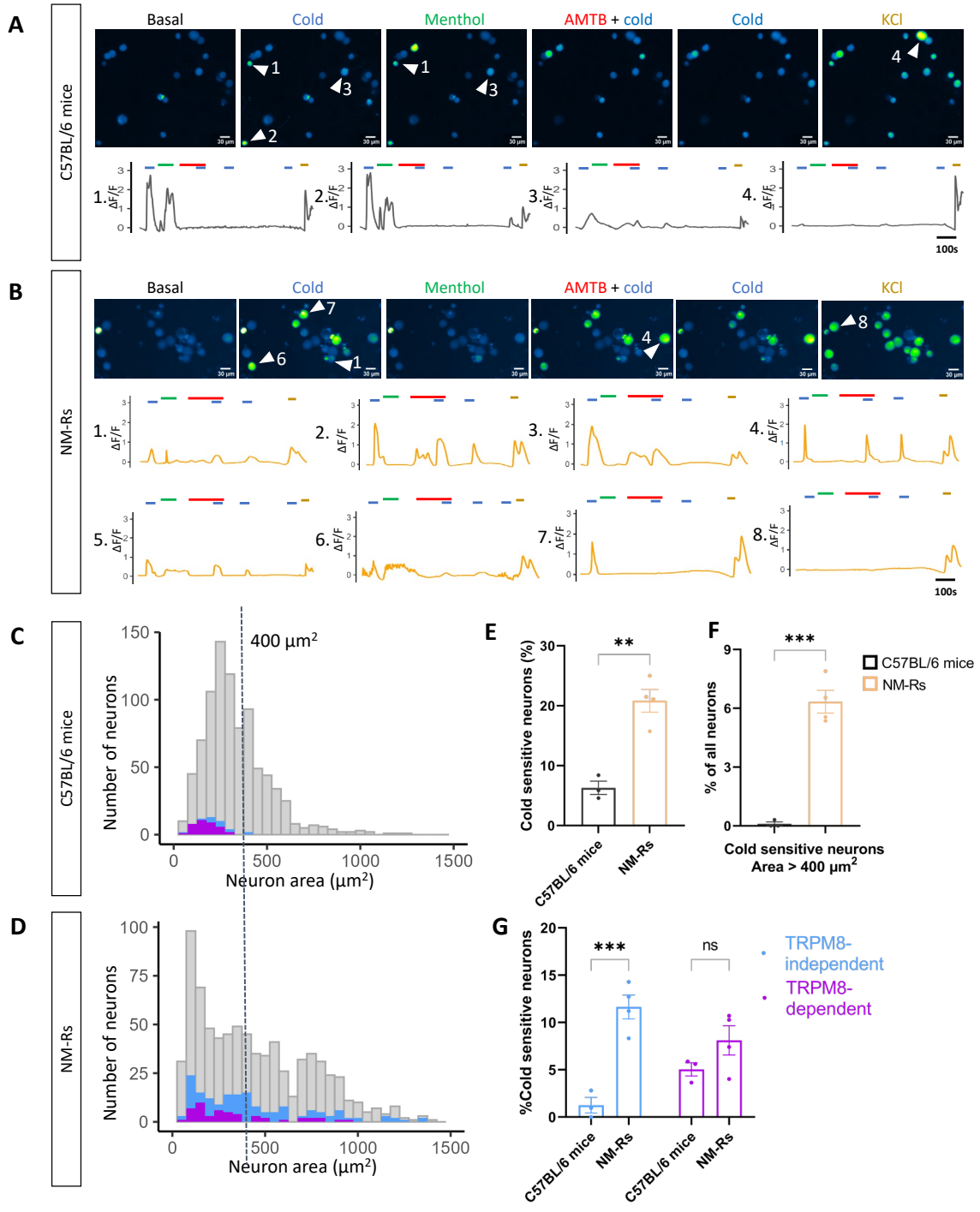

Figure 33. Comparative calcium imaging and neuronal area distribution in cultured DRG neurons from C57BL/6 mice and naked mole-rats.
(A). Representative images showing the fluorescence intensity in the DRG neurons from C57BL/6 mice under various conditions. From left to right: Basal conditions, Cold stimulus (blue lines, 16°C), Menthol (green lines, 200 µM), cold stimulus after pre-treatment with AMTB (red lines, 10 µM), repeated cold stimulus, and depolarization with KCl (dark yellow lines, 100 mM). (B). Representative images showing the fluorescence intensity in the DRG neurons from NM-Rs under various conditions. From left to right same stimulation as mouse experiments. Scale bar: 30 µm.

(C). Histogram showing the distribution of neuron areas in C57BL/6 mice, with cold-sensitive neurons highlighted. Neurons that are TRPM8-independent (blue) and TRPM8-dependent (purple) are predominantly found in the smaller size range (<400 μm²). (D). Histogram showing the distribution of neuron areas in NM-Rs, with a significant proportion of cold-sensitive neurons found in both smaller and larger size ranges. TRPM8-independent (blue) and TRPM8-dependent (purple) neurons are present across a broader range of neuron sizes, including those larger than 400 μm². (E). Bar graph comparing the percentage of cold-sensitive neurons between C57BL/6 mice and NM-Rs. (F). Bar graph showing the percentage of large cold-sensitive neurons relative to the total DRG population. (G). Bar graph depicting the percentage of TRPM8-independent (blue) and TRPM8-dependent (purple) cold-sensitive neurons in C57BL/6 mice and NM-Rs. Mice (n = 3, 860 neurons); NM-Rs (n = 4, 775 neurons). Data are presented as mean ± SEM. $**p<0.01$, $***p<0.001$ and ns (not significant) with Tukey's multiple comparisons test.

In C57BL/6 mice, cold-sensitive neurons were predominantly small, with cell areas measuring less than 400 μm² (Figure 33C). In contrast, NM-R DRG neurons exhibited a broader range of sizes, with a substantial number of cold-sensitive neurons having areas greater than 400 μm² (Figure 33D). Analysis revealed a significant difference between these two species, with NM-Rs having a substantially higher proportion of large cold-sensitive neurons that account for about 6.34 % of the total neuronal population ($p < 0.001$). However, such neurons were virtually absent in C57BL/6 mice (Figure 33F). The presence of these large cold-sensitive neurons in NM-Rs could indicate a distinct physiological mechanism for cold detection, potentially involving different receptor pathways or neuronal subtypes.

4.5.4 TRPM8-dependent and TRPM8-independent cold sensitivity in mouse and Naked mole-rat DRGs

Cold sensitivity neurons were classified as TRPM8-dependent (in purple), if they exhibited a menthol-induced calcium influx or the cold response was inhibited by AMTB, while TRPM8-independent neurons (in blue) were those where the cold response remained unaffected by TRPM8 modulation (Figure 33G).

In C57BL/6 mice, the majority of cold-sensitive neurons were TRPM8-dependent, indicating that cold sensation in mice primarily involves TRPM8 channels (Figure 33G). In contrast, NM-Rs displayed a marked increase in the proportion of TRPM8-independent cold-sensitive neurons ($p < 0.001$), suggesting that NM-Rs rely more heavily on alternative, TRPM8-independent pathways for detecting cold stimuli.

Interestingly, while TRPM8-independent neurons were more prevalent in NM-Rs, the proportion of TRPM8-dependent neurons did not differ significantly between the two species (Figure 33G, ns, not significant). This suggests that both mice and NM-Rs rely equally on TRPM8 for cold detection. However, the higher prevalence of TRPM8-independent neurons in

NM-Rs indicates that they may utilize additional mechanisms for cold sensation, potentially enhancing their ability to detect cold temperatures beyond what is observed in mice. This greater reliance on TRPM8-independent pathways in NM-Rs likely reflects an adaptive mechanism suited to their unique ecological niche, where a broader or more diversified set of sensory mechanisms is advantageous for detecting cold.

4.6 Comparative analysis of the physiological properties of sensory fibers in the hindpaw hairy skin

This study aimed to deepen our understanding of cold detection mechanisms in NM-Rs, with a primary focus on the peripheral nervous system, particularly at the skin nerve interface, which plays a critical role in initial sensory transduction. *Ex vivo* skin nerve preparation is a reliable preparation for studying the activation of primary sensory neurons in mouse skin. This method enables the measurement of action potentials from specific sensory nerve terminals located outside in the skin.

4.6.1 Cold sensory fibers in Naked mole-rat show faster conduction velocity compared to mouse

Analysis revealed that NM-Rs exhibited a broader and more variable response profile of cold-sensitive fibers compared to C57BL/6 mice, as indicated by the distribution conduction velocities (Figure 34A). C57BL/6 mice (n = 39 fibers) demonstrated a sharp, narrow peak around 0 to 3 m/s, indicating a relatively homogeneous population of cold-sensitive fibers with similar activation thresholds. In contrast, NM-Rs (n = 57 fibers) displayed a wider distribution with ranging from approximately 0 to 15 m/s, indicating a greater heterogeneity in their cold-sensitive fibers. Furthermore, NM-Rs exhibited faster CV in these fibers compared to C57BL/6 mice.

Conversely, analysis on the warm-sensitive fibers (n = 17 C57BL/6 mice fibers, n = 21 NM-R fibers; (Figure 34B) and mechanosensitive fibers (n = 97 C57BL/6 mice fibers, n = 81 NM-R fibers; Figure 34C) did not reveal significant differences between NM-Rs and C57BL/6. Both species showed comparable distributions in these sensory modalities, suggesting that while NM-Rs have evolved a distinct and more variable cold sensitivity with faster conduction velocities.

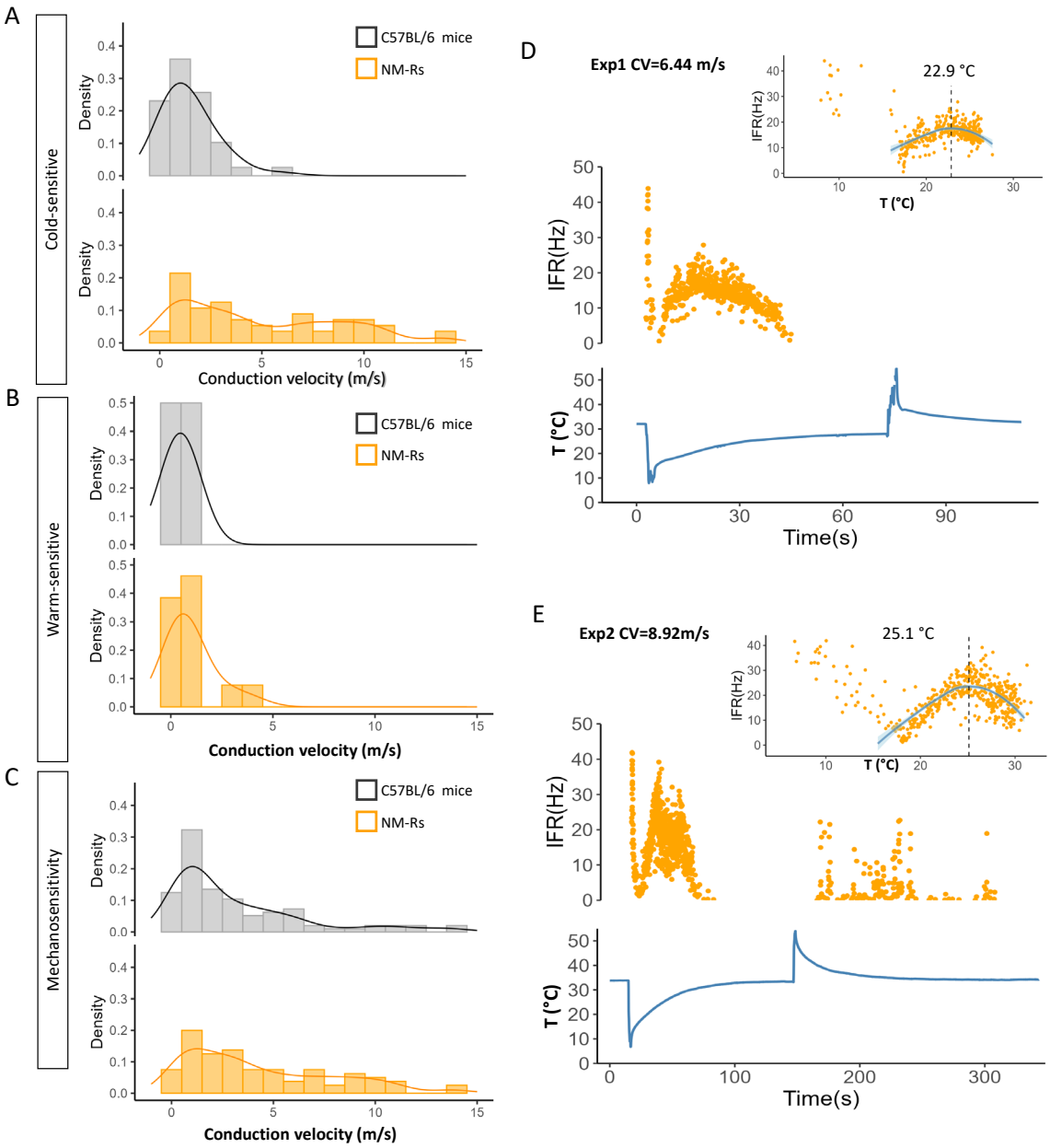

Figure 34. Comparative analysis of sensory fiber conduction velocities and cold sensitivity in naked mole-rats.

(A-C). Distribution of conduction velocities (CV) for cold-sensitive (A), warm-sensitive (B), and mechanosensitive (C) fibers in C57BL/6 mice (n=10) and NM-Rs (n=8). (A) Cold-sensitive fibers: 39 fibers from C57BL/6 mice and 57 fibers from NM-Rs. (B). Warm-sensitive fibers: 17 fibers from C57BL/6 mice and 21 fibers from NM-Rs. (C) Mechanosensitive fibers: 97 fibers from C57BL/6 mice and 81 fibers from NM-Rs. The histograms represent the density distribution of conduction velocities, with C57BL/6 mice shown in gray and NM-Rs in orange. Each panel highlights the differences in conduction velocity profiles between the two species across different sensory modalities. C57BL/6 mice display a more uniform distribution with higher density peaks in cold-

sensitive fibers, while NM-Rs exhibit broader and more variable distributions, indicating greater heterogeneity in their sensory fiber conduction velocities. (D-E). Examples of cold-sensitive fiber responses in NM-Rs, showing instantaneous firing rate (IFR) inresponse to temperature changes. The CV for these fibers are 6.44m/s (D) and 8.92m/s (E). The top panels present the relationship between IFR and temperature, with peak firing rates observed at 22.9°C (D) and 25.1°C (E). The middle panels illustrate the temporal dynamics of IFR during the cooling protocol, showing a rapid increase in firing rate followed by a gradual adaptation. The bottom panels depict the corresponding temperature profiles during the experiments, indicating the cooling stimulus applied to the fibers.

4.6.2 Examples of cold-sensitive fiber activity in Naked mole-rats skin

To further illustrate the characteristics of cold-sensitive fibers in NM-Rs, we presented two representative examples, focusing on their instantaneous firing rate (IFR) in response to temperature changes during controlled cooling protocols (Figure 34D and E).

In example 1 (Figure 34D, CV=6.44 m/s), the IFR of a cold-sensitive fiber was recorded during a controlled cooling protocol. The IFR, measured in Hertz (Hz), reflected the frequency of action potentials generated as the temperature dropped. The inset graph showed the relationship between IFR and temperature (°C), with a fitted curve highlighting fiber cold sensitivity. The peak firing rate occurred at 22.9°C, as indicated by the vertical dashed line. Below this threshold, the IFR increased sharply and peaked rapidly before gradually declining as the temperature continued to drop. The middle panel illustrated the time course of IFR during the cooling process, showing an initial rapid increase in firing rate which shortly reached its peak. This was followed by a gradual decrease in IFR, suggesting a possible adaptation mechanism in which the responsiveness of fibers diminished over time despite continued cold exposure. The bottom panel represented the corresponding temperature changes during this period.

The second example (Figure 34E, CV=8.92 m/s) provided another illustration of a cold-sensitive fiber, further emphasizing the variability in response patterns among different fibers. The IFR was again measured during a cooling protocol, but in this case, the peak firing rate was observed at a higher temperature of 25.1°C. As with the first example, this fiber demonstrated a robust response to cooling, as illustrated by a rapid initial increase in IFR. However, this response peaked at a higher temperature and exhibited a different adaptation profile, with the firing rate gradually declining as the temperature decreased further.

4.6.3 TRPM8-dependent cold-sensitive fibers in Naked mole-rats skin

To explore the role of TRPM8 channels in cold sensitivity, we investigated the effects of the TRPM8 antagonist AMTB on cold-sensitive fibers in NM-Rs. Due to experimental constraints and limited animal availability, we were able to test only two NM-Rs (n = 26 fibers). Nevertheless, the results provide valuable insights into the diversity of cold-sensitive fiber subtypes in NM-Rs and C57BL/6 mice.

We identified two distinct populations of cold-sensitive fibers in both NM-Rs and C57BL/6 mice: TRPM8-dependent and TRPM8-independent fibers. Figure 35A illustrated the proportion of TRPM8-dependent and independent fibers in both species. In C57BL/6 mice, a higher proportion of cold-sensitive fibers were TRPM8-dependent (approximately 93%), as AMTB inhibited 15 out of 16 cold-sensitive fibers (in purple). Conversely, in NM-Rs, there was a more balanced distribution between the two fiber types. AMTB inhibited 12 out of 26 cold-sensitive fibers (approximately 46%) in NM-Rs, indicating TRPM8-dependent cold-sensitive fibers, while around 54% cold-sensitive fibers were insensitive to AMTB, suggesting they were TRPM8-independent (in blue).

An example of the inhibitory effect of AMTB on a cold-sensitive fiber in NM-Rs was presented in Figure 35B (without AMTB) and Figure 35C (with AMTB). Without AMTB application, the mean firing rate (MFR) across the cooling protocol was shown in the top panel, with the firing rate peaking at approximately 27.5°C as the temperature decreased (dashed line). The middle panel showed a histogram of spike counts over time, demonstrating robust spiking activity in response to the cooling protocol. The bottom panel represented the corresponding temperature profile during the experiment. The cooling protocol showed a rapid drop in temperature, followed by a slow stabilization around 10°C.

Following AMTB application (Figure 35C), the MFR was dramatically reduced, with little firing rate peaking at approximately 27°C as before. The middle panel presented the spike count histogram, showing a near-complete inhibition of spiking activity following AMTB treatment. The bottom panel illustrates that the cooling protocol remained consistent with the AMTB condition, confirming that the reduction in spiking activity was due to AMTB inhibition of TRPM8, rather than changes in the cooling stimulus.

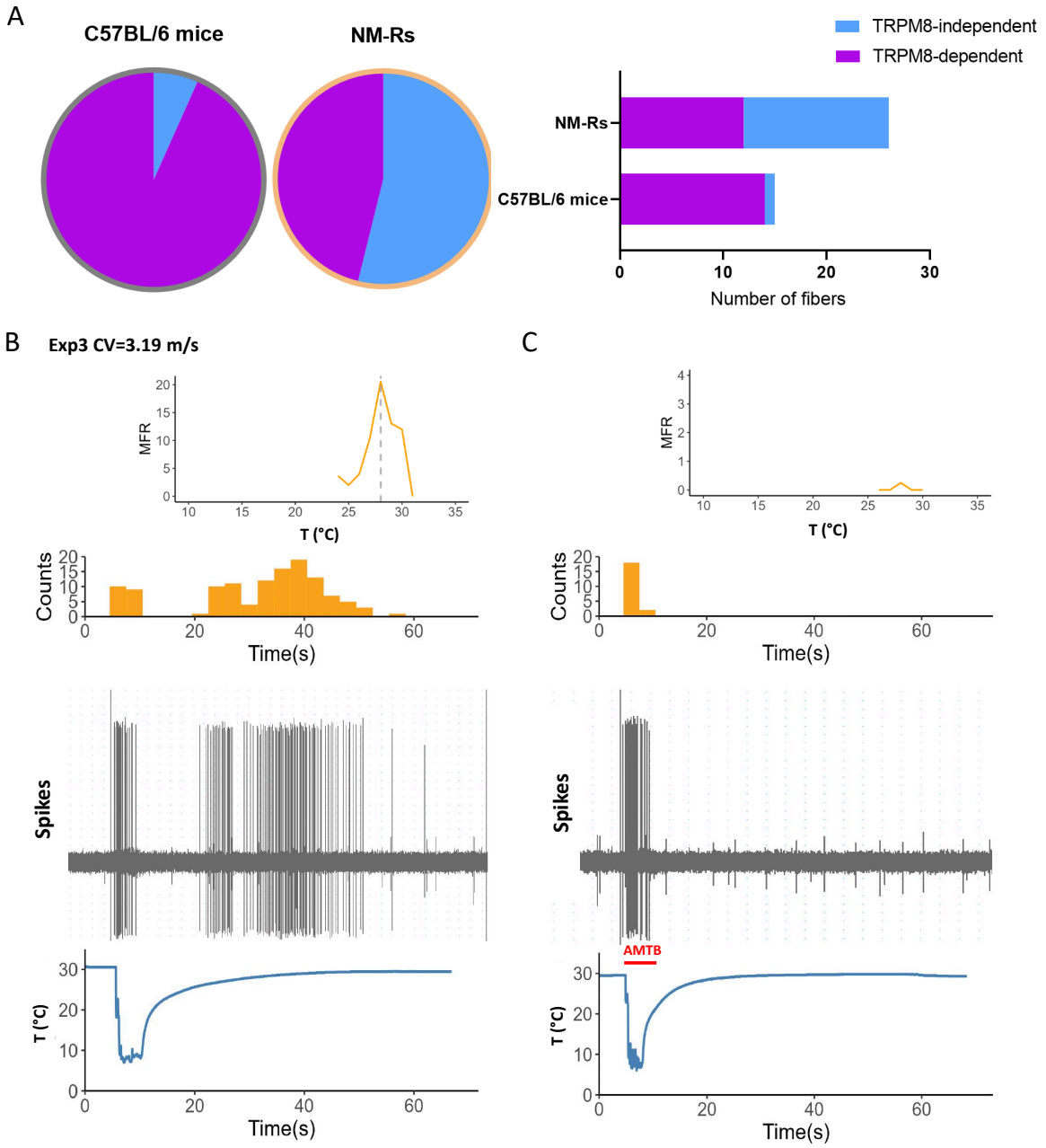

Figure 35. TRPM8-dependent cold-sensitive fibers in Naked mole-rats.
(A). Proportion of TRPM8-dependent and TRPM8-independent cold-sensitive fibers in C57BL/6 mice (16 fibers, n=5) and NM-Rs (26 fibers, n=2). The pie charts represent the relative distribution of TRPM8-dependent (purple) and TRPM8-independent (blue) fibers. The bar graph shows the number of cold-sensitive fibers that were inhibited by AMTB in each species. In mice, 15 out of 16 cold-sensitive fibers were TRPM8-dependent (~93%), while in NM-Rs, 12 out of 26 cold-sensitive fibers were TRPM8-dependent (~46%). (B-C). Effects of AMTB on cold-sensitive fiber activity in an NM-R during a controlled cooling protocol. (B) shows the baseline activity of a cold-sensitive fiber before AMTB application, while (C) shows the activity of the same fiber after the application of the TRPM8 antagonist AMTB. The top panels present the mean firing rate (MFR) as a function of temperature, with peak activity observed at 27.5°C. The middle panels display the spike count histograms, indicating robust spiking before AMTB and a marked reduction afterward. The bottom panels illustrate the temperature profile, showing a gradual temperature decrease to approximately 10°C during the experiment. The CV of this fiber is 3.19 m/s.

5 Discussion

While previous studies have explored the behavioral strategies in which NM-Rs use for thermoregulation, the molecular mechanisms underlying their thermosensation remain unclear (Begall et al., 2015; Buffenstein, Amoroso, et al., 2021; Krebs & Clutton-Brock, 1991; Šumbera, 2019; Vandewint et al., 2019; Yahav & Buffenstein, 1991). In this study, we aimed to investigate the role of TRPM8 in cold sensation in NM-Rs. Our work reveals two significant findings: first, we discovered that NM-R TRPM8 contains a unique extended N-terminal region, which inhibits the channel function and may modulate cold sensitivity in these animals. Second, NM-Rs utilize both TRPM8-dependent and TRPM8-independent mechanisms for cold sensation, suggesting unique evolutionary adaptations in their sensory system.

5.1 TRPM8 expression in sensory organs of Naked mole-rat

Our investigation demonstrated that TRPM8 is expressed in multiple sensory organs in NM-Rs, including the DRG, spinal cord, and skin.

5.1.1 Expression patterns of TRPM8 in NM-R DRGs

In most mammals, TRPM8 is predominantly expressed in the small-diameter, cold-sensitive neurons within the DRGs, where it plays a crucial role in cold detection and the mediation of nociceptive responses (Dhaka et al., 2008; Knowlton et al., 2013). However, in NM-Rs, the pattern of TRPM8 expression appears to have evolved in response to their unique subterranean environment. Before this study, NM-Rs *Trpm8* mRNA expression had been reported (Poulson et al., 2020). They used RNAscope with canonical *Trpm8* probe and found decreased *Trpm8* punctae in NM-Rs DRGs compared to mice (Poulson et al., 2020). This raised questions about the possible reasons for the insensitivity of NM-R to mild cold stimuli post-nerve injury.

Based on earlier studies from our group, we found that Trpm8 mRNA levels in mice and NM-Rs were similar (Figure 10). Here, using RNAscope and immunofluorescence techniques, we found high TRPM8 expression in NM-R DRGs, suggesting that TRPM8 may play a more integral and complex role in NM-R sensory processing than previously recognized (Section 4.1.1). The discrepancies between our results and those of Poulson et al., 2020, may be explained by the quantification methods used: they quantified mRNA puncta per cell, whereas we quantified the number of *Trpm8*-positive neurons in the DRG tissue of both species.

Our study revealed that the total expression of TRPM8 was significantly higher in NM-R (17.14% compared to 10% in mice). Contrary to its restricted expression in the small-diameter neurons in other mammals, TRPM8 in NM-Rs was distributed across a broader range of neuron types, including larger-diameter, myelinated neurons (Section 4.1.1), which is also observed to a lesser degree in rat (Kobayashi et al., 2005). Larger neuron size is often associated with faster signal conduction due to myelination (Abraira & Ginty, 2013; Meltzer et al., 2021; Omerbašić et al., 2015), and this could suggest that TRPM8-positive neurons in NM-Rs might have evolved to transmit sensory information more rapidly. The enhanced conduction velocity might be an adaptation to their subterranean lifestyle, allowing NM-Rs to respond more quickly to changes in environmental temperature.

Table 9. Comparison of TRPM8-expressing neurons in NM-R and Mouse DRGs.
Mouse data from: Matos-Cruz et al., 2017; Dhaka et al., 2008; Knowlton et al., 2013. The *Trpm8* reporter mouse line expressed EGFP under the TRPM8 promoter. EGFP expression was detected using an antibody against EGFP. ND: not detected.

	NM-R_RNAScope	NM-R_IF	Mouse_EGFP
NF200/TRPM8	**36.17%**	**33.70%**	**23.16%**
TRPV1/TRPM8	**25.99%**	**19.45%**	**12.20%**
IB4/TRPM8	**4.69%**	**1.28%**	**2.61%**
CGRP/TRPM8	**39.33%**	**ND**	**36.40%**
TRPM8/PGP9.5	**ND**	**17.41%**	**10%**

Further comparison of TRPM8 expression in NM-Rs and mice revealed a significant increase in TRPM8 co-localization with sensory neuron markers such as NF200 and TRPV1 in NM-R (Table 9). This difference could imply a broader functional role of TRPM8 in NM-R sensory neurons that extend beyond cold detection to potentially include also mechanosensation and nociception. In mice, TRPM8 co-localization with NF200 is around 23.16%, and with TRPV1, it is only 12.2% (Dhaka et al., 2008; Lippoldt et al., 2013). The higher co-localization with TRPV1 in NM-Rs is particularly notable, as TRPV1 is typically associated with heat and pain sensation, suggesting that the sensory pathways for cold and pain may be less distinctly separated in NM-Rs. This might explain the reduced sensitivity of NM-R towards mild cold

stimuli, as well as a diminished ability of them to differentiate between cold and pain after nerve injury (Poulson et al., 2020).

5.1.2 Expression of TRPM8 in NM-R spinal cord and skin

Our investigation of TRPM8 expression in the spinal cord and skin of NM-R using RNAscope and immunofluorescence techniques revealed notable discrepancies between mRNA and protein levels.

TRPM8 expression in the spinal cord of NM-Rs presented a complex picture (Section 4.1.2, Figure 18, Figure 19 and Figure 20). Our RNAscope analysis revealed widespread *Trpm8* mRNA expression throughout the gray matter of the spinal cord, extending beyond the superficial layers that are traditionally associated with thermal and nociceptive processing. This broad mRNA expression contrasts sharply with the immunofluorescence data showing the localization of TRPM8 protein to the superficial layers (I and II) which are crucial for pain and thermal sensation processing, coinciding with its known function in cold and pain sensation in peripheral sensory neurons (Dhaka et al., 2007). The superficial immunofluorescence staining is possibly located at the synaptic endings of sensory neurons.

A similar pattern of TRPM8 expression was observed in the skin of NM-Rs. While RNAscope analysis detected *Trpm8* mRNA in certain epidermal cells, immunofluorescence failed to show corresponding protein expression in these cells, suggesting that mRNA may not be efficiently translated into protein. Conversely, TRPM8 protein was observed in certain nerve fibers within the skin, co-localizing with NF200, despite the absence of detectable mRNA in these fibers. This further supports the notion that *Trpm8* mRNA may be synthesized and retained in neuronal cell bodies, while protein localization specific localized to nerve endings.

Interestingly, EGFP expression in a *Trpm8* reporter line was detected in epidermal cells (Dhaka et al., 2008). Additionally, PIEZO1 and TRPV3 further support the role of keratinocytes in sensory processing, suggesting a more expansive involvement of TRPM8 in cold sensitivity (Mikesell et al., 2022; Peier et al., 2002). Recent studies further indicate potential non-sensory roles for TRPM8, such as maintaining skin barrier integrity or regulating local inflammatory responses to cold stimuli. TRPM8 might also influence skin color changes and locomotion performance in response to cold potentially, expanding its functional roles in NM-Rs beyond cold sensation (Lippoldt et al., 2013; Malik et al., 2023)

Another possibility that must be considered is the sensitivity of the TRPM8 antibody used in the spinal cord and skin studies. The failure to detect TRPM8 protein in the grey matter outside the superficial layers might not necessarily indicate an absence of the protein but rather a limitation in the ability of antibody to detect low levels of TRPM8 or its different isoforms. Antibodies can vary in their affinity and may not equally recognize all protein conformations or post-translational modifications. This limitation could explain the apparent absence of TRPM8 protein where its mRNA is present. Moreover, despite stable or high levels of *Trpm8* mRNA, translation of the protein might be suppressed or delayed due to post-transcriptional regulatory mechanisms. Proteomics experiments are crucial for confirming whether TRPM8 protein is indeed present in other regions of the grey matter.

5.2 Sequence and structural analysis of Naked mole-rat TRPM8

5.2.1 Sequence conservation and structural insights

In silico analysis revealed the conservation of key amino acid residues of TRPM8 orthologs, responsible for sensitivity to cold and chemical stimuli in NM-Rs suggesting that the fundamental mechanisms of TRPM8 activation are preserved (Section 4.2.2). However, our findings uncovered an unique extended N-terminal region in NM-R TRPM8, consisting of an additional 71 amino acids which are not found in the TRPM8 protein of most other species (Section 4.2.1).

The exon coding for this extended N-terminal region was mapped using sequence alignment tools, confirming the presence of a species-specific splice variant in NM-R TRPM8 (Figure 36). In addition, we also identified an extended N-terminal region in the TRPM8 of the clawed frog, another cold-blooded species, although the amino acid sequences were are not conserved. The presence of this extended region in both NM-R and clawed frog suggests a potential evolutionary adaptation associated with their cold-blooded physiology, possibly modulating cold sensation to better suit environments where Tb is dependent on external temperature.

Interestingly, an extended N-terminal region is also found in other mammals such as the star-nosed mole and the wild yak (Ahmad et al., 2024; Ayalew et al., 2021; Tattersall & Campbell, 2023). However, amino acid sequences of the extended N-terminal region in these species are distinct from those in NM-R. Thus, the NM-R extended N-terminal sequence shows no evolutionary convergence, likely indicating its unique adaptation specific to NM-R.

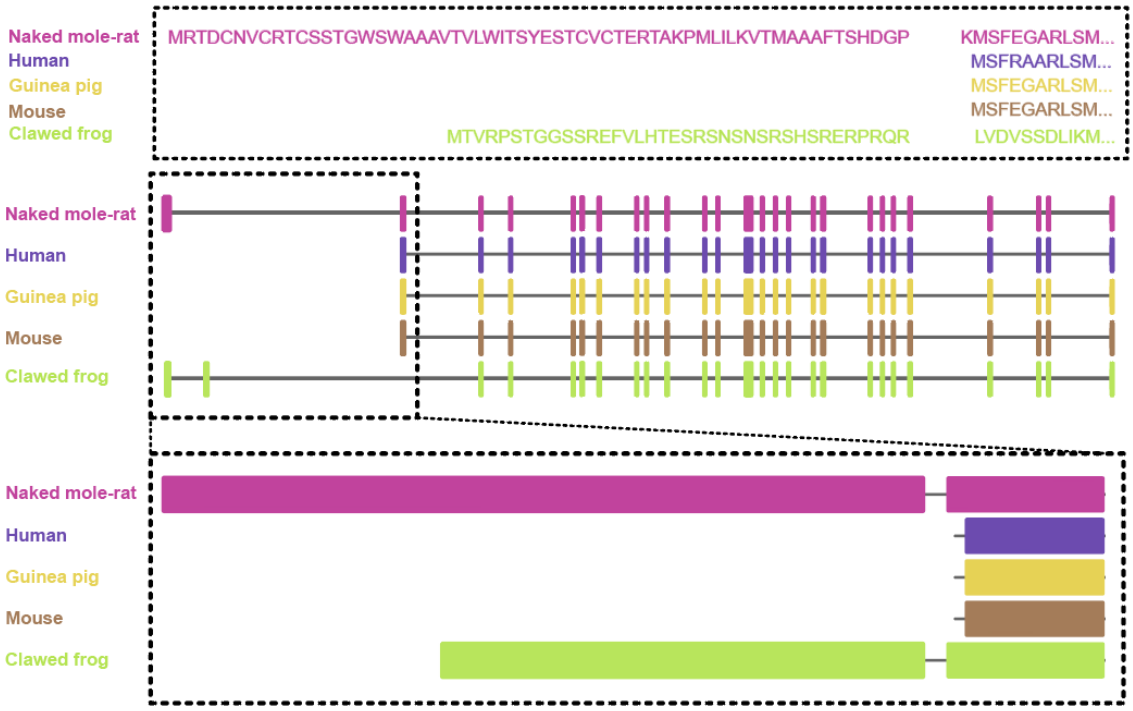

Figure 36. Sequence alignment and structural representation of TRPM8 across species. This figure illustrates the sequence alignment and structural comparison of TRPM8 across five species: NM-R, human, guinea pig, mouse, and clawed frog. The top panel shows the N-terminal region, highlighting the extended sequence unique to NM-R (highlighted in purple), which is absent in other species. The middle panel presents the exon structure of TRPM8 across species, demonstrating the conservation of key functional domains but the addition of the unique N-terminal exon in NM-R. The bottom panel depicts a simplified structural model of the full length TRPM8 channel, showing the extended N-terminal region in NM-R (in purple) compared to the shorter N-terminal regions in other species. Figure from Dr. D. Mendez-Aranda.

The N-terminal domain of ion channels typically plays a crucial role in determining the sensitivity of the channel by exerting a major impact on channel gating, localization, and interaction with cellular signaling pathways (Hellenthal et al., 2021; Hinman et al., 2006; Paulsen et al., 2015; Pertusa et al., 2014). This region usually includes distinct sequences or structural motifs essential for regulating the gating processes. For TRPM8, the N-terminal domain can regulate the channel response to cold temperatures and menthol, both of which are key triggers for activation. Changes in the N-terminal region could affect the responsiveness of channel to these stimuli by directly impacting its ability to open or close in response to external signals (Pertusa et al., 2014; Plaza-Cayón et al., 2022). Furthermore, the N-terminal domain has been implicated in the trafficking of TRPM8 to the cell surface, a crucial step for proper functioning in sensory neurons (Phelps & Gaudet, 2007; L. Zhang & Barritt, 2006).

The importance of the N-terminal domain extends across various ion channels. For instance, in TRPV1, it interacts with phosphoinositides like PIP2 to modulate the thermal and chemical sensitivity of the channel (Rohács et al., 2005). Similarly, in voltage-gated potassium channels, the N-terminal T1 domain is essential for subunit assembly and gating. In Nav1.5, a cardiac sodium channel, the N-terminal domain regulates gating properties, with mutations linked to Brugada syndrome (Chi et al., 2022; Gardill et al., 2018). Recent research on hTRPA1 found that truncations, particularly removing the N-terminal ARD, significantly altered its temperature sensitivity, with Δ1–688 hTRPA1 showing enhanced sensitivity to both cold and heat (Moparthi et al., 2022). Additionally, in hyperpolarization-activated cyclic nucleotide–gated channels the N-terminal domain regulates interactions with cyclic nucleotides like cAMP, which is essential for modulating channel opening and pacemaker activity in both the heart and brain (Porro et al., 2019).

5.2.2 Expression of TRPM8 extended N-terminal variant

Using RNAscope with the *Ex-trpm8* probe, which specifically detects the extended sequence, and the canonical *Trpm8* probe, we identified three neuronal subpopulations in NM-R DRGs: *Trpm8*$^{+}$ *Ex-trpm8*$^{+}$ neurons (co-expressing both the canonical and extended variants), *Trpm8*$^{–}$ *Ex-trpm8*$^{+}$ neurons (expressing only the extended variant) and *Trpm8*$^{+}$ *Ex-trpm8*$^{–}$ neurons (expressing only the canonical variant). Thus, the extended N-terminal variant is broadly expressed in NM-R DRGs (Section 4.3.2). This suggests the presence of two potential isoforms or splice variants of TRPM8 in NM-Rs, each potentially playing distinct functional roles in cold sensitivity.

The presence of two isoforms in NM-Rs, including the extended N-terminal variant, suggests that splicing plays a crucial role in regulating cold sensitivity of TRPM8. While splice variants have been observed in human and mouse *Trpm8* (see in NCBI), our findings demonstrate the inhibitory function of the long variant (*Trpm8*$^{+}$ *Ex-trpm8*$^{+}$*)* in NM-R DRGs—a function not previously identified in mice. This variant may contribute to adapting NM-R sensory physiology to the specific demands of their subterranean habitat.

5.3 Physiological properties of NM-R TRPM8 isoforms

Isoform-specific specialization is well-documented in sensory neurons. For example, in TRPV1-expressing neurons, alternative splicing can generate isoforms with varying responses

to thermal and chemical stimuli, allowing these neurons to fine-tune their sensitivity based on the environmental cues (Caterina et al., 1997; Laursen et al., 2016). Similarly, we identified at least two distinct TRPM8 isoforms in NM-R DRGs: one featuring the extended N-terminal region and another without, resembling the canonical mouse TRPM8 (Section 4.3). We found that the full-length NM-R TRPM8 isoform (with the extended N-terminal region) is not sensitive to cold or menthol, whereas the isoform lacking this region is sensitive to both stimuli (Section 4.4.2 and 4.4.3). Given the role of TRPM8 in cold detection, this raises the question of whether these isoforms interact functionally with each other when co-expressed in DRGs. We tested TRPM8 function in heterologous expression systems using HEK293 cells co-transfected with both NM-R full length TRPM8 (with the extended N-terminal) and mouse TRPM8 (without the N-terminal extension) in various co-transfection scenarios (Section 4.4.6). Our results indicate that the extended N-terminal region in NM-R TRPM8 does not affect the cold sensitivity of the canonical mouse-like TRPM8 isoform, suggesting it may not have a significant inhibitory effect in vivo through direct isoform competition. Neurons expressing both *Trpm8*$^{+}$ and *Ex-trpm8*$^{+}$ variants may still exhibit nuanced cold sensitivity, but this likely occurs through indirect mechanisms, such as post-translational modifications or context-specific interactions in DRG neurons, which are not replicated in HEK293 cells.

Given that co-expression did not diminish mouse TRPM8 function, it is more likely that the *Ex-trpm8*$^{+}$ variant plays distinct roles, potentially beyond cold detection. For example, TRPM8 has been implicated in pain modulation and mechanosensation (Julius, 2013; Lewin & Moshourab, 2004), and the *Ex-trpm8*$^{+}$ variant may participate in such processes within the DRG. Its involvement in conditions such as cold allodynia and nerve injury (Liu et al., 2020; Morenilla-Palao et al., 2014; Myers et al., 2009; Poulson et al., 2020) further suggests that this isoform may regulate sensory modulation in a manner that reflects the unique physiological demands of NM-Rs, particularly under conditions of nerve damage.

While information on the coexistence and interaction of TRPM8 isoforms in a single organism remains limited, our findings are consistent with isoform-specific functions observed in other ion channels. For instance, in Drosophila, distinct TRPA1 isoforms exhibit different thermal sensitivities, allowing selective responses to chemical or thermal stimuli (Kang et al., 2012). Similarly, the extended N-terminal region in NM-R TRPM8 may serve a modulatory role by reducing the channel thermosensitivity, as supported by the presence of DRG neurons expressing only *Ex-trpm8* without *Trpm8* signals (Section 4.3.2).

5.4 TRPM8-dependent and independent cold detection in Naked Mole-Rats

Temperature is a critical environmental factor that influences various aspects of mammalian behavior including foraging and reproduction. Studies indicate that mammals adjust their foraging behavior based on the ambient temperature. In colder environments, mammals tend to consume higher calorie food to compensate for energy losses, whereas in warmer environments, lower-calorie options are preferred (Adamczyk et al., 2015). Similarly, reproduction rates tend to decrease in colder conditions but can increase in warmer climates, demonstrating the significant impact of temperature on reproductive strategies. Recent studies have revealed that temperature perception can also impact the cognitive functions including learning and memory (Maille & Schradin, 2017; Soravia et al., 2021). For example, animals might experience a decline in their learning and memory abilities under warmer conditions.

From the perspectives of sensory perception, temperature triggers distinct behavioral and psychological responses in animals (Lumpkin & Caterina, 2007). Temperature perception can roughly be categorized into harmless warmth or coolness and painful heat or coldness, all of which is responsible to drive specific behaviors. For instance, animals tend to actively seek harmless temperatures, but elicit strong avoidance responses against painful temperatures.

Temperature preference data already showed that NM-Rs tend to occupy warmer environments compared to mice (Section 1.5). At first glance, this behavior may seem to contradict our findings regarding the augmented cold sensitivity in NM-Rs. However, the tendency to stay in warmer regions could be a compensatory response to their increased sensitivity to cold. Despite their physiological adaptations that allow for the detection of cold more efficiently, NM-Rs may prefer warmer zones to avoid noxious cold stimuli which will be detected at a greater sensitivity by their nervous system.

Interestingly, our work identified that 17.14% of total NM-R DRG neurons express TRPM8. However, TRPM8-dependent cold-sensitive neurons account for only about 7.5% of the total neuronal population. In contrast, we found a significant population of TRPM8-independent cold-sensitive neurons, comprising approximately 11.64% of the total population, compared to only 1.26% in mice (Section 4.5). This finding underscores an increased sensitivity to cold stimuli exhibited by NM-Rs which can be further supported by the facts that such cold-sensitive

population is predominantly comprised of larger-diameter neurons (Section 4.5.3). Additionally, in *ex vivo* studies, a higher proportion of cold-sensitive fibers were TRPM8-dependent in mice (approximately 93%), while around 54% of cold-sensitive fibers in NM-Rs were TRPM8-independent (Section 4.6)

The increased cold sensitivity in NM-Rs is not only illustrated by the robust physiological responses but also the involvement of fibers with higher conduction velocities (Section 4.6.1). The larger cold-sensitive neurons identified in the DRG studies are likely to be myelinated, an important feature for the rapid conduction of sensory signals. Myelination significantly enhances the speed of signal transmission along nerve fibers, enabling a swift response to cold stimuli. The well-established correlation between neuron size and conduction velocity suggests that these larger neurons which are typically associated with Aδ and Aβ fibers, are myelinated and therefore exhibit faster conduction velocities compared to the smaller, unmyelinated C-fibers (Abraira & Ginty, 2013; Meltzer et al., 2021; Omerbašić et al., 2015).

Together, the results highlight a significant difference in cold detection mechanisms between NM-Rs and mice, suggests that NM-Rs rely on both TRPM8 and alternative pathways for cold sensation, reflecting species-specific adaptations. The presence of a substantial TRPM8-independent population in NM-Rs points toward the involvement of other ion channels in their cold detection mechanisms, which may contribute to their heightened sensitivity to cold stimuli.

Studies have shown that even when mice lack the *Trpm8* gene, they can still sense extreme cold (Daniels & McKemy, 2007). This also suggests the existence of other cold receptors that have yet to be identified, pointing to a broader mechanism of cold detection beyond what is currently known to be mediated by TRPM8. In line with this, our data suggest that NM-Rs not only rely on TRPM8 but also on alternative cold-sensitive pathways, to achieve efficient cold detection while behaviorally seeking warmer environments to mitigate cold exposure. Among the alternative cold-sensitive ion channels, TRPA1 emerges as a notable candidate. TRPA1, a channel that triggers Ca^{2+} influx and non-selective cation currents once activated in response to temperatures around 17°C, has been extensively studied for its role in sensing noxious cold (Bandell et al., 2004; Del Camino et al., 2010; Karashima et al., 2009; Story et al., 2003).

The exact contribution of TRPA1 to cold sensation in NM-Rs remains somewhat ambiguous. We and others have shown that *Trpa1* mRNA expression is notably higher in the DRGs of NM-Rs compared to mice (Figure 37A and Figure 37B) (Poulson et al., 2020). While TRPA1 is traditionally known for its roles to detect noxious cold and chemical irritants, as well as its ability to trigger robust nocifensive responses to the TRPA1 agonist mustard oil in NM-Rs, there is conflicting evidence regarding its role in cold detection (Poulson et al., 2020).

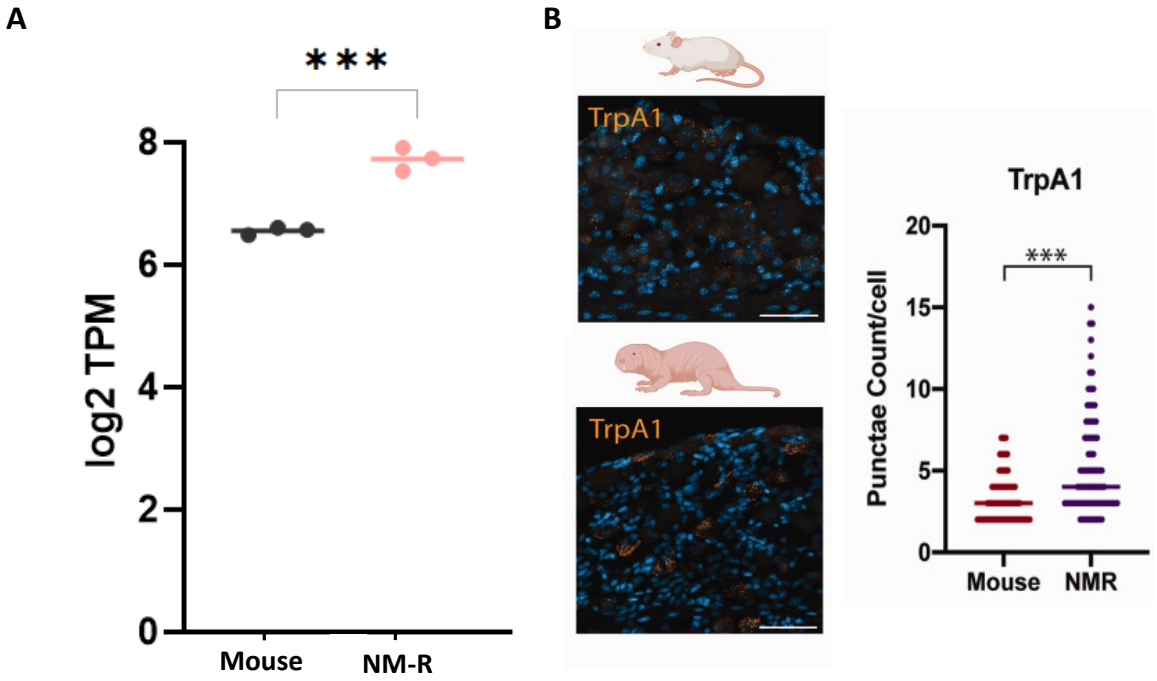

Figure 37. TRPA1 expression and function in NM-Rs compared to Mice.
(A). Transcriptomic analysis of *Trpa1* in DRGs of NM-R. Data from Eigendbrod O, unpublished. (B). Expression of *Trpa1* mRNA in DRG of NM-Rs. This figure is adapted from Poulson et al., 2020.

Altogether, TRPA1 function may reflect species-specific differences. While TRPA1 has been shown to respond to cold in rats and mice, it does not seem to mediate cold sensation in humans and rhesus monkeys (Chen et al., 2013; Cordero-Morales et al., 2011; Jordt et al., 2004; Zurborg et al., 2007). These findings broaden our understanding of the complex mechanisms underlying temperature perception in NM-Rs. Another cold-sensitive channel candidate, TRPC5 (Bernal et al., 2021; Zimmermann et al., 2011), was not detected in our mole-rat database. However, NM-R TRPC5 sequences are available in NCBI (Gene ID: 101709576), though no published studies have yet explored the role of TRPC5 in NM-R cold sensation. The identification of cold-sensitive channels in NM-R requires further investigation using additional techniques and cold-induced behavioral assays.

5.5 Evolutionary adaptations of Naked mole-rat TRPM8

5.5.1 Diversity of TRPM8 across species

The TRPM8 channel plays a critical role in cold detection across a variety of species, but its presence, function, and activation threshold exhibit significant variability due to evolutionary pressures and habitat adaptations. TRPM8 is entirely absent in many fish species, such as zebrafish and carp, indicating that cold detection in these species relies on alternative mechanisms or channels (York & Zakon, 2022). This absence may reflect an adaptation to extreme ecological niches, such as the Antarctic, where fish species thrive without TRPM8. Instead, fish likely employ other cold-sensitive channels, such as TRPV1/2, TRPV4, and TRPA1, which are known to participate in temperature sensing in certain aquatic vertebrates (Saito & Shingai, 2006; York & Zakon, 2022).

In amphibians, particularly the African clawed frog (*Xenopus laevis*), TRPM8 is present, but with a higher activation threshold than in mammals. This correlates with the lower basal Tb of amphibians, reflecting their ectothermic physiology, which depends heavily on environmental temperatures to regulate body heat. A higher activation threshold for TRPM8 allows these amphibians to sense potentially harmful cold stimuli, while not being overly sensitive to their generally cooler environments (Myers et al., 2009). This pattern extends to birds, such as chickens, where TRPM8 activation temperatures are higher compared to mammals, reflecting their elevated core Tb (Lu et al., 2022; Myers et al., 2009).

The evolutionary history of TRPM8 provides additional insight into how this channel has adapted across different lineages. Studies suggest that TRPM8 evolved from gene duplication and exon shuffling events, specifically from the *Trpm2* gene, in lobe-finned fishes, which are considered the precursors of terrestrial vertebrates (Lu et al., 2022; Myers et al., 2009). This gene duplication likely occurred during the transition from water to land, a pivotal evolutionary event in vertebrate history. During this time, the need for precise cold detection became more pronounced as animals moved to terrestrial environments, where temperature fluctuations are more extreme compared to aquatic habitats. As such, the evolutionary development of TRPM8 in these species involved significant structural changes that enhanced cold sensitivity (Lu et al., 2022; Myers et al., 2009).

When examining NM-R TRPM8, unique adaptations to their subterranean environment are apparent. NM-Rs maintain a stable Tb around 32°C due to their poikilothermic nature and constant exposure to the relatively mild temperatures of underground habitats temperature (Buffenstein, Amoroso, et al., 2021). Unlike many mammals, NM-Rs do not exhibit circadian rhythms—a unique adaptation to their constant, subterranean environment, which is devoid of natural light cycles (Riccio & Goldman, 2000). Absence of such circadian regulation suggests a significant evolutionary shift in their sensory and regulatory systems which may have reshaped their thermosensory and thermoregulatory mechanisms (Tan & Knight, 2018).

5.5.2 Comparative adaptations in other mole-rats

While our study focuses primarily on the NM-R, it is important to consider other mole-rat species within the *Bathyergidae* family, as their thermoregulatory strategies offer valuable insights into the diversity of TRPM8 function and adaptation. Our findings on NM-R TRPM8 reveal the presence of an extended N-terminal region, a feature that is significantly shorter in other mole-rat species (Figure 38A). The evolutionary tree we constructed demonstrates the differentiation between NM-R full-length TRPM8 and its counterparts in other mole-rat species (Figure 38B).{Citation}

The *Bathyergidae* family is composed of species that live in a wide range of habitats, from arid deserts to moutain regions, and these environmental differences have likely shaped their distinct physiological responses to temperature. For instance, Damaraland mole-rats (*Fukomys damarensis*), which are desert-adapted, rely heavily on behavioral strategies such as huddling, as well as physiological mechanisms like metabolic adjustments, to maintain body heat in fluctuating ambient temperatures. Their burrow systems provide thermal buffering, minimizing the need for extreme physiological adaptations seen in species exposed to harsher climates (Montoya-Sanhueza, Šaffa, et al., 2022; Šumbera, 2019; Vejmělka et al., 2021). On the other hand, species like *Georychus capensis*, which inhabits regions with higher rainfall and cooler climates, possibly relying more on conductive heat loss through their body surfaces and feet to dissipate heat in warm conditions (Vejmělka et al., 2021). Similarly, species like the Natal mole-rat (*Cryptomys hottentotus natalensis*), which inhabit moutain regions where temperatures can fall below freezing, display even more pronounced adaptations to cold (Finn et al., 2022; Oosthuizen et al., 2021). Although residing in cold environments with limited resources, Natal mole-rats have the highest resting metabolic rates among the mole-rat species examined, indicating that they prioritize heat generation and insulation against heat loss (Finn

et al., 2022; Oosthuizen et al., 2021). Such variations across mole-rat species underscore the ecological pressures that shape the evolution of TRPM8 and other thermosensory channels.

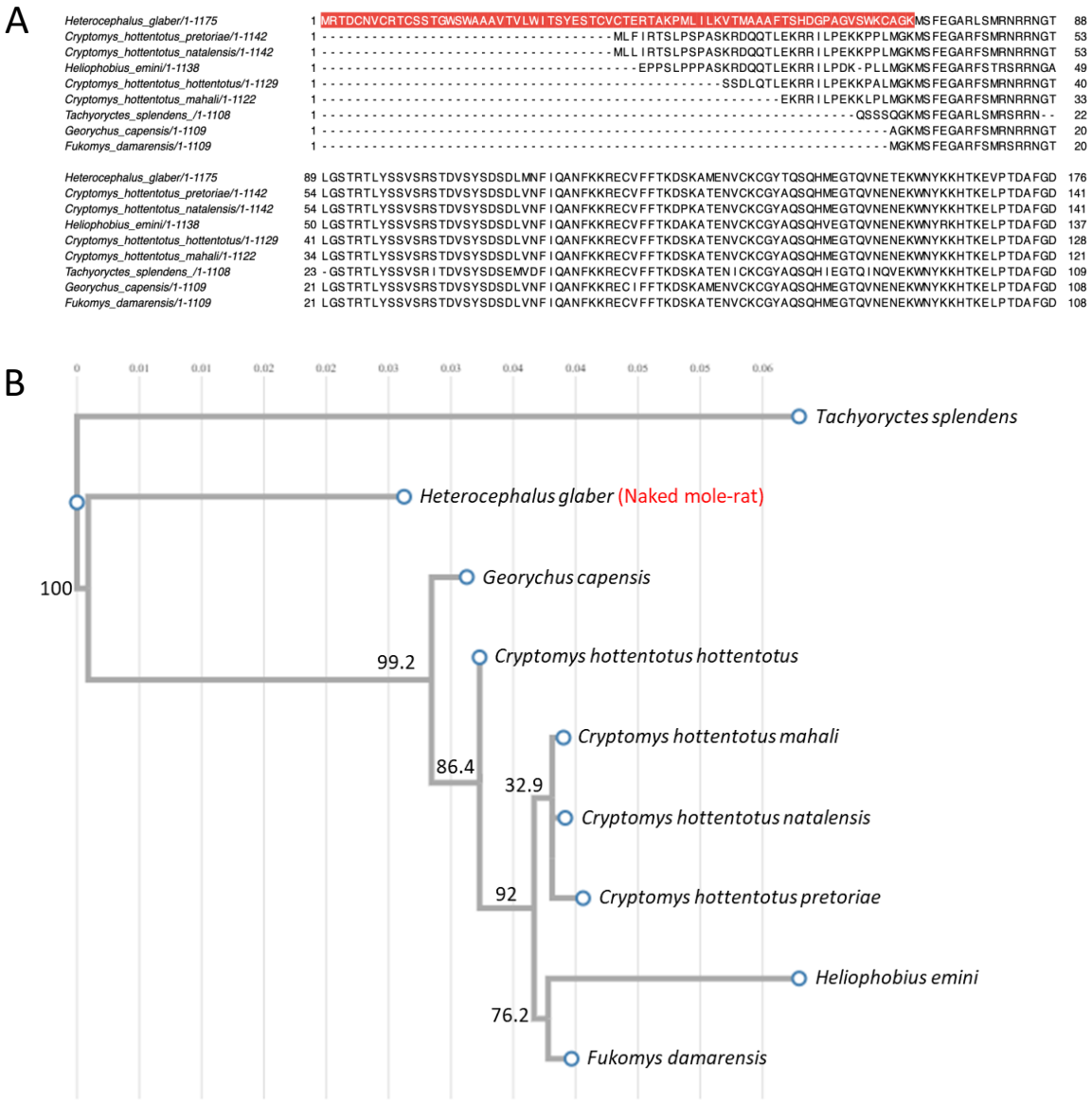

Figure 38: Comparative analysis of TRPM8 protein sequences among African mole-rat species.
(A). Comparative alignment of TRPM8 extended N-terminal sequences between African mole-rat species. This alignment compares the extended N-terminal regions of TRPM8 across African mole-rat species. The NM-R sequence, highlighted in red, emphasizes its unique features. Sequences were aligned using Serial Cloner software. Phylogenic analysis of TRPM8 proteins between African mole-rat species. (B). This phylogenetic tree illustrates the evolutionary relationships and genetic distances of TRPM8 proteins across African mole-rat species, with the NM-R highlighted in red. Bootstrap values at each node indicate the reliability of the branching points. The tree was constructed using CLUSTALW.

5.6 Summary of TRPM8 function, expression, and cold sensitivity in NM-R

With all observations made during the expression and function of TRPM8 in NM-R, the following working model is proposed (Figure 39).

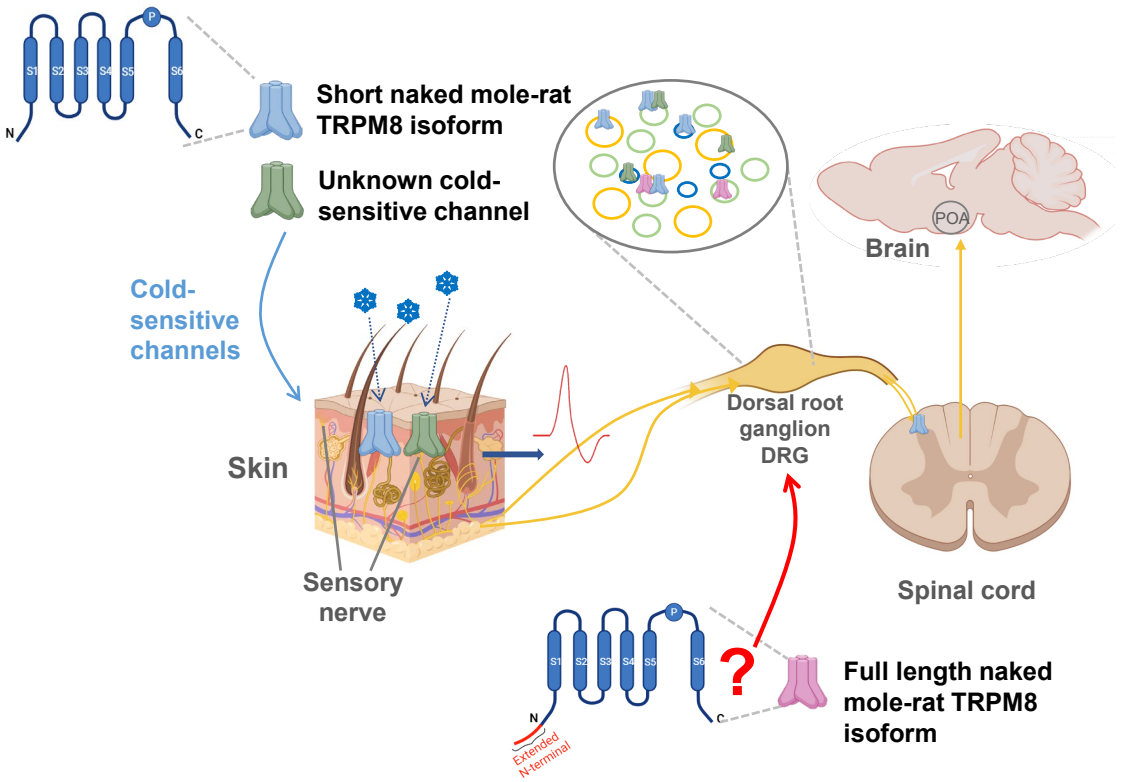

Figure 39: Overview of TRPM8 function, expression, and cold sensitivity mechanisms in NM-R.
This figure illustrates the cold sensitivity mechanisms in NM-R, highlighting both TRPM8-dependent and TRPM8-independent pathways, as well as the expression of TRPM8 isoforms in NM-R DRG neurons. Full-length NM-R TRPM8 isoform (bottom right, in pink): this isoform contains an extended N-terminal region (1-71 amino acids), which may serve another role in NM-R DRG neurons. Short NM-R TRPM8 isoform (top left, in blue): a shorter variant of TRPM8, similar to the canonical TRPM8 found in mice, is also expressed in NM-R skin and DRG neurons. Unknown cold-sensitive channel (bottom left, in green): represents TRPM8-independent cold-sensitive pathways, potentially involving other ion channels. These pathways account for a significant portion of NM-R cold-sensitive neurons and contribute to the ability of NM-R to detect cold.

5.7 Limitations of the study

Despite the robust findings of this study, several limitations still must be considered, particularly regarding experimental constraints and the complexity of TRPM8 expression and function in NM-R.

5.7.1 Technical challenges

This limitation severely restricted our ability to quantify TRPM8 expression at the protein level in NM-R tissues and to directly assess the expression of different isoforms because of lack of antibodies working for western blot. This lack of reliable reagents points to the need for the development of custom antibodies or alternative detection methods, such as mass spectrometry-based proteomics, to overcome this bottleneck.

Another critical limitation of this study pertains to the range of cold temperatures tested in our experimental setup. The lowest temperature tested in our calcium imaging and functional assays was 16°C, which may not fully capture the threshold of TRPM8 cold activation in NM-Rs. Given the poikilothermic nature of NM-Rs, and their stable body temperature of approximately 32°C, it is possible that the TRPM8 cold-sensitivity threshold in this species may lie below 16°C. Future studies incorporating lower-temperature conditions are necessary to precisely characterize the cold-sensing thresholds of NM-R TRPM8, particularly in relation to the unique structural features of its extended isoform.

5.7.2 TRPM8 comparative splice

This study predominantly compared NM-Rs to mice, a well-characterized model for TRPM8 research. However, future research should extend these comparisons to other species that are either adapted to extreme cold environments (e.g., Arctic mammals) or are thermophilic species adapted to hot climates. Comparative analysis with such species will provide a broader evolutionary context for understanding how TRPM8 and other thermoreceptors have evolved to meet the specific demands of diverse thermal environments. Such studies could also elucidate whether the extended N-terminal region in NM-R TRPM8 represents an evolutionary adaptation unique to their poikilothermic physiology or whether similar mechanisms exist in other species.

The presence of an extended N-terminal region in NM-R TRPM8 suggests potential alternative splicing mechanisms that may generate isoforms with distinct functional properties. Our study focused on the most prominent TRPM8 isoform observed, but there is a possibility of other splice variants playing critical roles in cold sensation. To thoroughly investigate these variants, future research could benefit from employing third-generation sequencing technologies, such as Pacific Biosciences (PacBio) or Oxford Nanopore sequencing, which are capable of capturing full length cDNA sequences and defining the complete landscape of splice variants in NM-Rs.

5.7.3 Discrepancies in mRNA and protein localization

We observed discrepancies between mRNA and protein localization in NM-R spinal cord and skin. This could be indicative of post-transcriptional regulatory mechanisms, or a lack of sufficient protein translation in certain tissues. Further validation using single-cell RNA sequencing and proteomic approaches will be crucial to clarify the expression patterns of TRPM8 and its isoforms at both transcriptomic and proteomic levels.

6 Conclusions

The primary objective of this study was to investigate the paradox of cold sensation in NM-R. Unlike other rodents, NM-Rs do not display typical thermoregulatory behaviors or cold-induced nociceptive responses observed in most mammals. This prompted the hypothesis that the mechanisms underlying cold perception in NM-Rs are distinct and specific. While previous studies have explored the behavioral strategies in which NM-Rs use for thermoregulation, the molecular mechanisms underlying their thermosensation remain unclear. The centre of this investigation was TRPM8 ion channel which is widely recognized as the principal mediator of cold sensation in mammals.

This study confirmed the presence of TRPM8 mRNA and protein in various NM-R tissues, including the DRGs, spinal cord, and skin, using RNAscope and immunofluorescence techniques. Notably, expression levels of TRPM8 in the NM-R DRGs were comparable to, or even higher, than those observed in murine models. However, the distribution of TRPM8-positive neurons within the DRGs of NM-Rs differed significantly from that in mice. While TRPM8 is typically localized in the small-diameter, cold-sensitive neurons in other rodents, TRPM8 expression is present in a broader range of neuron sizes in NM-Rs, including larger-diameter neurons.

This study also uncovered a significant population of TRPM8-independent cold-sensitive neurons in the NM-R DRGs. Approximately 20.83% of NM-R DRG neurons, a substantially higher level compared to those in mice, were responsive to cold. Notably, a considerable fraction of these cold-sensitive neurons in NM-Rs were large-diameter neurons and did not rely on TRPM8 for cold detection. This finding suggests the existence of alternative cold sensation pathways in NM-Rs which may compensate for the reduced functionality of TRPM8.

Further analysis of the skin-nerve preparation revealed a broader and more variable response profile in cold-sensitive fibers of NM-R compared to mice. These fibers exhibited higher conduction velocities, indicating a probable adaptation required for rapid cold detection despite the reduced sensitivity of TRPM8. Application of TRPM8 inhibitors like AMTB significantly reduced the firing rate of these fibers, confirming the involvement of TRPM8 in cold sensitivity, albeit with a complex interplay between TRPM8-dependent and independent mechanisms.

A novel and significant finding of this research was the identification of a unique extended N-terminal sequence (1–71 amino acids) in NM-R TRPM8, a feature absent in over thirty other

species. We also showed that the functional regions of TRPM8 responsible for cold and chemical sensitivity are highly conserved across species. Furthermore, functional assays, including calcium imaging of transfected HEK293T cells, demonstrated that NM-R TRPM8 exhibited a significantly reduced response to cold, menthol, and icilin compared to mouse TRPM8. This diminished sensitivity was especially pronounced in the presence of the extended N-terminal sequence. These results suggest that the N-terminal extension in NM-R TRPM8 serves as a regulatory element, dampening the channel sensitivity to cold and chemical stimuli.

Future directions:

1. Investigation of TRPM8 isoforms under stress conditions

To examine the expression of different TRPM8 isoforms in NM-R DRG neurons under varying stress conditions, such as different temperature environments (at 30–32°C and cold). By applying distinct *Trpm8* probes (targeting the canonical and extended variants), we can analyze the spatial distribution of these isoforms. This approach will help determine whether specific TRPM8 isoforms are differentially expressed in larger-diameter neurons and provide insights into potential species variants (see Section 5.2.3). Following this, spatial proteomics can be employed to examine the protein distribution between neurons positive for different probes, providing deeper insights into the functional and structural differences of these TRPM8 isoforms under stress conditions.

2. Exploration of TRPM8-independent cold-sensitive channels

A direct approach would involve investigating known cold-sensitive ion channels, such as TRPA1 and TRPC5. Applying candidate cold channel agonists and antagonists to cultured NM-R DRG neurons, followed by calcium imaging, can provide valuable insights into the role of these channels in cold sensation.

7 References

Abraira, V. E., & Ginty, D. D. (2013). The Sensory Neurons of Touch. *Neuron*, *79*(4), 618–639. https://doi.org/10.1016/j.neuron.2013.07.051

Adamczyk, K., Górecka-Bruzda, A., Nowicki, J., Gumułka, M., Molik, E., Schwarz, T., Earley, B., & Klocek, C. (2015). Perception of environment in farm animals – A review. *Annals of Animal Science*, *15*(3), 565–589. https://doi.org/10.1515/aoas-2015-0031

Ahmad, H. I., Mahmood, S., Hassan, M., Sajid, M., Ahmed, I., Shokrollahi, B., Shahzad, A. H., Abbas, S., Raza, S., Khan, K., Muhammad, S. A., Fouad, D., Ataya, F. S., & Li, Z. (2024). Genomic insights into Yak (Bos grunniens) adaptations for nutrient assimilation in high-altitudes. *Scientific Reports*, *14*(1), 5650. https://doi.org/10.1038/s41598-024-55712-3

Ayalew, W., Chu, M., Liang, C., Wu, X., & Yan, P. (2021). Adaptation Mechanisms of Yak (Bos grunniens) to High-Altitude Environmental Stress. *Animals*, *11*(8), 2344. https://doi.org/10.3390/ani11082344

Bagriantsev, S. N., & Gracheva, E. O. (2015). Molecular mechanisms of temperature adaptation. *The Journal of Physiology*, *593*(16), 3483–3491. https://doi.org/10.1113/jphysiol.2014.280446

Baldwin, M. W., & Ko, M.-C. (2020). Functional evolution of vertebrate sensory receptors. *Hormones and Behavior*, *124*, 104771. https://doi.org/10.1016/j.yhbeh.2020.104771

Bandell, M., Story, G. M., Hwang, S. W., Viswanath, V., Eid, S. R., Petrus, M. J., Earley, T. J., & Patapoutian, A. (2004). Noxious Cold Ion Channel TRPA1 Is Activated by Pungent Compounds and Bradykinin. *Neuron*, *41*(6), 849–857. https://doi.org/10.1016/S0896-6273(04)00150-3

Basbaum, A. I., Bautista, D. M., Scherrer, G., & Julius, D. (2009). Cellular and Molecular Mechanisms of Pain. *Cell*, *139*(2), 267–284. https://doi.org/10.1016/j.cell.2009.09.028

Bautista, D. M., Jordt, S.-E., Nikai, T., Tsuruda, P. R., Read, A. J., Poblete, J., Yamoah, E. N., Basbaum, A. I., & Julius, D. (2006). TRPA1 Mediates the Inflammatory Actions of Environmental Irritants and Proalgesic Agents. *Cell*, *124*(6), 1269–1282. https://doi.org/10.1016/j.cell.2006.02.023

References

Bautista, D. M., Siemens, J., Glazer, J. M., Tsuruda, P. R., Basbaum, A. I., Stucky, C. L., Jordt, S.-E., & Julius, D. (2007). The menthol receptor TRPM8 is the principal detector of environmental cold. *Nature*, *448*(7150), 204–208. https://doi.org/10.1038/nature05910

Beery, A. K., Bicks, L., Mooney, S. J., Goodwin, N. L., & Holmes, M. M. (2016). Sex, social status, and CRF receptor densities in naked mole-rats. *Journal of Comparative Neurology*, *524*(2), 228–243. https://doi.org/10.1002/cne.23834

Begall, S., Berendes, M., Schielke, C. K. M., Henning, Y., Laghanke, M., Scharff, A., Van Daele, P., & Burda, H. (2015). Temperature preferences of African mole-rats (family Bathyergidae). *Journal of Thermal Biology*, *53*, 15–22. https://doi.org/10.1016/j.jtherbio.2015.08.003

Bégay, V., Cirovic, B., Barker, A. J., Klopfleisch, R., Hart, D. W., Bennett, N. C., & Lewin, G. R. (2022). *Immune competence and spleen size scale with colony status in the naked mole-rat*. https://doi.org/10.1098/rsob.210292

Bernal, L., Sotelo-Hitschfeld, P., König, C., Sinica, V., Wyatt, A., Winter, Z., Hein, A., Touska, F., Reinhardt, S., Tragl, A., Kusuda, R., Wartenberg, P., Sclaroff, A., Pfeifer, J. D., Ectors, F., Dahl, A., Freichel, M., Vlachova, V., Brauchi, S., … Zimmermann, K. (2021). Odontoblast TRPC5 channels signal cold pain in teeth. *Science Advances*, *7*(13), eabf5567. https://doi.org/10.1126/sciadv.abf5567

Betz, M. J., & Enerbäck, S. (2018). Targeting thermogenesis in brown fat and muscle to treat obesity and metabolic disease. *Nature Reviews Endocrinology*, *14*(2), 77–87. https://doi.org/10.1038/nrendo.2017.132

Bonnet, C., Oh, D., Mei, H., Robertson, S., Chang, D., Bourges, J.-L., Behar-Cohen, F., Zheng, J. J., & Deng, S. X. (2021). Wnt6 plays a complex role in maintaining human limbal stem/progenitor cells. *Scientific Reports*, *11*(1), 20948. https://doi.org/10.1038/s41598-021-00273-y

Browe, B. M., Vice, E. N., & Park, T. J. (2020). Naked Mole-Rats: Blind, Naked, and Feeling No Pain. *The Anatomical Record*, *303*(1), 77–88. https://doi.org/10.1002/ar.23996

Buffenstein, R., Amoroso, V., Andziak, B., Avdieiev, S., Azpurua, J., Barker, A. J., Bennett, N. C., Brieño-Enríquez, M. A., Bronner, G. N., Coen, C., Delaney, M. A., Dengler-Crish, C. M., Edrey, Y. H., Faulkes, C. G., Frankel, D., Friedlander, G., Gibney, P. A., Gorbunova, V., Hine, C., … Smith, E. St. J. (2021). The naked truth: A comprehensive clarification and classification of current 'myths' in naked mole-rat biology. *Biological Reviews*, brv.12791. https://doi.org/10.1111/brv.12791

Buffenstein, R., Park, T. J., & Holmes, M. M. (Eds.). (2021). *The Extraordinary Biology of the Naked Mole-Rat* (Vol. 1319). Springer International Publishing. https://doi.org/10.1007/978-3-030-65943-1

Cai, W., Zhang, W., Zheng, Q., Hor, C. C., Pan, T., Fatima, M., Dong, X., Duan, B., & Xu, X. Z. S. (2024). The kainate receptor GluK2 mediates cold sensing in mice. *Nature Neuroscience*. https://doi.org/10.1038/s41593-024-01585-8

Cao, E., Cordero-Morales, J. F., Liu, B., Qin, F., & Julius, D. (2013). TRPV1 Channels Are Intrinsically Heat Sensitive and Negatively Regulated by Phosphoinositide Lipids. *Neuron*, *77*(4), 667–679. https://doi.org/10.1016/j.neuron.2012.12.016

Caterina, M. J., Schumacher, M. A., Tominaga, M., Rosen, T. A., Levine, J. D., & Julius, D. (1997). The capsaicin receptor: A heat-activated ion channel in the pain pathway. *Nature*, *389*(6653), 816–824. https://doi.org/10.1038/39807

Chen, J., Kang, D., Xu, J., Lake, M., Hogan, J. O., Sun, C., Walter, K., Yao, B., & Kim, D. (2013). Species differences and molecular determinant of TRPA1 cold sensitivity. *Nature Communications*, *4*(1), 2501. https://doi.org/10.1038/ncomms3501

Chen, X., Sooch, G., Demaree, I. S., White, F. A., & Obukhov, A. G. (2020). Transient Receptor Potential Canonical (TRPC) Channels: Then and Now. *Cells*, *9*(9), 1983. https://doi.org/10.3390/cells9091983

Cheng, H., Sebaa, R., Malholtra, N., Lacoste, B., El Hankouri, Z., Kirby, A., Bennett, N. C., Van Jaarsveld, B., Hart, D. W., Tattersall, G. J., Harper, M.-E., & Pamenter, M. E. (2021). Naked

mole-rat brown fat thermogenesis is diminished during hypoxia through a rapid decrease in UCP1. *Nature Communications*, *12*(1), 6801. https://doi.org/10.1038/s41467-021-27170-2

Chi, G., Liang, Q., Sridhar, A., Cowgill, J. B., Sader, K., Radjainia, M., Qian, P., Castro-Hartmann, P., Venkaya, S., Singh, N. K., McKinley, G., Fernandez-Cid, A., Mukhopadhyay, S. M. M., Burgess-Brown, N. A., Delemotte, L., Covarrubias, M., & Dürr, K. L. (2022). Cryo-EM structure of the human Kv3.1 channel reveals gating control by the cytoplasmic T1 domain. *Nature Communications*, *13*(1), 4087. https://doi.org/10.1038/s41467-022-29594-w

Colditz, I. G., & Hine, B. C. (2016). Resilience in farm animals: Biology, management, breeding and implications for animal welfare. *Animal Production Science*, *56*(12), 1961. https://doi.org/10.1071/AN15297

Cordero-Morales, J. F., Gracheva, E. O., & Julius, D. (2011). Cytoplasmic ankyrin repeats of transient receptor potential A1 (TRPA1) dictate sensitivity to thermal and chemical stimuli. *Proceedings of the National Academy of Sciences*, *108*(46). https://doi.org/10.1073/pnas.1114124108

Cox, P. G., Faulkes, C. G., & Bennett, N. C. (2020). Masticatory musculature of the African mole-rats (Rodentia: Bathyergidae). *PeerJ*, *8*, e8847. https://doi.org/10.7717/peerj.8847

Craig, A. D., & Dostrovsky, J. O. (2001). Differential Projections of Thermoreceptive and Nociceptive Lamina I Trigeminothalamic and Spinothalamic Neurons in the Cat. *Journal of Neurophysiology*, *86*(2), 856–870. https://doi.org/10.1152/jn.2001.86.2.856

Daniels, R. L., & McKemy, D. D. (2007). Mice Left Out in the Cold: Commentary on the Phenotype of TRPM8-Nulls. *Molecular Pain*, *3*, 1744-8069-3–23. https://doi.org/10.1186/1744-8069-3-23

Del Camino, D., Murphy, S., Heiry, M., Barrett, L. B., Earley, T. J., Cook, C. A., Petrus, M. J., Zhao, M., D'Amours, M., Deering, N., Brenner, G. J., Costigan, M., Hayward, N. J., Chong, J. A., Fanger, C. M., Woolf, C. J., Patapoutian, A., & Moran, M. M. (2010). TRPA1 Contributes to Cold Hypersensitivity. *The Journal of Neuroscience*, *30*(45), 15165–15174. https://doi.org/10.1523/JNEUROSCI.2580-10.2010

Dhaka, A., Earley, T. J., Watson, J., & Patapoutian, A. (2008). Visualizing Cold Spots: TRPM8-Expressing Sensory Neurons and Their Projections. *Journal of Neuroscience*, *28*(3), 566–575. https://doi.org/10.1523/JNEUROSCI.3976-07.2008

Dhaka, A., Murray, A. N., Mathur, J., Earley, T. J., Petrus, M. J., & Patapoutian, A. (2007). TRPM8 Is Required for Cold Sensation in Mice. *Neuron*, *54*(3), 371–378. https://doi.org/10.1016/j.neuron.2007.02.024

Díaz-Franulic, I., Raddatz, N., Castillo, K., González-Nilo, F. D., & Latorre, R. (2020). A folding reaction at the C-terminal domain drives temperature sensing in TRPM8 channels. *Proceedings of the National Academy of Sciences*, *117*(33), 20298–20304. https://doi.org/10.1073/pnas.2004303117

Dragoni, I., Guida, E., & McIntyre, P. (2006). The Cold and Menthol Receptor TRPM8 Contains a Functionally Important Double Cysteine Motif. *Journal of Biological Chemistry*, *281*(49), 37353–37360. https://doi.org/10.1074/jbc.M607227200

Eigenbrod, O., Debus, K. Y., Reznick, J., Bennett, N. C., Sánchez-Carranza, O., Omerbašić, D., Hart, D. W., Barker, A. J., Zhong, W., Lutermann, H., Katandukila, J. V., Mgode, G., Park, T. J., & Lewin, G. R. (2019). Rapid molecular evolution of pain insensitivity in multiple African rodents. *Science*, *364*(6443), 852–859. https://doi.org/10.1126/science.aau0236

Erler, I., Al-Ansary, D. M. M., Wissenbach, U., Wagner, T. F. J., Flockerzi, V., & Niemeyer, B. A. (2006). Trafficking and Assembly of the Cold-sensitive TRPM8 Channel. *Journal of Biological Chemistry*, *281*(50), 38396–38404. https://doi.org/10.1074/jbc.M607756200

Fajardo, O., Meseguer, V., Belmonte, C., & Viana, F. (2008). TRPA1 Channels Mediate Cold Temperature Sensing in Mammalian Vagal Sensory Neurons: Pharmacological and Genetic Evidence. *The Journal of Neuroscience*, *28*(31), 7863–7875. https://doi.org/10.1523/JNEUROSCI.1696-08.2008

References

Faulkes, C. G., & Bennett, N. C. (2013). Plasticity and constraints on social evolution in African mole-rats: Ultimate and proximate factors. *Philosophical Transactions of the Royal Society B: Biological Sciences*, *368*(1618), 20120347. https://doi.org/10.1098/rstb.2012.0347

Finn, K. T., Janse van Vuuren, A. K., Hart, D. W., Süess, T., Zöttl, M., & Bennett, N. C. (2022). Seasonal Changes in Locomotor Activity Patterns of Wild Social Natal Mole-Rats (Cryptomys hottentotus natalensis). *Frontiers in Ecology and Evolution*, *10*, 819393. https://doi.org/10.3389/fevo.2022.819393

Follmann, R., Goldsmith, C. J., & Stein, W. (2018). Multimodal sensory information is represented by a combinatorial code in a sensorimotor system. *PLOS Biology*, *16*(10), e2004527. https://doi.org/10.1371/journal.pbio.2004527

Gardill, B. R., Rivera-Acevedo, R. E., Tung, C.-C., Okon, M., McIntosh, L. P., & Van Petegem, F. (2018). The voltage-gated sodium channel EF-hands form an interaction with the III-IV linker that is disturbed by disease-causing mutations. *Scientific Reports*, *8*(1), 4483. https://doi.org/10.1038/s41598-018-22713-y

Gau, P., Poon, J., Ufret-Vincenty, C., Snelson, C. D., Gordon, S. E., Raible, D. W., & Dhaka, A. (2013). The Zebrafish Ortholog of TRPV1 Is Required for Heat-Induced Locomotion. *The Journal of Neuroscience*, *33*(12), 5249–5260. https://doi.org/10.1523/JNEUROSCI.5403-12.2013

Geiser, F. (2004). Metabolic Rate and Body Temperature Reduction During Hibernation and Daily Torpor. *Annual Review of Physiology*, *66*(1), 239–274. https://doi.org/10.1146/annurev.physiol.66.032102.115105

Gomes Rodrigues, H., Šumbera, R., & Hautier, L. (2016). Life in Burrows Channelled the Morphological Evolution of the Skull in Rodents: The Case of African Mole-Rats (Bathyergidae, Rodentia). *Journal of Mammalian Evolution*, *23*(2), 175–189. https://doi.org/10.1007/s10914-015-9305-x

Gong, J., Liu, J., Ronan, E. A., He, F., Cai, W., Fatima, M., Zhang, W., Lee, H., Li, Z., Kim, G.-H., Pipe, K. P., Duan, B., Liu, J., & Xu, X. Z. S. (2019). A Cold-Sensing Receptor Encoded by a Glutamate Receptor Gene. *Cell*, *178*(6), 1375-1386.e11. https://doi.org/10.1016/j.cell.2019.07.034

González-Muñiz, R., Bonache, M. A., Martín-Escura, C., & Gómez-Monterrey, I. (2019). Recent Progress in TRPM8 Modulation: An Update. *International Journal of Molecular Sciences*, *20*(11), 2618. https://doi.org/10.3390/ijms20112618

Gorshkova, E. A., Gubernatorova, E. O., Dvorianinova, E. M., Yurakova, T. R., Marey, M. V., Averina, O. A., Holtze, S., Hildebrandt, T. B., Dmitriev, A. A., Drutskaya, M. S., Vyssokikh, M. Yu., & Nedospasov, S. A. (2023). Macrophages from naked mole-rat possess distinct immunometabolic signatures upon polarization. *Frontiers in Immunology*, *14*, 1172467. https://doi.org/10.3389/fimmu.2023.1172467

Gracheva, E. O., Cordero-Morales, J. F., González-Carcacía, J. A., Ingolia, N. T., Manno, C., Aranguren, C. I., Weissman, J. S., & Julius, D. (2011). Ganglion-specific splicing of TRPV1 underlies infrared sensation in vampire bats. *Nature*, *476*(7358), 88–91. https://doi.org/10.1038/nature10245

Hellenthal, K. E. M., Brabenec, L., Gross, E. R., & Wagner, N.-M. (2021). TRP Channels as Sensors of Aldehyde and Oxidative Stress. *Biomolecules*, *11*(10), 1401. https://doi.org/10.3390/biom11101401

Hilton, H. G., Rubinstein, N. D., Janki, P., Ireland, A. T., Bernstein, N., Fong, N. L., Wright, K. M., Smith, M., Finkle, D., Martin-McNulty, B., Roy, M., Imai, D. M., Jojic, V., & Buffenstein, R. (2019). Single-cell transcriptomics of the naked mole-rat reveals unexpected features of mammalian immunity. *PLOS Biology*, *17*(11), e3000528. https://doi.org/10.1371/journal.pbio.3000528

Hinman, A., Chuang, H., Bautista, D. M., & Julius, D. (2006). TRP channel activation by reversible covalent modification. *Proceedings of the National Academy of Sciences*, *103*(51), 19564–19568. https://doi.org/10.1073/pnas.0609598103

References

Hoffstaetter, L. J., Bagriantsev, S. N., & Gracheva, E. O. (2018). TRPs et al.: A molecular toolkit for thermosensory adaptations. *Pflügers Archiv - European Journal of Physiology*, *470*(5), 745–759. https://doi.org/10.1007/s00424-018-2120-5

Iftinca, M., & Altier, C. (2020). The cool things to know about TRPM8! *Channels*, *14*(1), 413–420. https://doi.org/10.1080/19336950.2020.1841419

Izquierdo, C., Martín-Martínez, M., Gómez-Monterrey, I., & González-Muñiz, R. (2021). TRPM8 Channels: Advances in Structural Studies and Pharmacological Modulation. *International Journal of Molecular Sciences*, *22*(16), 8502. https://doi.org/10.3390/ijms22168502

Jacobs, P. J., & Oosthuizen, M. K. (2023). Laterality in the Damaraland Mole-Rat: Insights from a Eusocial Mammal. *Animals*, *13*(4), 627. https://doi.org/10.3390/ani13040627

Jessen, C. (1981). Independent clamps of peripheral and central temperatures and their effects on heat production in the goat. *The Journal of Physiology*, *311*(1), 11–22. https://doi.org/10.1113/jphysiol.1981.sp013570

Jordt, S.-E., Bautista, D. M., Chuang, H., McKemy, D. D., Zygmunt, P. M., Högestätt, E. D., Meng, I. D., & Julius, D. (2004). Mustard oils and cannabinoids excite sensory nerve fibres through the TRP channel ANKTM1. *Nature*, *427*(6971), 260–265. https://doi.org/10.1038/nature02282

Jordt, S.-E., & Julius, D. (2002). Molecular Basis for Species-Specific Sensitivity to "Hot" Chili Peppers. *Cell*, *108*(3), 421–430. https://doi.org/10.1016/S0092-8674(02)00637-2

Julius, D. (2013). TRP Channels and Pain. *Annual Review of Cell and Developmental Biology*, *29*(1), 355–384. https://doi.org/10.1146/annurev-cellbio-101011-155833

Julius, D., & Basbaum, A. I. (2001). *Molecular mechanisms of nociception*. *413*.

Kang, K., Panzano, V. C., Chang, E. C., Ni, L., Dainis, A. M., Jenkins, A. M., Regna, K., Muskavitch, M. A. T., & Garrity, P. A. (2012). Modulation of TRPA1 thermal sensitivity enables sensory discrimination in Drosophila. *Nature*, *481*(7379), 76–80. https://doi.org/10.1038/nature10715

Karashima, Y., Talavera, K., Everaerts, W., Janssens, A., Kwan, K. Y., Vennekens, R., Nilius, B., & Voets, T. (2009). TRPA1 acts as a cold sensor in vitro and in vivo. *Proceedings of the National Academy of Sciences*, *106*(4), 1273–1278. https://doi.org/10.1073/pnas.0808487106

Kashio, M., & Tominaga, M. (2022). TRP channels in thermosensation. *Current Opinion in Neurobiology*, *75*, 102591. https://doi.org/10.1016/j.conb.2022.102591

Kim, T. K., & Eberwine, J. H. (2010). Mammalian cell transfection: The present and the future. *Analytical and Bioanalytical Chemistry*, *397*(8), 3173–3178. https://doi.org/10.1007/s00216-010-3821-6

Knowlton, W. M., Palkar, R., Lippoldt, E. K., McCoy, D. D., Baluch, F., Chen, J., & McKemy, D. D. (2013). A Sensory-Labeled Line for Cold: TRPM8-Expressing Sensory Neurons Define the Cellular Basis for Cold, Cold Pain, and Cooling-Mediated Analgesia. *The Journal of Neuroscience*, *33*(7), 2837–2848. https://doi.org/10.1523/JNEUROSCI.1943-12.2013

Kobayashi, K., Fukuoka, T., Obata, K., Yamanaka, H., Dai, Y., Tokunaga, A., & Noguchi, K. (2005). Distinct expression of TRPM8, TRPA1, and TRPV1 mRNAs in rat primary afferent neurons with aδ/c-fibers and colocalization with trk receptors. *Journal of Comparative Neurology*, *493*(4), 596–606. https://doi.org/10.1002/cne.20794

Koltzenburg, M., Stucky, C. L., & Lewin, G. R. (1997). Receptive Properties of Mouse Sensory Neurons Innervating Hairy Skin. *Journal of Neurophysiology*, *78*(4), 1841–1850. https://doi.org/10.1152/jn.1997.78.4.1841

Krebs, E. J. R., & Clutton-Brock, T. (1991). *MONOGRAPHS IN BEHAVIOR AND ECOLOGY*.

Latorre, R., Brauchi, S., Orta, G., Zaelzer, C., & Vargas, G. (2007). ThermoTRP channels as modular proteins with allosteric gating. *Cell Calcium*, *42*(4–5), 427–438. https://doi.org/10.1016/j.ceca.2007.04.004

Laursen, W. J., Schneider, E. R., Merriman, D. K., Bagriantsev, S. N., & Gracheva, E. O. (2016). Low-cost functional plasticity of TRPV1 supports heat tolerance in squirrels and camels.

Proceedings of the National Academy of Sciences, *113*(40), 11342–11347. https://doi.org/10.1073/pnas.1604269113

Lewin, G. R., & Moshourab, R. (2004). Mechanosensation and pain. *Journal of Neurobiology*, *61*(1), 30–44. https://doi.org/10.1002/neu.20078

Li, J., Zumpano, K. T., & Lemon, C. H. (2024). Separation of Oral Cooling and Warming Requires TRPM8. *The Journal of Neuroscience*, *44*(11), e1383232024. https://doi.org/10.1523/JNEUROSCI.1383-23.2024

Li, L., Rutlin, M., Abraira, V. E., Cassidy, C., Kus, L., Gong, S., Jankowski, M. P., Luo, W., Heintz, N., Koerber, H. R., Woodbury, C. J., & Ginty, D. D. (2011). The Functional Organization of Cutaneous Low-Threshold Mechanosensory Neurons. *Cell*, *147*(7), 1615–1627. https://doi.org/10.1016/j.cell.2011.11.027

Lin, T. D., Rubinstein, N. D., Fong, N. L., Smith, M., Craft, W., Martin-McNulty, B., Perry, R., Delaney, M. A., Roy, M. A., & Buffenstein, R. (2024). Evolution of T cells in the cancer-resistant naked mole-rat. *Nature Communications*, *15*(1), 3145. https://doi.org/10.1038/s41467-024-47264-x

Lippoldt, E. K., Elmes, R. R., McCoy, D. D., Knowlton, W. M., & McKemy, D. D. (2013). Artemin, a Glial Cell Line-Derived Neurotrophic Factor Family Member, Induces TRPM8-Dependent Cold Pain. *Journal of Neuroscience*, *33*(30), 12543–12552. https://doi.org/10.1523/JNEUROSCI.5765-12.2013

Liu, Y., Mikrani, R., He, Y., Faran Ashraf Baig, M. M., Abbas, M., Naveed, M., Tang, M., Zhang, Q., Li, C., & Zhou, X. (2020). TRPM8 channels: A review of distribution and clinical role. *European Journal of Pharmacology*, *882*, 173312. https://doi.org/10.1016/j.ejphar.2020.173312

Lu, X., Yao, Z., Wang, Y., Yin, C., Li, J., Chai, L., Dong, W., Yuan, L., Lai, R., & Yang, S. (2022). The acquisition of cold sensitivity during TRPM8 ion channel evolution. *Proceedings of the National Academy of Sciences*, *119*(21), e2201349119. https://doi.org/10.1073/pnas.2201349119

Lumpkin, E. A., & Caterina, M. J. (2007). Mechanisms of sensory transduction in the skin. *Nature*, *445*(7130), 858–865. https://doi.org/10.1038/nature05662

Maille, A., & Schradin, C. (2017). Ecophysiology of cognition: How do environmentally induced changes in physiology affect cognitive performance? *Biological Reviews*, *92*(2), 1101–1112. https://doi.org/10.1111/brv.12270

Malik, H. R., Bertolesi, G. E., & McFarlane, S. (2023). TRPM8 thermosensation in poikilotherms mediates both skin colour and locomotor performance responses to cold temperature. *Communications Biology*, *6*(1), 127. https://doi.org/10.1038/s42003-023-04489-8

Malkia, A., Pertusa, M., Fernández-Ballester, G., Ferrer-Montiel, A., & Viana, F. (2009). Differential Role of the Menthol-Binding Residue Y745 in the Antagonism of Thermally Gated TRPM8 Channels. *Molecular Pain*, *5*, 1744-8069-5–62. https://doi.org/10.1186/1744-8069-5-62

Matos-Cruz, V., Schneider, E. R., Mastrotto, M., Merriman, D. K., Bagriantsev, S. N., & Gracheva, E. O. (2017). Molecular Prerequisites for Diminished Cold Sensitivity in Ground Squirrels and Hamsters. *Cell Reports*, *21*(12), 3329–3337. https://doi.org/10.1016/j.celrep.2017.11.083

McCoy, E. S., Taylor-Blake, B., & Zylka, M. J. (2012). CGRPα-Expressing Sensory Neurons Respond to Stimuli that Evoke Sensations of Pain and Itch. *PLoS ONE*, *7*(5), e36355. https://doi.org/10.1371/journal.pone.0036355

McKemy, D. D. (2018). Molecular basis of peripheral innocuous cold sensitivity. In *Handbook of Clinical Neurology* (Vol. 156, pp. 57–67). Elsevier. https://doi.org/10.1016/B978-0-444-63912-7.00003-5

McKemy, D. D., Neuhausser, W. M., & Julius, D. (2002). Identification of a cold receptor reveals a general role for TRP channels in thermosensation. *Nature*, *416*(6876), 52–58. https://doi.org/10.1038/nature719

Meltzer, S., Santiago, C., Sharma, N., & Ginty, D. D. (2021). The cellular and molecular basis of somatosensory neuron development. *Neuron*, *109*(23), 3736–3757. https://doi.org/10.1016/j.neuron.2021.09.004

Mikesell, A. R., Isaeva, O., Moehring, F., Sadler, K. E., Menzel, A. D., & Stucky, C. L. (2022). Keratinocyte PIEZO1 modulates cutaneous mechanosensation. *ELife*, *11*, e65987. https://doi.org/10.7554/eLife.65987

Milenkovic, N., Wetzel, C., Moshourab, R., & Lewin, G. R. (2008). Speed and Temperature Dependences of Mechanotransduction in Afferent Fibers Recorded From the Mouse Saphenous Nerve. *Journal of Neurophysiology*, *100*(5), 2771–2783. https://doi.org/10.1152/jn.90799.2008

Milenkovic, N., Zhao, W.-J., Walcher, J., Albert, T., Siemens, J., Lewin, G. R., & Poulet, J. F. A. (2014). A somatosensory circuit for cooling perception in mice | Nature Neuroscience. *Nature Neuroscience*, *17*(11), 1560–1566. https://doi.org/10.1038/nn.3828

Molliver, D. C., Wright, D. E., Leitner, M. L., Parsadanian, A. S., Doster, K., Wen, D., Yan, Q., & Snider, W. D. (1997). IB4-Binding DRG Neurons Switch from NGF to GDNF Dependence in Early Postnatal Life. *Neuron*, *19*(4), 849–861. https://doi.org/10.1016/S0896-6273(00)80966-6

Montell, C., & Rubin, G. M. (1989). Molecular characterization of the drosophila trp locus: A putative integral membrane protein required for phototransduction. *Neuron*, *2*(4), 1313–1323. https://doi.org/10.1016/0896-6273(89)90069-X

Montoya-Sanhueza, G., Bennett, N. C., Chinsamy, A., & Šumbera, R. (2022). Functional anatomy and disparity of the postcranial skeleton of African mole-rats (Bathyergidae). *Frontiers in Ecology and Evolution*, *10*, 857474. https://doi.org/10.3389/fevo.2022.857474

Montoya-Sanhueza, G., Šaffa, G., Šumbera, R., Chinsamy, A., Jarvis, J. U. M., & Bennett, N. C. (2022). Fossorial adaptations in African mole-rats (Bathyergidae) and the unique appendicular phenotype of naked mole-rats. *Communications Biology*, *5*(1), 526. https://doi.org/10.1038/s42003-022-03480-z

Moparthi, L., Sinica, V., Moparthi, V. K., Kreir, M., Vignane, T., Filipovic, M. R., Vlachova, V., & Zygmunt, P. M. (2022). The human TRPA1 intrinsic cold and heat sensitivity involves separate

channel structures beyond the N-ARD domain. *Nature Communications*, *13*(1), 6113. https://doi.org/10.1038/s41467-022-33876-8

Morenilla-Palao, C., Luis, E., Fernández-Peña, C., Quintero, E., Weaver, J. L., Bayliss, D. A., & Viana, F. (2014). Ion Channel Profile of TRPM8 Cold Receptors Reveals a Role of TASK-3 Potassium Channels in Thermosensation. *Cell Reports*, *8*(5), 1571–1582. https://doi.org/10.1016/j.celrep.2014.08.003

Morhart, M. J. (2015). *Selective traits of pup ontogeny and reproduction in two captive naked mole-rat (Heterocephalus glaber) colonies*. https://doi.org/10.25365/THESIS.38400

Myers, B. R., Sigal, Y. M., & Julius, D. (2009). Evolution of Thermal Response Properties in a Cold-Activated TRP Channel. *PLoS ONE*, *4*(5), e5741. https://doi.org/10.1371/journal.pone.0005741

Nilius, B., & Owsianik, G. (2011). The transient receptor potential family of ion channels. *Genome Biology*, *12*(3), 218. https://doi.org/10.1186/gb-2011-12-3-218

Nilius, B., & Voets, T. (2008). A TRP channel-steroid marriage. *Nature Cell Biology*, *10*(12), 1383–1384. https://doi.org/10.1038/ncb1208-1383

Oelkrug, R., Polymeropoulos, E. T., & Jastroch, M. (2015). Brown adipose tissue: Physiological function and evolutionary significance. *Journal of Comparative Physiology B*, *185*(6), 587–606. https://doi.org/10.1007/s00360-015-0907-7

Oiwa, Y., Oka, K., Yasui, H., Higashikawa, K., Bono, H., Kawamura, Y., Miyawaki, S., Watarai, A., Kikusui, T., Shimizu, A., Okano, H., Kuge, Y., Kimura, K., Okamatsu-Ogura, Y., & Miura, K. (2020). Characterization of brown adipose tissue thermogenesis in the naked mole-rat (Heterocephalus glaber), a heterothermic mammal. *Scientific Reports*, *10*(1), 19488. https://doi.org/10.1038/s41598-020-74929-6

Okamura, Y., Nishino, A., Murata, Y., Nakajo, K., Iwasaki, H., Ohtsuka, Y., Tanaka-Kunishima, M., Takahashi, N., Hara, Y., Yoshida, T., Nishida, M., Okado, H., Watari, H., Meinertzhagen, I. A., Satoh, N., Takahashi, K., Satou, Y., Okada, Y., & Mori, Y. (2005). Comprehensive analysis of

the ascidian genome reveals novel insights into the molecular evolution of ion channel genes. *Physiological Genomics*, *22*(3), 269–282. https://doi.org/10.1152/physiolgenomics.00229.2004

Omerbašić, D., Schuhmacher, L.-N., Bernal Sierra, Y.-A., Smith, E. St. J., & Lewin, G. R. (2015). ASICs and mammalian mechanoreceptor function. *Neuropharmacology*, *94*, 80–86. https://doi.org/10.1016/j.neuropharm.2014.12.007

Oosthuizen, M. K., & Bennett, N. C. (2022). Clocks Ticking in the Dark: A Review of Biological Rhythms in Subterranean African Mole-Rats. *Frontiers in Ecology and Evolution*, *10*, 878533. https://doi.org/10.3389/fevo.2022.878533

Oosthuizen, M. K., Robb, G., Harrison, A., Froneman, A., Joubert, K., & Bennett, N. C. (2021). Flexibility in body temperature rhythms of free-living natal mole-rats (Cryptomys hottentotus natalensis). *Journal of Thermal Biology*, *99*, 102973. https://doi.org/10.1016/j.jtherbio.2021.102973

Palchevskyi, S., Czarnocki-Cieciura, M., Vistoli, G., Gervasoni, S., Nowak, E., Beccari, A. R., Nowotny, M., & Talarico, C. (2023). Structure of human TRPM8 channel. *Communications Biology*, *6*(1), 1065. https://doi.org/10.1038/s42003-023-05425-6

Pamenter, M. E. (2022). Adaptations to a hypoxic lifestyle in naked mole-rats. *Journal of Experimental Biology*, *225*(4), jeb196725. https://doi.org/10.1242/jeb.196725

Paricio-Montesinos, R., Schwaller, F., Udhayachandran, A., Rau, F., Walcher, J., Evangelista, R., Vriens, J., Voets, T., Poulet, J. F. A., & Lewin, G. R. (2020). The Sensory Coding of Warm Perception. *Neuron*, *106*(5), 830-841.e3. https://doi.org/10.1016/j.neuron.2020.02.035

Park, T. J., Lu, Y., Jüttner, R., Smith, E. St. J., Hu, J., Brand, A., Wetzel, C., Milenkovic, N., Erdmann, B., Heppenstall, P. A., Laurito, C. E., Wilson, S. P., & Lewin, G. R. (2008). Selective Inflammatory Pain Insensitivity in the African Naked Mole-Rat (Heterocephalus glaber). *PLoS Biology*, *6*(1), e13. https://doi.org/10.1371/journal.pbio.0060013

Patapoutian, A., Peier, A. M., Story, G. M., & Viswanath, V. (2003). ThermoTRP channels and beyond: Mechanisms of temperature sensation. *Nature Reviews Neuroscience*, *4*(7), 529–539. https://doi.org/10.1038/nrn1141

Paulsen, C. E., Armache, J.-P., Gao, Y., Cheng, Y., & Julius, D. (2015). Structure of the TRPA1 ion channel suggests regulatory mechanisms. *Nature*, *520*(7548), 511–517. https://doi.org/10.1038/nature14367

Pedretti, A., Marconi, C., Bettinelli, I., & Vistoli, G. (2009). Comparative modeling of the quaternary structure for the human TRPM8 channel and analysis of its binding features. *Biochimica et Biophysica Acta (BBA) - Biomembranes*, *1788*(5), 973–982. https://doi.org/10.1016/j.bbamem.2009.02.007

Peier, A. M., Reeve, A. J., Andersson, D. A., Moqrich, A., Earley, T. J., Hergarden, A. C., Story, G. M., Colley, S., Hogenesch, J. B., McIntyre, P., Bevan, S., & Patapoutian, A. (2002). A Heat-Sensitive TRP Channel Expressed in Keratinocytes. *Science*, *296*(5575), 2046–2049. https://doi.org/10.1126/science.1073140

Pertusa, M., González, A., Hardy, P., Madrid, R., & Viana, F. (2014). Bidirectional Modulation of Thermal and Chemical Sensitivity of TRPM8 Channels by the Initial Region of the N-terminal Domain. *Journal of Biological Chemistry*, *289*(32), 21828–21843. https://doi.org/10.1074/jbc.M114.565994

Phelps, C. B., & Gaudet, R. (2007). The Role of the N Terminus and Transmembrane Domain of TRPM8 in Channel Localization and Tetramerization. *Journal of Biological Chemistry*, *282*(50), 36474–36480. https://doi.org/10.1074/jbc.M707205200

Plaza-Cayón, A., González-Muñiz, R., & Martín-Martínez, M. (2022). Mutations of TRPM8 channels: Unraveling the molecular basis of activation by cold and ligands. *Medicinal Research Reviews*, *42*(6), 2168–2203. https://doi.org/10.1002/med.21920

Poole, K., Herget, R., Lapatsina, L., Ngo, H.-D., & Lewin, G. R. (2014). Tuning Piezo ion channels to detect molecular-scale movements relevant for fine touch. *Nature Communications*, *5*(1), 3520. https://doi.org/10.1038/ncomms4520

Porro, A., Saponaro, A., Gasparri, F., Bauer, D., Gross, C., Pisoni, M., Abbandonato, G., Hamacher, K., Santoro, B., Thiel, G., & Moroni, A. (2019). The HCN domain couples voltage gating and cAMP response in hyperpolarization-activated cyclic nucleotide-gated channels. *ELife*, *8*, e49672. https://doi.org/10.7554/eLife.49672

Poulson, S. J., Aldarraji, A., Arain, I. I., Dziekonski, N., Motlana, K., Riley, R., Holmes, M. M., & Martin, L. J. (2020). Naked mole-rats lack cold sensitivity before and after nerve injury. *Molecular Pain*, *16*, 174480692095510. https://doi.org/10.1177/1744806920955103

Prober, D. A., Zimmerman, S., Myers, B. R., McDermott, B. M., Kim, S.-H., Caron, S., Rihel, J., Solnica-Krezel, L., Julius, D., Hudspeth, A. J., & Schier, A. F. (2008). Zebrafish TRPA1 Channels Are Required for Chemosensation But Not for Thermosensation or Mechanosensory Hair Cell Function. *The Journal of Neuroscience*, *28*(40), 10102–10110. https://doi.org/10.1523/JNEUROSCI.2740-08.2008

Reimúndez, A., Fernández-Peña, C., García, G., Fernández, R., Ordás, P., Gallego, R., Pardo-Vazquez, J. L., Arce, V., Viana, F., & Señarís, R. (2018). Deletion of the Cold Thermoreceptor TRPM8 Increases Heat Loss and Food Intake Leading to Reduced Body Temperature and Obesity in Mice. *The Journal of Neuroscience*, *38*(15), 3643–3656. https://doi.org/10.1523/JNEUROSCI.3002-17.2018

Reimúndez, A., Fernández-Peña, C., Ordás, P., Hernández-Ortego, P., Gallego, R., Morenilla-Palao, C., Navarro, J., Martín-Cora, F., Pardo-Vázquez, J. L., Schwarz, L. A., Arce, V., Viana, F., & Señarís, R. (2023). The cold-sensing ion channel TRPM8 regulates central and peripheral clockwork and the circadian oscillations of body temperature. *Acta Physiologica*, *237*(3), e13896. https://doi.org/10.1111/apha.13896

Riccio, A. P., & Goldman, B. D. (2000). Circadian rhythms of locomotor activity in naked mole-rats (Heterocephalus glaber). *Physiology & Behavior*, *71*(1–2), 1–13. https://doi.org/10.1016/S0031-9384(00)00281-X

Rivera, B., Moreno, C., Lavanderos, B., Hwang, J. Y., Fernández-Trillo, J., Park, K.-S., Orio, P., Viana, F., Madrid, R., & Pertusa, M. (2021). Constitutive Phosphorylation as a Key Regulator of TRPM8 Channel Function. *The Journal of Neuroscience*, *41*(41), 8475–8493. https://doi.org/10.1523/JNEUROSCI.0345-21.2021

Roberts, W. W. (1988). *Differential Thermosensor Control of Thermoregulatory Grooming, Locomotion, and Relaxed Postural Extension*".

Rohács, T., Lopes, C. M. B., Michailidis, I., & Logothetis, D. E. (2005). PI(4,5)P2 regulates the activation and desensitization of TRPM8 channels through the TRP domain. *Nature Neuroscience*, *8*(5), 626–634. https://doi.org/10.1038/nn1451

Romanovsky, A. A. (2014). Skin temperature: Its role in thermoregulation. *Acta Physiologica*, *210*(3), 498–507. https://doi.org/10.1111/apha.12231

Rosenblum, E. B., Poorten, T. J., Settles, M., Murdoch, G. K., Robert, J., Maddox, N., & Eisen, M. B. (2009). Genome-Wide Transcriptional Response of Silurana (Xenopus) tropicalis to Infection with the Deadly Chytrid Fungus. *PLoS ONE*, *4*(8), e6494. https://doi.org/10.1371/journal.pone.0006494

Sahd, L. (2021). *THE ANATOMY OF SEISMIC SIGNALLING: MORPHOLOGICAL ADAPTATIONS OF THE HIND LIMB IN DRUMMING AND NON-DRUMMING AFRICAN MOLE-RATS (BATHYERGIDAE)* [Stellenbosch University]. http://hdl.handle.net/10019.1/110315

Saito, S., & Shingai, R. (2006). Evolution of thermoTRP ion channel homologs in vertebrates. *Physiological Genomics*, *27*(3), 219–230. https://doi.org/10.1152/physiolgenomics.00322.2005

Seebacher, F. (2009). Responses to temperature variation: Integration of thermoregulation and metabolism in vertebrates. *Journal of Experimental Biology*, *212*(18), 2885–2891. https://doi.org/10.1242/jeb.024430

Simone, D. A., & Kajander, K. C. (1997). Responses of Cutaneous A-Fiber Nociceptors to Noxious Cold. *Journal of Neurophysiology*, *77*(4), 2049–2060. https://doi.org/10.1152/jn.1997.77.4.2049

Soravia, C., Ashton, B. J., Thornton, A., & Ridley, A. R. (2021). The impacts of heat stress on animal cognition: Implications for adaptation to a changing climate. *WIREs Climate Change*, *12*(4), e713. https://doi.org/10.1002/wcc.713

Story, G. M., Peier, A. M., Reeve, A. J., Eid, S. R., Mosbacher, J., Hricik, T. R., Earley, T. J., Hergarden, A. C., Andersson, D. A., Hwang, S. W., McIntyre, P., Jegla, T., Bevan, S., & Patapoutian, A. (2003). ANKTM1, a TRP-like Channel Expressed in Nociceptive Neurons, Is Activated by Cold Temperatures. *Cell*, *112*(6), 819–829. https://doi.org/10.1016/S0092-8674(03)00158-2

Šumbera, R. (2019). Thermal biology of a strictly subterranean mammalian family, the African mole-rats (Bathyergidae, Rodentia)—A review. *Journal of Thermal Biology*, *79*, 166–189. https://doi.org/10.1016/j.jtherbio.2018.11.003

Takashima, Y., Daniels, R. L., Knowlton, W., Teng, J., Liman, E. R., & McKemy, D. D. (2007). Diversity in the Neural Circuitry of Cold Sensing Revealed by Genetic Axonal Labeling of Transient Receptor Potential Melastatin 8 Neurons. *Journal of Neuroscience*, *27*(51), 14147–14157. https://doi.org/10.1523/JNEUROSCI.4578-07.2007

Tan, C. L., & Knight, Z. A. (2018). Regulation of Body Temperature by the Nervous System. *Neuron*, *98*(1), 31–48. https://doi.org/10.1016/j.neuron.2018.02.022

Tattersall, G. J., & Campbell, K. L. (2023). Thermoconforming rays of the star-nosed mole. *Journal of Experimental Biology*, *226*(3), jeb245127. https://doi.org/10.1242/jeb.245127

Usoskin, D., Furlan, A., Islam, S., Abdo, H., Lönnerberg, P., Lou, D., Hjerling-Leffler, J., Haeggström, J., Kharchenko, O., Kharchenko, P. V., Linnarsson, S., & Ernfors, P. (2015). Unbiased

classification of sensory neuron types by large-scale single-cell RNA sequencing. *Nature Neuroscience*, *18*(1), 145–153. https://doi.org/10.1038/nn.3881

Vandewauw, I., De Clercq, K., Mulier, M., Held, K., Pinto, S., Van Ranst, N., Segal, A., Voet, T., Vennekens, R., Zimmermann, K., Vriens, J., & Voets, T. (2018). A TRP channel trio mediates acute noxious heat sensing. *Nature*, *555*(7698), 662–666. https://doi.org/10.1038/nature26137

Vandewint, A. L., Zhu-Pawlowsky, A. J., Kirby, A., Tattersall, G. J., & Pamenter, M. E. (2019). Evaporative cooling and vasodilation mediate thermoregulation in naked mole-rats during normoxia but not hypoxia. *Journal of Thermal Biology*, *84*, 228–235. https://doi.org/10.1016/j.jtherbio.2019.07.011

Vejmělka, F., Okrouhlík, J., Lövy, M., Šaffa, G., Nevo, E., Bennett, N. C., & Šumbera, R. (2021). Heat dissipation in subterranean rodents: The role of body region and social organisation. *Scientific Reports*, *11*(1), 2029. https://doi.org/10.1038/s41598-021-81404-3

Viswanath, V., Story, G. M., Peier, A. M., Petrus, M. J., Lee, V. M., Hwang, S. W., Patapoutian, A., & Jegla, T. (2003). Opposite thermosensor in fruitfly and mouse. *Nature*, *423*(6942), 822–823. https://doi.org/10.1038/423822a

Vriens, J., Nilius, B., & Voets, T. (2014). Peripheral thermosensation in mammals. *Nature Reviews Neuroscience*, *15*(9), 573–589. https://doi.org/10.1038/nrn3784

Walcher, J., Ojeda-Alonso, J., Haseleu, J., Oosthuizen, M. K., Rowe, A. H., Bennett, N. C., & Lewin, G. R. (2018). Specialized mechanoreceptor systems in rodent glabrous skin: Glabrous skin mechanoreceptors. *The Journal of Physiology*, *596*(20), 4995–5016. https://doi.org/10.1113/JP276608

Wang, Y. (Ed.). (2017). *Transient Receptor Potential Canonical Channels and Brain Diseases* (Vol. 976). Springer Netherlands. https://doi.org/10.1007/978-94-024-1088-4

Wetsel, W. C. (2011). Sensing hot and cold with TRP channels. *International Journal of Hyperthermia*, *27*(4), 388–398. https://doi.org/10.3109/02656736.2011.554337

Wong, H.-S., Freeman, D. A., & Zhang, Y. (2022). Not just a cousin of the naked mole-rat: Damaraland mole-rats offer unique insights into biomedicine. *Comparative Biochemistry and Physiology Part B: Biochemistry and Molecular Biology*, *262*, 110772. https://doi.org/10.1016/j.cbpb.2022.110772

Xu, L., Han, Y., Chen, X., Aierken, A., Wen, H., Zheng, W., Wang, H., Lu, X., Zhao, Z., Ma, C., Liang, P., Yang, W., Yang, S., & Yang, F. (2020). Molecular mechanisms underlying menthol binding and activation of TRPM8 ion channel. *Nature Communications*, *11*(1), 3790. https://doi.org/10.1038/s41467-020-17582-x

Yahav, S., & Buffenstein, R. (1991). Huddling Behavior Facilitates Homeothermy in the Naked Mole Rat *Heterocephalus glaber*. *Physiological Zoology*, *64*(3), 871–884. https://doi.org/10.1086/physzool.64.3.30158212

Yang, S., Lu, X., Wang, Y., Xu, L., Chen, X., Yang, F., & Lai, R. (2020). A paradigm of thermal adaptation in penguins and elephants by tuning cold activation in TRPM8. *Proceedings of the National Academy of Sciences*, *117*(15), 8633–8638. https://doi.org/10.1073/pnas.1922714117

Yin, Y., Le, S. C., Hsu, A. L., Borgnia, M. J., Yang, H., & Lee, S.-Y. (2019). Structural basis of cooling agent and lipid sensing by the cold-activated TRPM8 channel. *Science*, *363*(6430), eaav9334. https://doi.org/10.1126/science.aav9334

Yin, Y., Park, C.-G., Zhang, F., G. Fedor, J., Feng, S., Suo, Y., Im, W., & Lee, S.-Y. (2024). Mechanisms of sensory adaptation and inhibition of the cold and menthol receptor TRPM8. *Science Advances*, *10*(31), eadp2211. https://doi.org/10.1126/sciadv.adp2211

Yin, Y., Wu, M., Zubcevic, L., Borschel, W. F., Lander, G. C., & Lee, S.-Y. (2018). *Structure of the cold- and menthol- sensing ion channel TRPM8*. 6.

York, J. M. (2023). Temperature activated transient receptor potential ion channels from Antarctic fishes. *Open Biology*, *13*(10), 230215. https://doi.org/10.1098/rsob.230215

York, J. M., & Zakon, H. H. (2022). Evolution of Transient Receptor Potential (TRP) Ion Channels in Antarctic Fishes (Cryonotothenioidea) and Identification of Putative Thermosensors. *Genome Biology and Evolution*, *14*(2), evac009. https://doi.org/10.1093/gbe/evac009

Zakharian, E., Cao, C., & Rohacs, T. (2010). Gating of Transient Receptor Potential Melastatin 8 (TRPM8) Channels Activated by Cold and Chemical Agonists in Planar Lipid Bilayers. *The Journal of Neuroscience*, *30*(37), 12526–12534. https://doi.org/10.1523/JNEUROSCI.3189-10.2010

Zhang, H., Wang, C., Zhang, K., Kamau, P. M., Luo, A., Tian, L., & Lai, R. (2022). The role of TRPA1 channels in thermosensation. *Cell Insight*, *1*(6), 100059. https://doi.org/10.1016/j.cellin.2022.100059

Zhang, L., & Barritt, G. J. (2006). TRPM8 in prostate cancer cells: A potential diagnostic and prognostic marker with a secretory function? *Endocrine-Related Cancer*, *13*(1), 27–38. https://doi.org/10.1677/erc.1.01093

Zimmermann, K., Hein, A., Hager, U., Kaczmarek, J. S., Turnquist, B. P., Clapham, D. E., & Reeh, P. W. (2009). Phenotyping sensory nerve endings in vitro in the mouse. *Nature Protocols*, *4*(2), 174–196. https://doi.org/10.1038/nprot.2008.223

Zimmermann, K., Lennerz, J. K., Hein, A., Link, A. S., Kaczmarek, J. S., Delling, M., Uysal, S., Pfeifer, J. D., Riccio, A., & Clapham, D. E. (2011). Transient receptor potential cation channel, subfamily C, member 5 (TRPC5) is a cold-transducer in the peripheral nervous system. *Proceedings of the National Academy of Sciences*, *108*(44), 18114–18119. https://doi.org/10.1073/pnas.1115387108

Zurborg, S., Yurgionas, B., Jira, J. A., Caspani, O., & Heppenstall, P. A. (2007). Direct activation of the ion channel TRPA1 by Ca2+. *Nature Neuroscience*, *10*(3), 277–279. https://doi.org/10.1038/nn1843